CNR, INC.

CNR, INC.
220 RESERVOIR STREET • NEEDHAM HEIGHTS, MASSACHUSETTS 02194 • (617) 449-4902

November 1978

HF MODEM EVALUATIONS FOR THE ADVANCED NARROWBAND DIGITAL VOICE TERMINAL (ANDVT)

FINAL REPORT

Contract No. N00173-78-C-0041

Prepared for

Naval Research Laboratory
Washington, DC 20375
(Code 5420)

and

Naval Electronic System Command
Washington, DC 20360
(Code ELEX 3103)

Prepared by

CNR, Inc.
220 Reservoir Street
Needham, Massachusetts 02194

David Chase
Phillip A. Bello
Charles Boardman
Leslie Pickering
Robert Pinto

(1)

ABSTRACT

During this program, the specifications for the ANDVT HF modem have been refined and detailed evaluation and simulation of the new technical features within this modem have been conducted. These include a multiple-tone signal detection format with an adaptive threshold, a multiple-tone/multiple-stage Doppler estimation algorithm, a matched filter frame estimation algorithm utilizing PN correlation properties, a low-rate error-correction coding approach for protection of the KG sync sequences, an error-correction coding approach specifically designed to protect the critical speech parameters, use of soft-decision (channel measurement) information obtained from the demodulator, and decision-directed Doppler tracking utilizing information from all data tones. The analytical and simulation results provide the desirable result that the preamble can be successfully received at a lower SNR than is required for the reception of high-quality 2400-b/s digitized voice. On a previous effort, high-quality digitized voice reception was obtained over a time-varying multipath HF fading channel model at a signal-to-noise ratio per information bit, E_b/N_0, in the range of 11 to 14 dB. The preamble functions evaluated during this program typically required several dB lower signal-to-noise ratio than is required for successful reception of digitized voice.

TABLE OF CONTENTS

LIST OF ILLUSTRATIONS

LIST OF ILLUSTRATIONS (Continued)

LIST OF ILLUSTRATIONS (Continued)

LIST OF ILLUSTRATIONS (Continued)

LIST OF TABLES

SECTION 1

INTRODUCTION AND RECOMMENDATIONS

This report represents a continuation of the previous work done by CNR [1.1] and the Naval Research Laboratory [1.2] on the design and evaluation of an HF modem for the advanced narrowband digital voice terminal (ANDVT). The emphasis in this report has been on computer simulations, whereas the previous report [1.1] emphasized the specifications and theoretical analysis of the signaling formats. As a result of this effort, a high degree of confidence can be placed on the advanced modem techniques specified. Table 1-1 summarizes the technical advances in HF modem design which have resulted from this and the previous study [1.1] sponsored by the Navy.

The recommended format is illustrated on Figure 1.1.

Signal detection and Doppler estimation is accomplished in approximately 0.355 sec by first detecting the presence of a signal and then estimating the Doppler offset which may be as large as $\pm$ 75 Hz. A probability of detection of below 10^{-2} and negligible probability of a false alarm is achievable by this format. The Doppler estimation error is well below 0.5 Hz. Reference [1.1] and the simulations presented in Section 3 of this report are in excellent agreement and indicate that the above performance results can be achieved at a signal-to-noise density ratio* of 40 dB-Hz, which corresponds to a signal-to-noise ratio measured in a 2400-Hz bandwidth of only 6.2 dB.

---

*The signal to noise density ratio P/N_0 is related to the E_b/N_0 for a 2400-b/s voice modem by:

$$\frac{P}{N_0} = \left(\frac{E_b}{N_0}\right)_{voice} + 33.8 \text{ dB}$$

TABLE 1-1

TECHNICAL ADVANCES IN ANDVT MODEM

- MULTIPLE-TONE SIGNAL DETECTION FORMAT WITH ADAPTIVE THRESHOLD.
- MULTIPLE-TONE/MULTIPLE-STAGE DOPPLER ESTIMATION ALGORITHM.
- MATCHED FILTER FRAME ESTIMATION ALGORITHM UTILIZING PN CORRELATION PROPERTIES.
- LOW-RATE ERROR-CORRECTION CODING APPROACH FOR PROTECTION OF THE KG SYNC SEQUENCES.
- ERROR-CORRECTION CODING IS SPECIFICALLY DESIGNED TO PROTECT THE CRITICAL SPEECH PARAMETERS AND TO USE SOFT-DECISION (CHANNEL MEASUREMENT) INFORMATION OBTAINED FROM THE DEMODULATOR.
- DECISION-DIRECTED DOPPLER TRACKING UTILIZING INFORMATION FROM ALL DATA TONES.

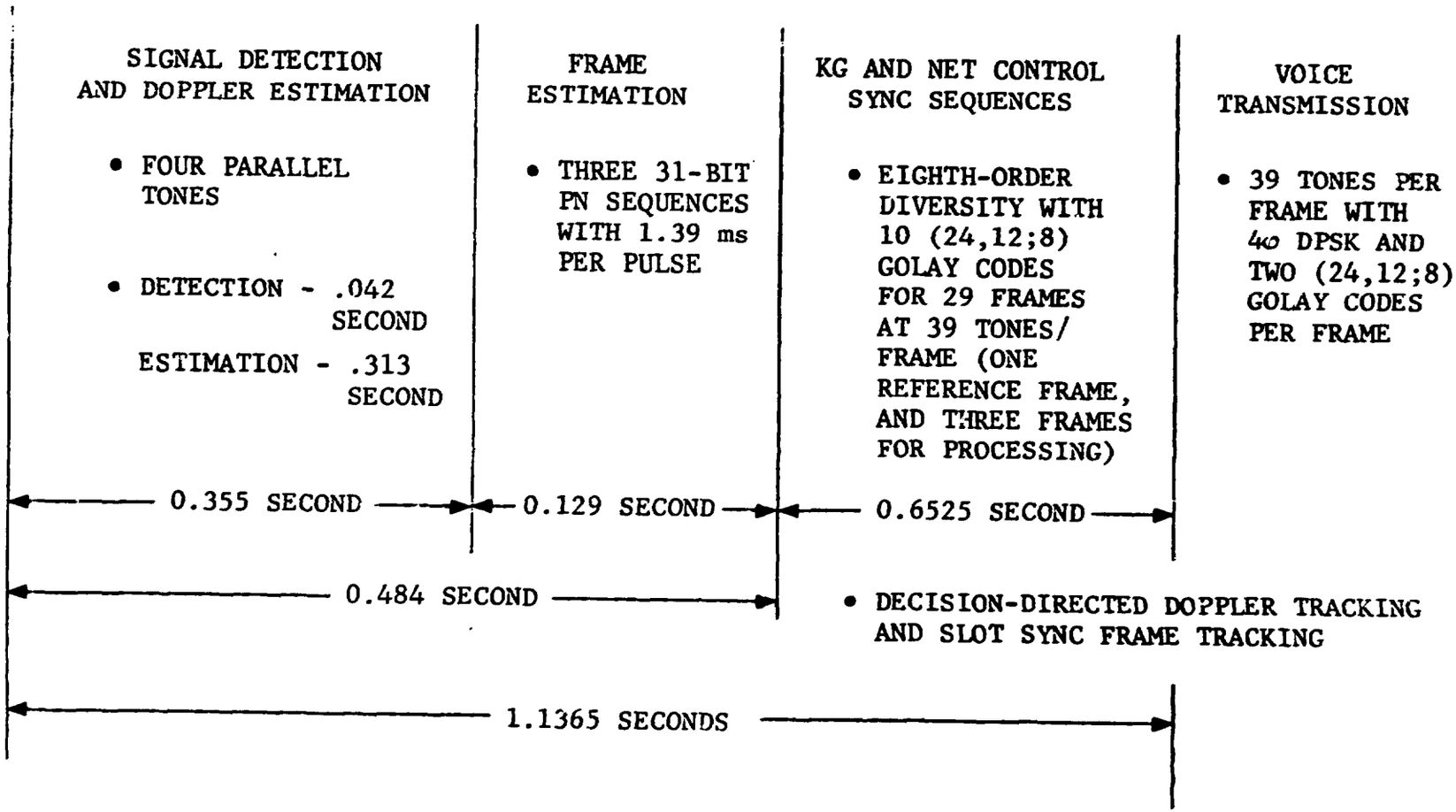

Figure 1.1 A Recommended Half-Duplex Format

noise ratio measured in a 2400-Hz bandwidth of only 6.2 dB.

Following the signal detection and Doppler estimation format, a frame estimation signaling format composed of wideband ($\approx$ 1440 Hz) pulses forming three PN sequences, each of length 31 pulses, is transmitted. This framing technique is shown in Section 2 of this report to be superior to the Carley framing technique specified in [1.1]. The simulation of this framing format, documented in Section 3, indicates that framing errors of below 1 ms are achieved at signal-to-noise density ratios of 40 dB-Hz for realistic 2- and 6-path HF channel models. It should be noted that the simulations reported on in Section 3 include the entire sequence of events, i.e., signal detection, Doppler estimation, and frame estimation, in a manner suitable for hardware implementation.

Following the PN frame estimation format, the 39-tone four-phase PSK modem begins transmission. The next 0.6525 second is devoted to the reception of the KG synchronization sequence. Ten Golay codes, with eighth-order diversity, are transmitted over 25 frames. The first 22.5-ms frame is used as a phase reference and the last three frames are used for soft decoding of these Golay codes. Since the actual data rate is very low, i.e., 120 bits are transmitted in 0.6525 sec, results are obtained in terms of the signal-to-noise per tone* E_T/N_0, which is closely related to the signal-to-noise ratio measured in a 2400-Hz bandwidth, i.e., $\left(\frac{E_b}{N_0}\right)_{voice}$. For the two-path HF channel modem, the

*As noted in Appendix B, the signal-to-noise ratio per tone E_T/N_0 is related to P/N_0 by:

$$\frac{P}{N_0} = \left(\frac{E_T}{N_0}\right)_{KG} + 33.4 \text{ dB}$$

simulation results in Section 4 indicate that a probability of a block error on 120 bits of below 10^{-3} is achievable at a $E_T/N_0 = 8$ dB or $\frac{P}{N_0} = 41.4$ dB-Hz. For the six-path split ray model, a probability of a block error of below 10^{-3} is achievable at $E_T/N_0 = 3$ dB or $\frac{P}{N_0} = 36.4$ dB-Hz. These results are consistent with our design goals of requiring the preamble, including the KG sync sequences, to operate at an SNR below that required for acceptable voice quality.

Tapes of voice transmission, based on the NRL LPC-10, which were made during the previous effort [1.1] indicated that an E_b/N_0 of 14 dB, or $\frac{P}{N_0} = 47.8$ dB-Hz, is required for the two-path model, and an E_b/N_0 of 11 dB, or $\frac{P}{N_0} = 44.8$ dB-Hz, is required for the six-path split ray model. Thus, the entire preamble, signal presence, Doppler estimation, frame estimation, and KG synchronization can be received at several dB lower than that required for intelligible voice receptions. Unfortunately, no new voice tapes have been made during this effort since the FORTRAN version of the latest LPC-10 format supplied by the Government was inoperative.

During the reception of the KG synchronization sequence and the reception of voice transmission, Doppler and frame tracking is required. Simulated results for the new Doppler tracking algorithm are given in Section 3 of this report and compared to the more conventional single-tone tracking algorithm. The new algorithm, which is based on using all of the modulated data tones, offers better performance than the single-tone Doppler tracking loops and has the added advantage that no additional bandwidth or power is required for Doppler tracking. Frame tracking is achieved by using early and late integration gates within an empty tone slot "slot sync", which, incidentally, is the only conventional HF modem technique used in this modem.

REFERENCES

[1.1] D. Chase, et al., "HF Modem Design for the Advanced Narrowband Digital Voice Terminal (ANDVT)," CNR Final Report on Contract No. N00039-77-C-0190, November 1977.

[1.2] W. M. Jewett and R. Cole, "Modulation and Coding Study for the Advanced Narrowband Digital Voice Terminal," NRL Memorandom Report 3811, Naval Research Laboratory, August 1978.

SECTION 2

SYNCHRONIZATION PREAMBLE PERFORMANCE

2.1 Introduction

In this section we make a careful examination of the synchronization preamble performance. Recall from earlier work that the correlation peaks at the matched filter outputs and other properties of sync preamble performance (e.g., effect of Doppler offset) are all derived from consideration of a transmitted sync preamble of the form

$$z_0(t) = \sum_{i=0}^{M-1} \gamma_i \, p(t - i\Delta) \tag{2.1}$$

where the discrete elements $\{\gamma_i;\ i = 1, \ldots, M - 1\}$ constitute the synchronization sequence and are chosen for their correlation properties. Because there is no periodicity in (2.1) the discrete matched filter response to the synchronization sequence in (2.1) has a special form and is referred to as the aperiodic correlation function.

For completeness and future comparisons, the aperiodic correlation function is developed in Appendix A [see Eq. (9) for explicit representations]. In this section we approach the problem from a more general point of view which incorporates features of both the periodic and aperiodic correlation functions. This topic is treated in Section 2.2 which has as its main objective an ambiguity function analysis of the performance of a sync preamble using PN sequences and an analysis of the edge effects due to

non-periodicities at the beginning and end of the preamble. In both cases we are interested in the magnitude of sidelobes in the matched filter output; in particular, we are interested in the extent to which the sidelobe levels are modified in the presence of a channel Doppler shift.

In Section 2.3 we address the problem of evaluating the rms estimation error associated with the determination of frame synchronization. The signal processing is the same as that described in an earlier report [2.1] at least up to the output of the discrete matched filter. Samples of a PN sequence correlation function, distorted by channel and noise, are available at that point. To this collection of samples we now apply a selection rule whereby one selects the maximum energy sample in a segment of the discrete matched filter output that is equal in duration to one period of the sync preamble. In Section 2.3 we analyze this situation and present results which demonstrate, in terms of rms estimation error, that excellent performance is obtained.

2.2 Ambiguity Function Analysis

In this section we perform a rather general ambiguity function analysis of the sync preamble. We recall that we are interested in the sidelobe level in the output of the matched filter receiver. With no Doppler shift present, the matched filter output corresponds to the correlation function of the discrete sequence used to generate the sync preamble. When there is a Doppler offset, the output corresponds to the discrete ambiguity function of the preamble and degradation can result. It is one purpose of this section to determine that degradation.

Generally, each of the functions above has a different value depending on whether the correlator acts to calculate the periodic or aperiodic correlation function. When PN sequences are used one must be concerned with the periodic correlation function. However, transmission of a finite duration preamble necessitates examination of edge effects at the beginning and end of the preamble. This topic is also treated in this section.

We can generally refer to the sync preamble as repeated versions of a fundamental preamble element

$$z_0(t) = \sum_{i=0}^{M-1} \gamma_i p(t - i\Delta) \tag{2.2}$$

If we make the following definitions:

$P \equiv$ length of period (integer multiples of Δ)

$N \equiv$ number of repetitions

we can write the total transmitted sync preamble

$$z(t) = \sum_{j=0}^{N-1} z_0(t - jP\Delta) \tag{2.3}$$

Thus, we see that the total sync preamble consists of repeated versions of $z_0(t)$ with zeroes between ($P > M$) or directly abutting ($P = M$). It is convenient to use the representation

$$P = qM + n \tag{2.4}$$

where q and n are integers with the restrictions $q \geq 1$ and $0 \leq n \leq N$. The fact that q can not be equal to zero rules out the

possibility of overlap which would be equivalent to a redefinition of the sequence.

It is helpful to write out (2.3) in a way that exhibits the dependence on the discrete sequence $\{\gamma_i;\ i = 0, \ldots, M - 1\}$. From (2.2) we have

$$z(t) = \sum_{i=0}^{M-1} \sum_{j=0}^{N-1} \gamma_i\ p[t - (i + jP)\Delta] \tag{2.5}$$

We are interested in evaluating sync preamble performance in the presence of a Doppler shift of F Hz. Thus, the received signal at the input of the received pulse matched filter is obtained by multiplying (2.5) by $\exp\{j2\pi Ft\}$. After doing this and rearranging we have

$$z(t) = \sum_{i=0}^{M-1} \sum_{k=0}^{N-1} \gamma_i\ e^{j2\pi(i+kP)F\Delta}\ \tilde{p}[t - (i+kP)\Delta] \tag{2.6}$$

where

$$\tilde{p}(t) = p(t)e^{j2\pi Ft} \tag{2.7}$$

Thus, a comparison of (2.6) with the result that is obtained when F = 0 indicates a multiplication of the original coefficients by a cissoid and the pulse modification in (2.7).

It is our goal to determine the output of the receiving pulse filter which has an impulse response q(-t), i.e., is ideally matched to some pulse shape q(t). Denoting this response $w_1(t)$, we compute

$$w_1(t) = z(t) \otimes q(-t) \tag{2.8}$$

to obtain

$$w_1(t) = \sum_{i=0}^{M-1} \sum_{k=0}^{N-1} \gamma_i \, e^{j2\pi(i+kP)F\Delta} \; r[t - (i+kP)\Delta, F] \tag{2.9}$$

where

$$r(t,F) = \tilde{p}(t) \otimes q^*(-t)$$

$$= \int p(\tau) q^*(\tau - t) e^{+j2\pi F\tau} \, d\tau \tag{2.10}$$

Because the Doppler offset F is small and causes a negligible shift in the spectrum of p(t) [see (2.7)], we can write

$$r(t,F) \approx r(t,0) = r(t) \tag{2.11}$$

We then have

$$w_1(t) \approx w(t) \tag{2.12}$$

where

$$w(t) = \sum_{i=0}^{M-1} \sum_{k=0}^{N-1} \gamma_i \, e^{j2\pi F(i+kP)\Delta} \; r[t - (i+kP)\Delta] \tag{2.13}$$

It is perfectly reasonable to assume that pulse filter design can yield the interpolating pulse property

$$r(n\Delta) = \begin{cases} 1 & n = 0 \\ 0 & n \neq 0 \end{cases} \tag{2.14}$$

Thus, we deal with the matched filter output samples

$$w_m = \sum_{k=0}^{M-1} \sum_{i=0}^{N-1} \gamma_i \, e^{j2\pi F(i+kP)\Delta} \; r\{[m - (i+kP)]\Delta\} \tag{2.15}$$

On the inner sum the only contribution occurs when $i = m - kP$, and the contribution takes place only if the inequality

$$0 \leq m - kP \leq M - 1 \tag{2.16}$$

To simplify matters we use the function

$$[a,b](n) = \begin{cases} 1 & a \leq n \leq b \\ 0 & \text{otherwise} \end{cases} \tag{2.17}$$

and, accordingly, reduce the double sum in (2.13) to a single sum

$$w_m = \sum_{k=0}^{N-1} \gamma_{m-kP} \, e^{j2\pi Fm\Delta} \, [0, M-1](m - kP) \tag{2.18}$$

It is a simple matter to determine the form of w_m for the L'th period; specifically we have

$$w_m = \begin{cases} \gamma_{m-(L-1)P} \, e^{j2\pi Fm\Delta} & (L-1)P \leq m \leq (L-1)P+M-1 \\ 0 & (L-1)P+M-1 < m \leq LP \end{cases} \tag{2.19}$$

The representation in (2.18), however, is simpler to apply analytically.

The response of an (FIR) filter of length M - 1 to the discrete input in (2.18) is given by

$$y_n = \sum_{i=0}^{M-1} h_i w_{n-i} \tag{2.20}$$

For the particular application we use a discrete matched filter

$$h_i = \gamma^*_{M-1-i} \tag{2.21}$$

The difference between this choice and that used in Eq. (4) of Appendix A is that here we have made the minimum shift to the right required to guarantee causality. We have

$$y_n = \sum_{k=0}^{N-1} \sum_{i=0}^{M-1} \gamma_{n-i-kP} \gamma^*_{M-1-i} e^{j2\pi F(n-i)\Delta} \quad [0, M-1](n-i-kP) \tag{2.22}$$

With the change of variable q = n-i we have

$$w_n = \sum_{k=0}^{N-1} \sum_{q=n-(M-1)}^{n} \gamma_{q-kP} \gamma^*_{(M-1)+q-n} e^{j2\pi Fq\Delta} [0, M-1](q - kP) \tag{2.23}$$

We shall find considerable use for this expression.

One reduction of interest occurs when we consider just one period, i.e., when we set N=1, we obtain

$$w_n = \sum_{q=n-(M-1)}^{n} \gamma_q \, \gamma^*_{(M-1)+q-n} \, e^{j2\pi Fq\Delta} \, [0, M-1](q) \qquad (2.24)$$
$$(N=1)$$

For convenience in comparison it facilitates matters to evaluate (2.24) at $n = p + (M-1)$. We get

$$w_{p+(M-1)}(F) = \sum_{q=p}^{M-1} \gamma_q \gamma^*_{q-p} \, e^{j2\pi Fq\Delta} \qquad (2.25)$$

which, unlike (2.24) which peaks at $q = M-1$, peaks at $p = 0$. This result agrees exactly with an earlier result [2.1, p. 2-84]. In (2.24), however, we have the peak explicitly taking place at $n = M-1$ which makes this expression more suitable for our present purposes, especially when it involves keeping track of the timing.

Using the general expression (2.23) we have calculated the ambiguity functions for several cases of interest. The matched filter output for a length-31 PN sequence is shown in Fig. 2.1 for Doppler shifts of 0.0, 2.0, and 10.0 Hz. The leading portion of each curve illustrates the forementioned edge effect. The right-hand section shows the internal structure of the matched filter output when total periodicity applies; in this segment the peak-to-sidelobe ratio takes on the value M (where M is the sequence length) when the Doppler shift F is zero.

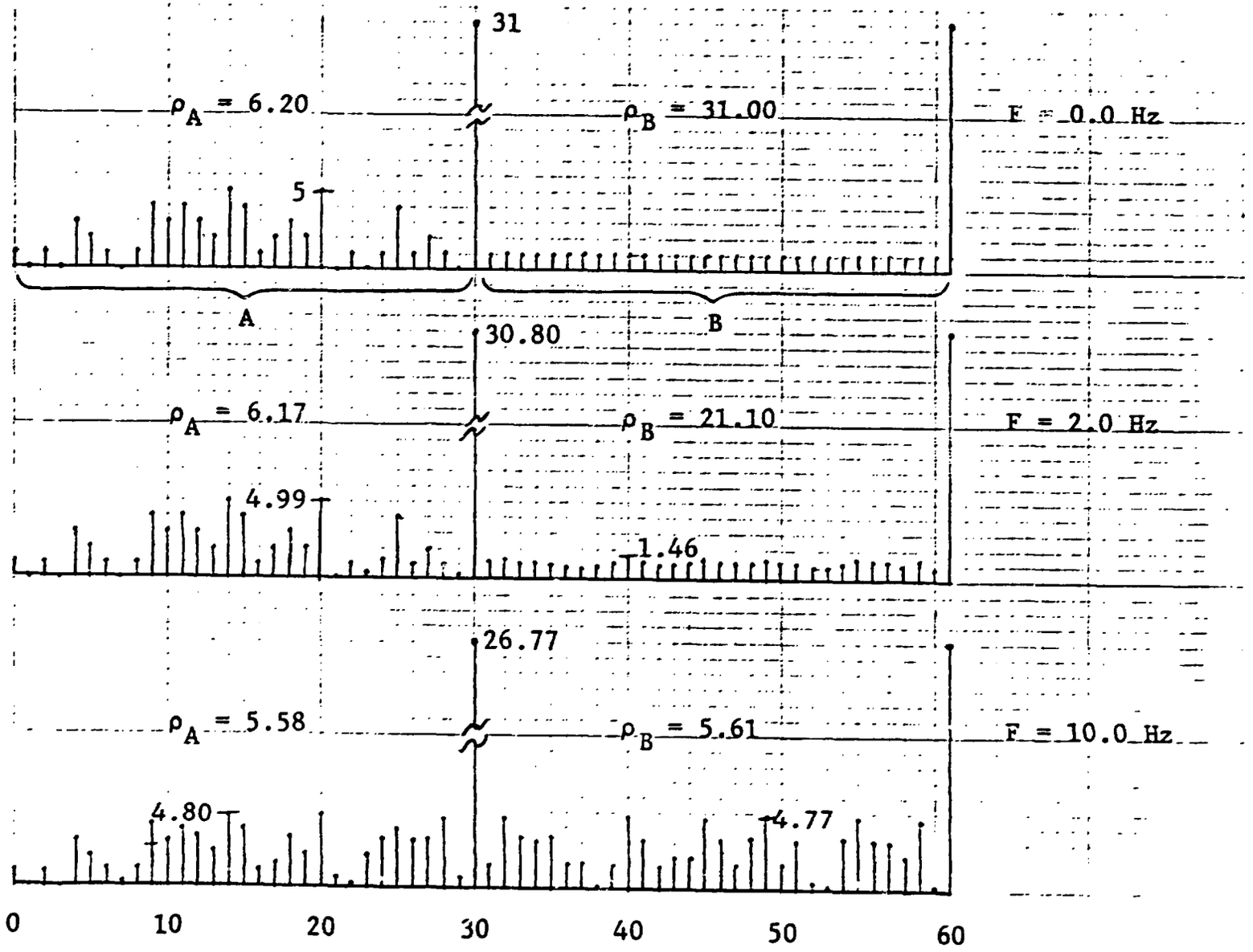

Figure 2.1 Magnitude of Discrete Matched Filter Output for Length-31 PN Sequence (If sequence is repeated n times the output consists of segment A followed by n-1 repeats of segment B followed by a time reverse of segment A.) ρ_A and ρ_B are the peak-to-sidelobe ratios in the respective segments.

For a Doppler shift of 2 Hz (the maximum that need be allowed), we see that ρ_B, the sidelobe level in the region of interest, has a value in excess of 21 for the 31 element sequence. This degradation does not seriously degrade the performance probabilities relative to peak detection.

For purposes of comparison we have also provided data for the F = 10 Hz Doppler shift in Fig. 2.1. Here we see that the sidelobe ratio has degraded from 31 to 5.61 in the region of periodicity whereas at the edges it has only degraded from 6.20 to 5.28, i.e., the two sidelobes are of comparable level. We re-emphasize, however, that this Doppler shift far exceeds the shift after Doppler correction.

For purposes of completeness, the edge effects for various sequences of lengths 3 through 7 are shown in Fig. 2.2. It can be seen that the degradation can be quite substantial (e.g., M = 11). For this reason, gating out of the areas at the edges is recommended generally.

A particularly interesting sequence is shown in Fig. 2.3. This sequence is the only known optimal binary sequence. Its sidelobes are <u>zero</u> when there is no Doppler offset, and the peak-to-sidelobe ratio is 80 when F = 2.0 Hz. Despite its extremely favorable sidelobe properties, this sequence is not useful in our current context as we shall see in Section 2.3.

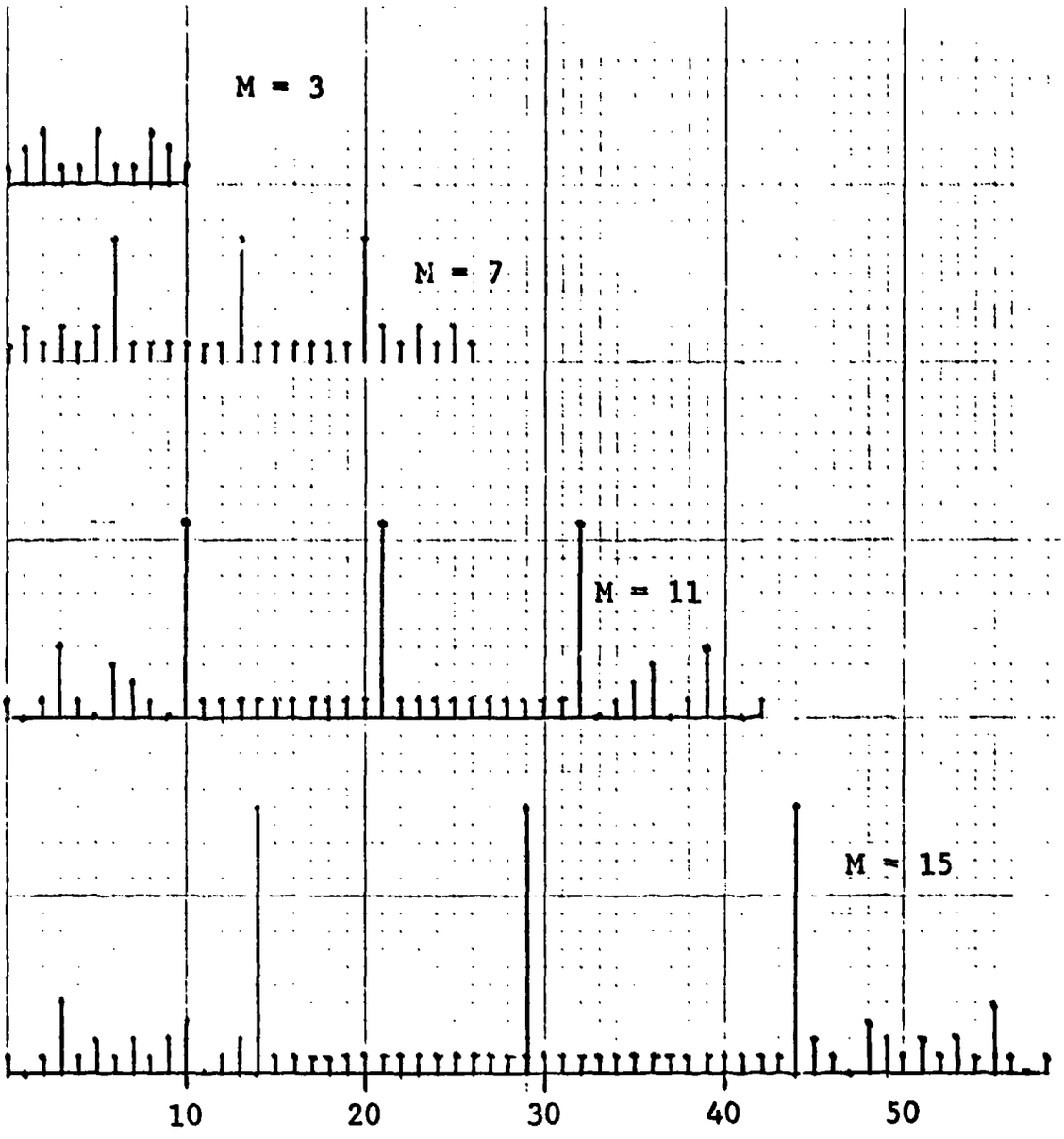

Figure 2.2 Illustration of Edge Effects for PN Sequence Correlation Functions

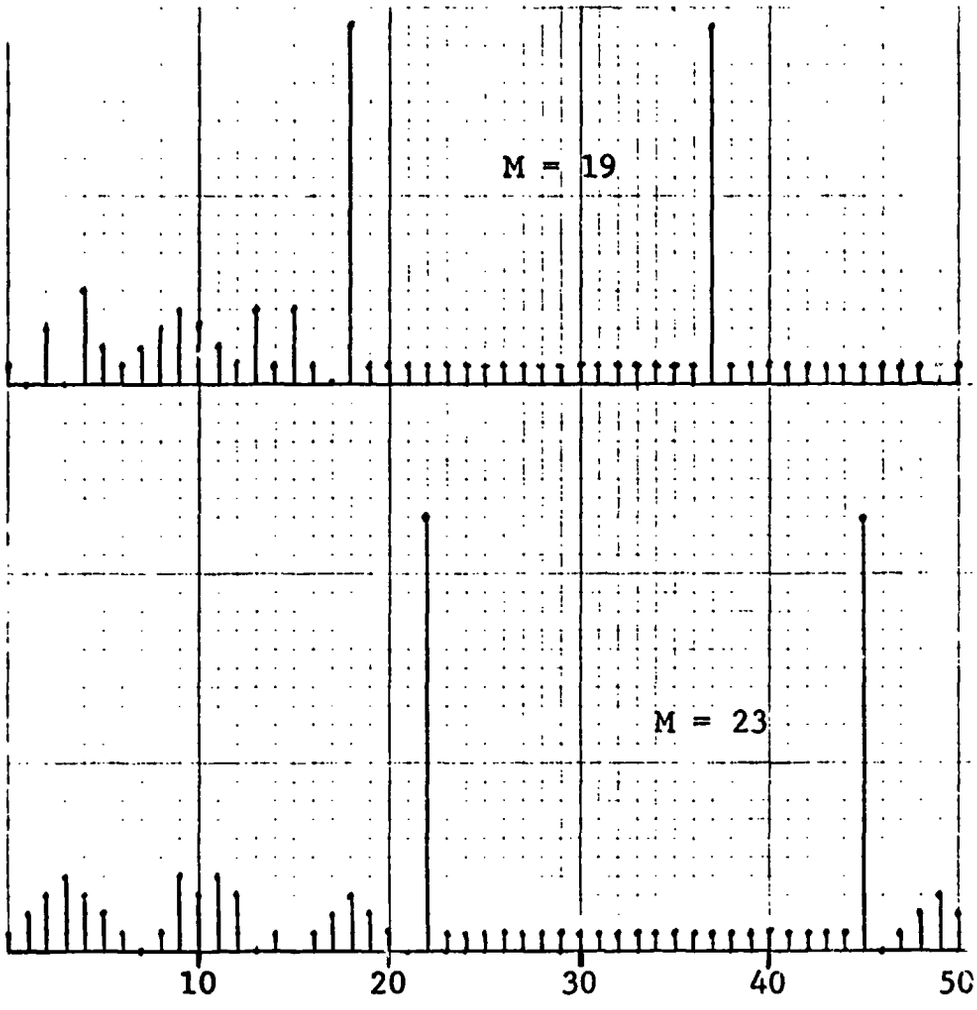

Figure 2.2 (Continued)

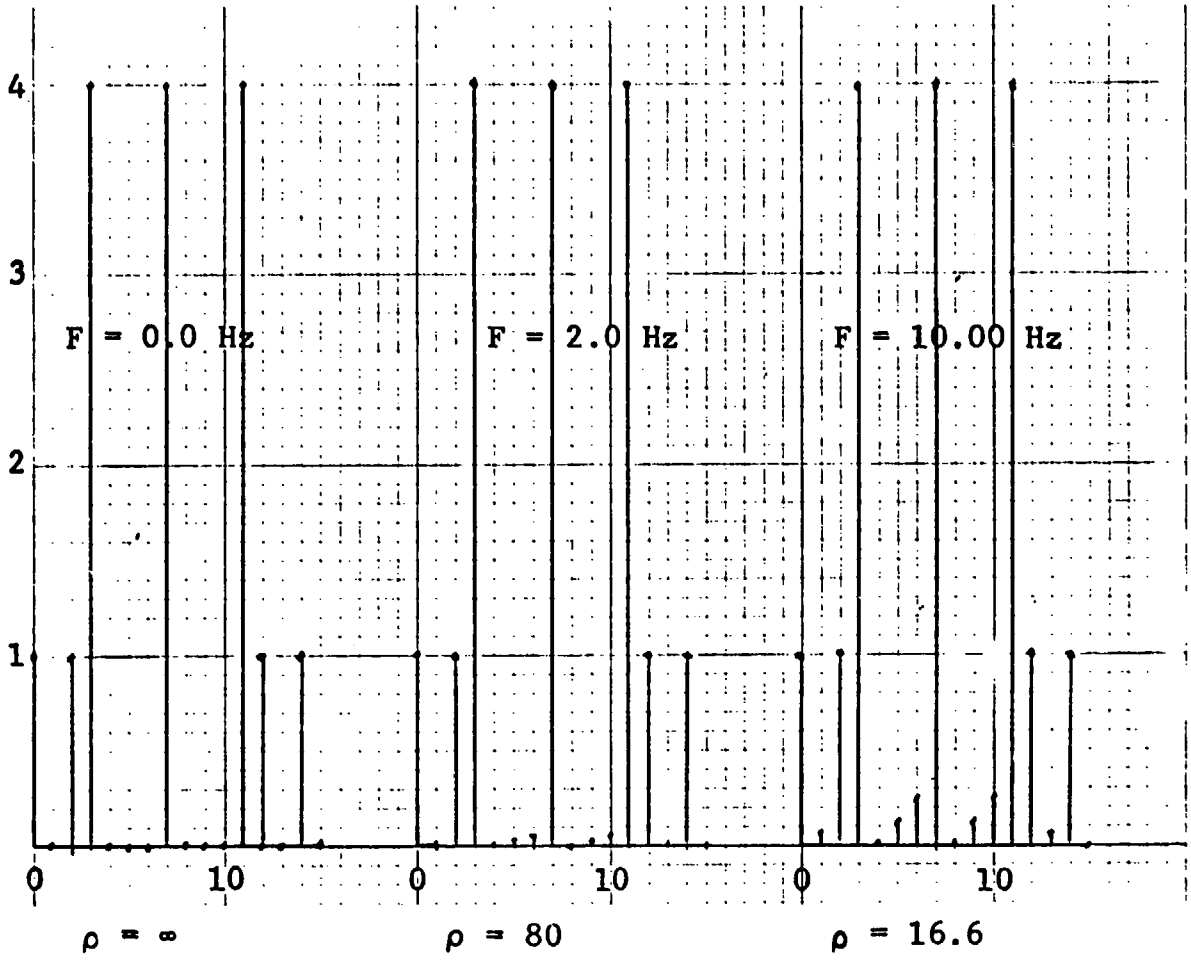

Figure 2.3 Magnitude of Discrete Matched Filter for Optimal Length-4 Sequence (1,0,0,0)

2.3 Evaluation of Frame Sync Estimation Error

This section addresses the problem of evaluating the estimation error associated with the determination of frame synchronization. The signal processing is exactly the same as that described in an earlier report [2.1] at least up to the output of the discrete matched filter. Recall that samples of the PN sequence correlation function, distorted by channel and noise, are available at that point. To this collection of samples we now apply a selection rule whereby one selects the maximum energy sample in a segment of the discrete matched filter output that is equal in duration to one period of the sync preamble. This section provides an analysis of this situation and presents results which demonstrate, in terms of rms estimation error, that very good performance is obtained. The processing is indicated schematically in Figure 2.4.

Our previous calculations implicitly assumed ideal sampling at the pulse repetition rate, hence our results which depended on the discrete autocorrelation function of the sequence (PN) that modulates the pulse train. In practice, the synchronization pulse duration will be some multiple of the basic sampling interval Δ, e.g., $k_0\Delta$. In such a case, because we cannot a priori separate the peaks from the sidelobes, we must correlate k_0 sets of N_{seq} variables corresponding to the samples taken $k_0\Delta$ seconds apart. The three sets, of course, arise from the three possible "guesses" of the "ideal" sampling times. The best choice of sample point sets, i.e., the one that provides the sample closest to the peak, is marked with arrows in Figure 2.5. Note that the choice of the best set does not provide a sample corresponding precisely to the peak; however, the sample corresponding to the peak will be in error by only one sampling interval at most. In order to simplify our calculations, it is assumed in the remainder of this development that the peak value can be obtained precisely.

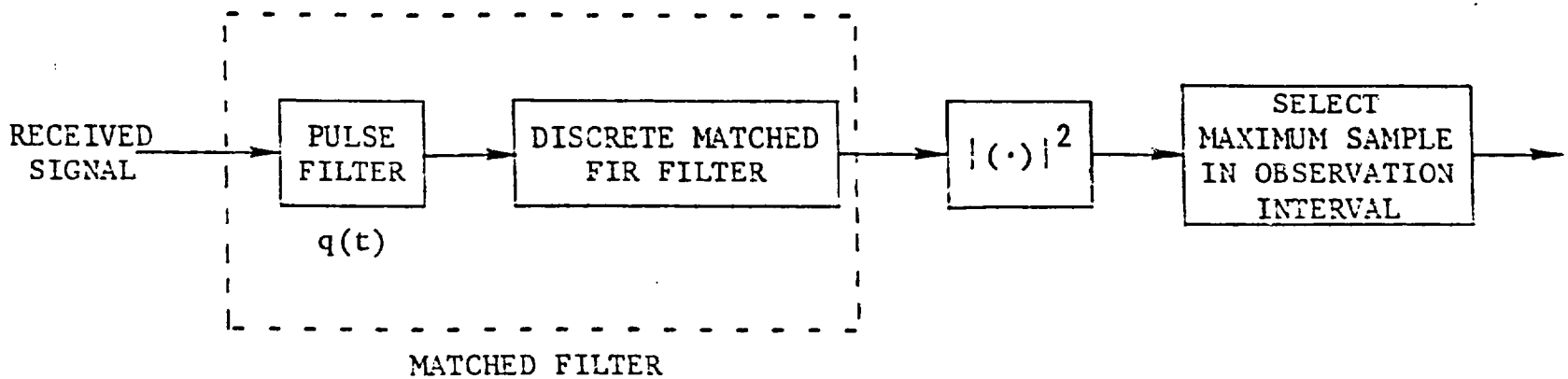

Figure 2.4 Sync Preamble Processing

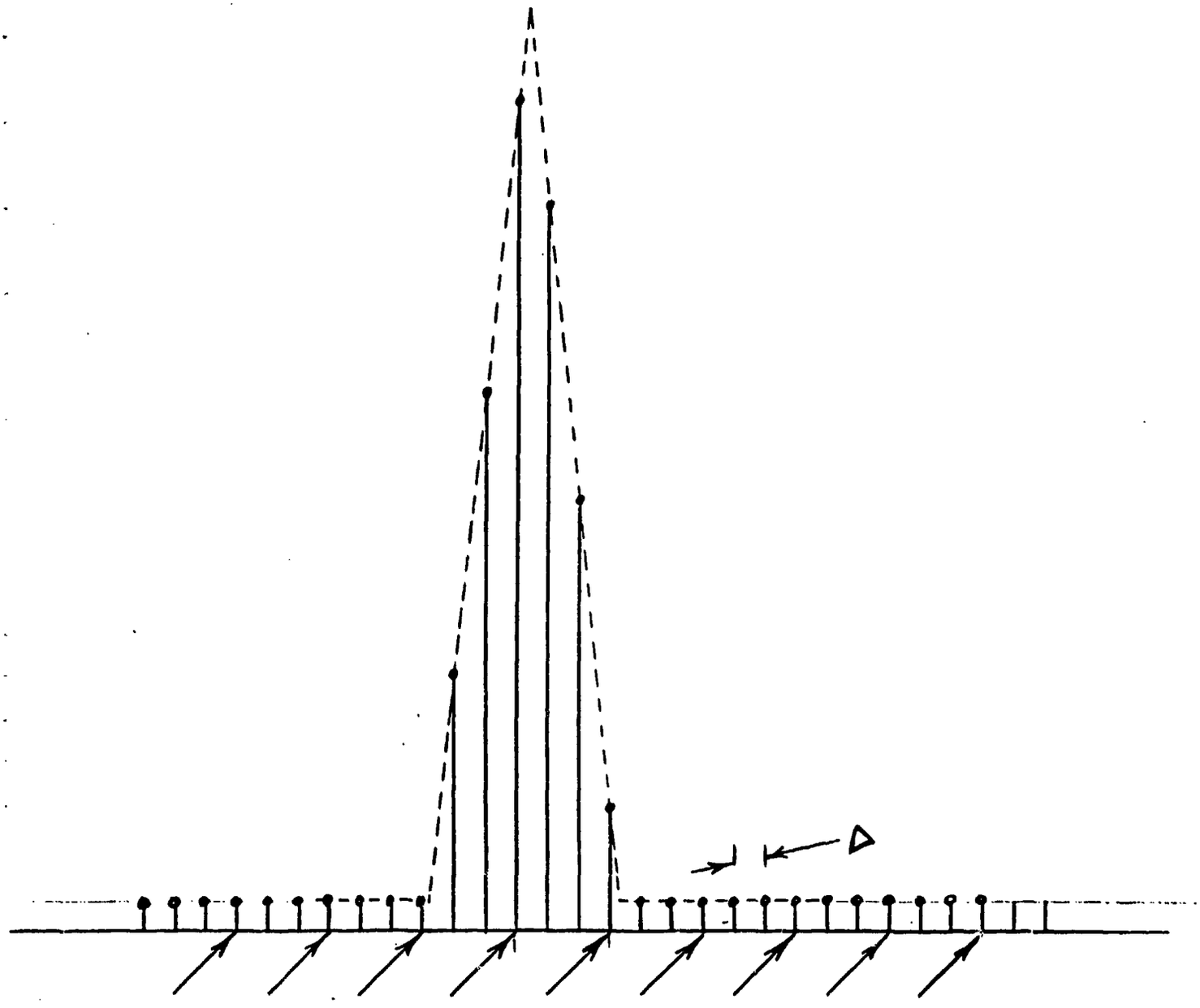

Figure 2.5 Correlator Output with "Best Choice" of Sample Point Set Spaced at the Pulse Duration (here 3Δ)

Selecting the peak value according to the rule described above is mathematically equivalent to simply choosing the maximum of the $k_0 N_{seq}$ sample points.

For the purposes of our analysis we view the time axis as being divided into two mutually exclusive sets:

(1) Received pulse (and multipath) interval

(2) Noise interval.

The first region is occupied with (multipath-distorted) signal energy. The second region, because of the extremely low side-lobes, is taken to be occupied by noise energy only. We ignore fluctuation in estimated frame boundary due to multipath since multipath spread is small compared to frame duration. When pulses overlap due to multipath, the peak can be reduced and in the limit of overlap one must consider a single path. Since we calculate as a function of non-overlapping pulses, we span the calculation range of interest. For those errors caused by noise, the characterization of the pulse with a single value corresponds to a worst-case calculation.

The notation for this problem is shown in Figure 2.6. Generally, the multipath components are assigned the subscripts $\{n_i;\ i = 1, \ldots, L\}$. Defining the multipath centroid

$$\bar{x} = \frac{1}{L} \sum_{i=1}^{L} x_{n_i} \tag{2.26}$$

the error under consideration is taken to be the weighted sum over all N sample slots

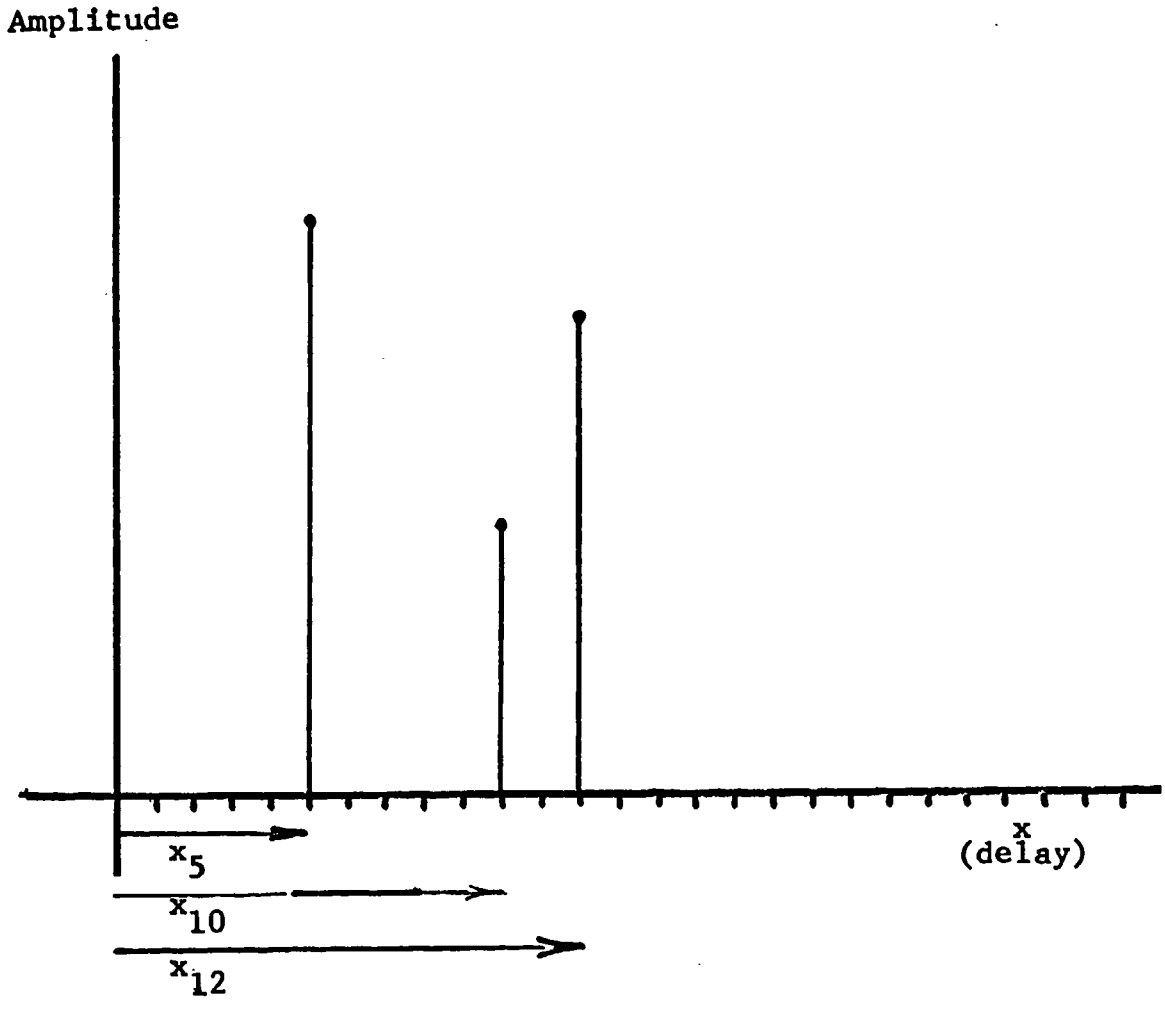

$x_n = n\Delta$

TOTAL OBSERVATION INTERVAL = $N\Delta$

Figure 2.6 Nomenclature and Notation for 3-Path Channel

$$e^2 = \sum_{j=1}^{N} \left(x_j - \bar{x} \right)^2 p_j \qquad (2.27)$$

where p_j is the probability that the energy in the sample slot at x_j exceeds the energy in all the other slots. This sum can be divided up in the following way:

$$e^2 = \sum_{\substack{j=1 \\ j \neq n_1, n_2, \ldots, n_L}}^{N} \left(x_j - \bar{x} \right)^2 p_j + \sum_{i=1}^{L} \left(x_{n_i} - \bar{x} \right)^2 p_i \qquad (2.28)$$

Note that the first sum in (2.28) is over those slots that contain no signal energy; i.e., it represents a measure of the error due to noise only. The second sum in (2.28) represents an error arising from the combined effects of noise and fading. Recalling that the word "selection" will be used to indicate choice of the sample slot with maximal energy, we make the following definitions:

(1) p is defined as the probability that a sample slot containing noise energy only will be selected.*

(2) q is defined as the probability that a sample slot containing noise energy and signal energy will be selected.

---

* Implicit in this development, of course, is our assumption that the noise samples are independent and identically distributed. This assumption is not strictly true, of course, because of smearing by the pulse filters, but is in keeping with our commitment not to utilize assumptions that favor system operation.

Using the definitions in (2.28) we have , after some rearranging,

$$e^2 = p \sum_{j=1}^{N} \left(x_j - \bar{x}\right)^2 + (q-p) \sum_{i=1}^{L} \left(x_{n_i} - \bar{x}\right)^2 \qquad (2.29)$$

In the absence of noise, p=0 and q=1/L (recall the assumption of equal strength paths). Hence we obtain

$$e^2 = \sigma_m^2 \qquad (2.30)$$

as the mean-squared error in the no-noise case. In (2.30)

$$\sigma_m^2 = \frac{1}{L} \sum_{i=1}^{L} \left(x_{n_i} + \bar{x}\right)^2 \qquad (2.31)$$

is a measure of multipath spread (multipath spread = $2\sigma_m$).

Returning to (2.29) we have

$$e^2 = p \sum_{j=1}^{N} \left(x_j - \bar{x}\right)^2 + L \left(q-p\right) \sigma_m^2 \qquad (2.32)$$

Some thought about the second term in this expression indicates that it is just slightly less than σ_m^2 for all practical situations. In the sequel we refer to it as the multipath error and neglect it. It can always be reasonably approximated by (2.30) once the multipath spread of the particular channel under study is known. The remaining error term

$$e_1^2 = p \sum_{j=1}^{N} \left(x_j - \bar{x}\right)^2 \tag{2.33}$$

we refer to as "the error in excess of multipath spread" and calculate below.

To evaluate the sum in (2.33) we recall that $x_j = j\Delta$ and assume for simplicity that $\bar{x} = m\Delta$ where m is an integer satisfying the inequality $1 \leq m \leq N$. This assumption at worst introduces an error less than $\Delta/2$. Applying the identities

$$\sum_{i=1}^{m} i = \frac{m}{2}(m + 1) \tag{2.34}$$

and

$$\sum_{i=1}^{m} i^2 = \frac{m}{6}(m + 1)(2m + 1) \tag{2.35}$$

some manipulation yields

$$e^2 = p\Delta^2 \left[\frac{N^3}{3} + \frac{N^2}{2} + \frac{N}{6} + f(m) \right] \tag{2.36}$$

where

$$f(m) = mN\,(m - N - 1) \tag{2.37}$$

Equation (2.37) is a function of the random variable m which represents the centroid location within the observation interval.

It is entirely reasonable to assume that the signal centroid, and thus m, is uniformly distributed throughout the observation interval. This yields

$$\overline{f} = -\frac{1}{6} N\,(N+1)(N+2) \tag{2.38}$$

as the mean value of f(m). For the average error we obtain

$$e^2 = \frac{\Delta^2}{6} N(N^2-1)p \tag{2.39}$$

It remains to evaluate the probability p that a sample slot containing noise energy only will be the one selected. Such a slot must contain more energy than all the other slots; this includes slots with signal and noise energy as well as other slots with noise energy alone. In the noise only slots, we assume that z_i, which represents the magnitude squared value of the signal, is distributed according to the probability density function (pdf)

$$p_0(z) = \frac{1}{2\sigma_0^2} \exp\left\{-\frac{z}{2\sigma_0^2}\right\} \tag{2.40}$$

When the signal is present the pdf is

$$p_1(z) = \frac{1}{2\sigma_1^2} \exp\left\{-\frac{z}{2\sigma_1^2}\right\} \tag{2.41}$$

In (2.40) σ_0^2 represents the noise amplitude variance; in (2.41) σ_1^2 represents the signal-plus-noise amplitude variance. The multidimensional pdf of all of these random variables (assumed to be independent) is given by

$$p(z_1,z_2,\ldots,z_N) = \prod_{i=1}^{N-L} p_0(z_i) \prod_{j=1}^{L} p_1(z_j) \tag{2.42}$$

The desired probability p is given by

$$p = \int_0^\infty P(z_s)p_0(z_s)\, dz_s \tag{2.43}$$

where $P(z_s)$ is the probability that the energy sample z_s in a noise slot exceeds the energy samples in all the other slots. It is given by

$$P(z_s) = F_0^{N-1-L}(z_s)\, F_1^L(z_s) \tag{2.44}$$

where $F_0(z_s)$ and $F_1(z_s)$ are the cumulative distributions corresponding to the pdf's given in (2.40) and (2.41) For either case the distribution has the generic form

$$F(z) = \int_0^z p(z)\, dz \tag{2.45}$$

$$= 1 - \exp\left\{-\frac{z}{2\sigma^2}\right\}$$

for which the appropriate subscript can be added to σ.

Using these results in (2.43) we have

$$p = \frac{1}{2\sigma_0^2} \int_0^\infty \left(1 - \exp\left\{-\frac{z}{2\sigma_0^2}\right\}\right)^{N-1-L} \left(1 - \exp\left\{-\frac{z}{2\sigma_1^2}\right\}\right)^{L} \exp\left\{-\frac{z}{2\sigma_0^2}\right\} dz \tag{2.46}$$

Defining

$$r = \sigma_0^2/\sigma_1^2 \tag{2.47}$$

and making the change of variables

$$u = \exp\left\{-\frac{z}{2\sigma_0^2}\right\} \tag{2.48}$$

we obtain

$$p = \int_0^1 (1 - u)^{N-1-L}(1 - u^r)^L \, du \tag{2.49}$$

Before evaluating this integral we note that

$$\sigma_1^2 = \frac{1}{2} GC^2(0) + \sigma_0^2 \tag{2.50}$$

In this expression σ_0^2 is half the complex noise power, C(0) is the peak correlation function value, and G is the path strength, i.e., $G = \overline{|g_i|^2}$ where g_i is the complex path gain of the i^{th} path. Note that equal strength paths have been assumed.

Recalling that the noise power is given by

$$2\sigma_0^2 = 2N_0C(0) \tag{2.51}$$

we can substitute into (2.47) and obtain

$$r = \frac{1}{1 + \frac{T_s}{L}\left(\frac{1}{T_s}\ \frac{LGC(0)}{2N_0}\right)} \tag{2.52}$$

where T_s is the duration of one cycle of the preamble. It is more useful to write (2.52) in the form

$$r = \frac{1}{1 + \frac{T_s\gamma_0}{L}} \tag{2.53}$$

where γ_0 the power-to-noise density ratio.

Returning now to the problem of evaluating the integral in (2.49) we observe, since L cannot be a very large integer, that there is no computational inconvenience in expanding the term $(1-u^r)^L$ using the binomial theorem. We obtain

$$p = \sum_{j=0}^{L} \binom{L}{j}(-1)^{L-j} \int_0^1 (1-u)^M\, u^{r(L-j)}\, du \tag{2.54}$$

where

$$M = N - 1 - L$$

The mathematical problem becomes one of evaluating the integral

$$I_a = \int_0^1 (1-x)^M x^a \, dx \tag{2.55}$$

This is accomplished via successive integration by parts. Initially we use the substitutions

$$u = (1-x)^M \tag{2.56}$$

and

$$dv = x^a \, dx \tag{2.57}$$

and obtain

$$I_a = (1-x)^M \frac{x^{a+1}}{a+1} \Bigg]_0^1 - \int_0^1 (-1)M \, (1-x)^{M-1} \frac{x^{a+1}}{a+1} dx$$

$$= \frac{M}{a+1} \int_0^1 (1-x)^{M-1} x^{a+1} \, dx \tag{2.58}$$

Proceeding similarly a second time, we obtain

$$I_a = \left(\frac{M}{a+1}\right)\left(\frac{M-1}{a+2}\right) \int_0^1 (1-x)^{M-2} x^{a+2} \, dx \tag{2.59}$$

For the M^{th} iteration, we obtain the simple result

$$I_a = \frac{M!}{\prod_{i=1}^{M+1} (a+i)} \tag{2.60}$$

Substituting back in (2.54) we obtain

$$p = \sum_{j=0}^{L} \binom{L}{j} (-1)^{L-j} \frac{M!}{\prod_{i=1}^{M+1} [r(L-j) + i]} \tag{2.61}$$

which after observing that

$$\prod_{i=1}^{M+1} [r(L-j)+i] = (M+1)! \prod_{i=1}^{M+1} \left[1+ \frac{r(L-j)}{i}\right] \tag{2.62}$$

and using the fact that

$$M = N-1-L$$

simplifies to

$$p = \frac{1}{N-L} \sum_{j=0}^{L} \binom{L}{j} (-1)^{L-j} \frac{1}{\prod_{i=1}^{N-L} \left[1 + \frac{r(L-j)}{i}\right]} \tag{2.63}$$

When used in conjunction with (2.53) and (2.39), this result yields the rms error e_1.

For a 31 length sequence and a pulse duration of 1.39 ms, the rms frame sync error is presented in Figure 2.7. The error is seen to decrease rapidly with increasing signal-to-noise-density ratio (SNDR) and number of paths. When the SNDR exceeds 40 dB-Hz, the rms error remains below 2 ms in all cases.

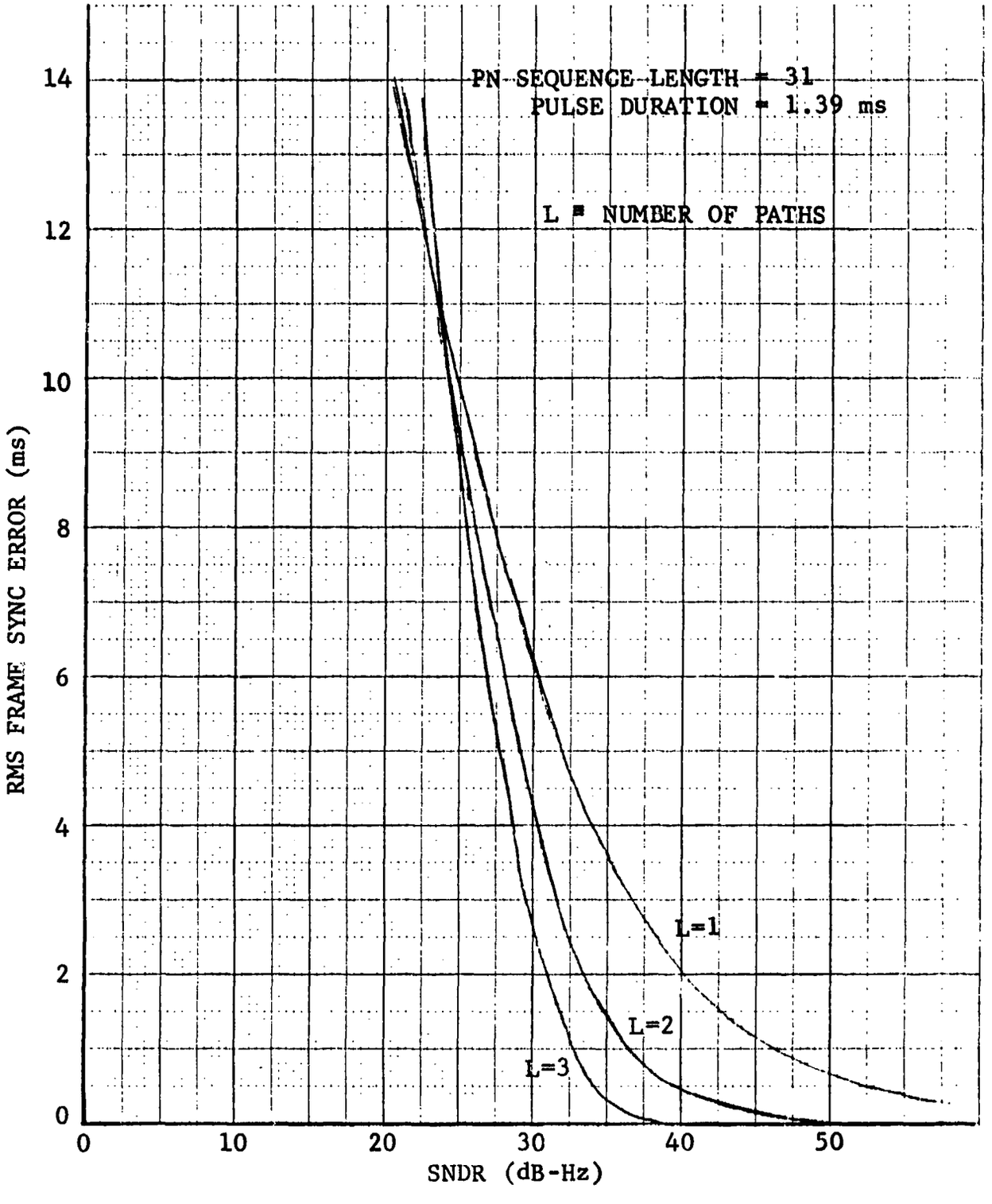

Figure 2.7 RMS Frame Sync Error in Excess of Multipath Error for an L-Path Channel with Equal Strength Independently Fading Paths

The curves presented in Figure 2.7 show the synchronization error due to noise only and should be thought of as an error in excess of the multipath error. Inclusion of the multipath error requires assumption of a specific path structure. In Figure 2.8 we show our calculated curves for a 2-path channel with 1 ms between the paths and a 6-path channel with 0.5 ms between adjacent paths. Plateaus are in evidence and the curves are seen to be more tightly clustered together than in the previous case.

It should be pointed out that the dependence on L in Figure 2.8 should not be considered as indicative of the dependence that will occur in practice. The wide range of multipath spreads and the possibility of overlap between the modes allow no generalization in this regard.

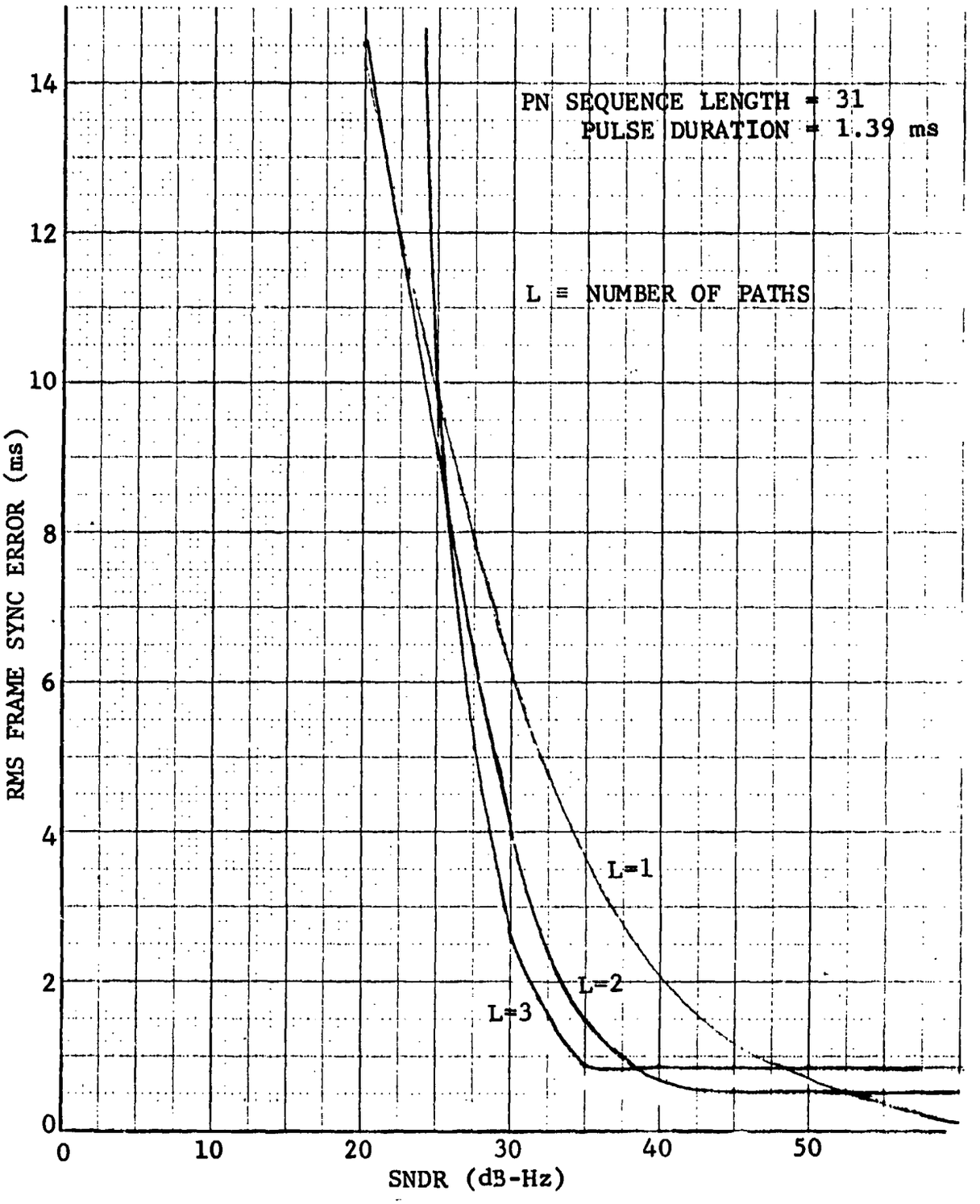

Figure 2.8 RMS Frame Sync Error with Multipath Spread Included

REFERENCES

[2.1] D. Chase, et al., "HF Modem Design for the Advanced Narrowband Digital Voice Terminal (ANDVT)," CNR Final Report on Contract No. N00039-77-C-0190, November 1977.

[2.2] J. Omara and T. Kailath, "Some Useful Probability Distributions," Technical Report No. 7050-6, Stanford Electronic Laboratories, Stanford University, September 1965.

SECTION 3

PREAMBLE SIMULATIONS

3.1 Signal Presence Detection and Doppler Estimation

3.1.1 Signal Model

Computer software for simulating modem signal presence detection and Doppler estimation has been developed. A detailed description of the modem signal processing is available in [3.1]. In the simulation these operations (bandpass filtering, frequency shifting, derivative estimation, etc.) are carried out exactly as would be done in the actual modem although floating point arithmetic was used. In the preamble simulations, the channel model was simplified to the extent that signal structure was fixed during the interval (approximately 350 ms) required for these operations. The small variation which would occur in a time-varying channel (bandwidth on the order of 1 Hz) can be expected to improve rather than degrade performance. Specifically, if s(t) is the complex envelope which would be received in the absence of distortion, the actual received signal is of the form

$$r(t) = \sum_{j=1}^{N_{path}} \alpha_j \, s(t - \tau_j) + n(t) \qquad (3.1)$$

where τ_j = delay of j^{th} path

$\overline{|\alpha_j|^2}$ = relative power of j^{th} path satisfying

$$\sum_{j=1}^{N_{path}} |\alpha_j|^2 = 1 \qquad (3.2)$$

During signal presence detection/Doppler estimation the signal consists of four unmodulated sinusoids located within an IF bandwidth less than W(≈2400)Hz, as shown in Figure 3.1:

$$s(t) = \sqrt{2P} \sum_{i=1}^{4} e^{j(2\pi f_i t + \varphi_i)} \tag{3.3}$$

Taken together with (3.2) this defines the per tone received power as P. Substituting this into (3.1) allows us to write the received signal in the simple form

$$r(t) = \sum_{i=1}^{4} z_i e^{j(2\pi f_i t + \varphi_i)} + n(t) \tag{3.4}$$

where

$$z_i = \sqrt{2P} \sum_{j=1}^{N_{path}} \alpha_j e^{-j2\pi f_i \tau_j} \tag{3.5}$$

is the resultant envelope for the i^{th} tone. In an exact model, α_j and, hence, z_i would vary slowly during the signal processing; this effect is of secondary importance and has been omitted in the current simulations.

In the simulation, r(t) was sampled W times per second, corresponding to the rate at which complex samples are processed in the actual modem. These samples are thus of the form

$$r_k = r\left(\frac{k}{W}\right) = \sum_{1}^{4} z_i e^{j\left(\frac{2\pi f_i k}{W} + \varphi_i\right)} + n\left(\frac{k}{W}\right) \tag{3.6}$$

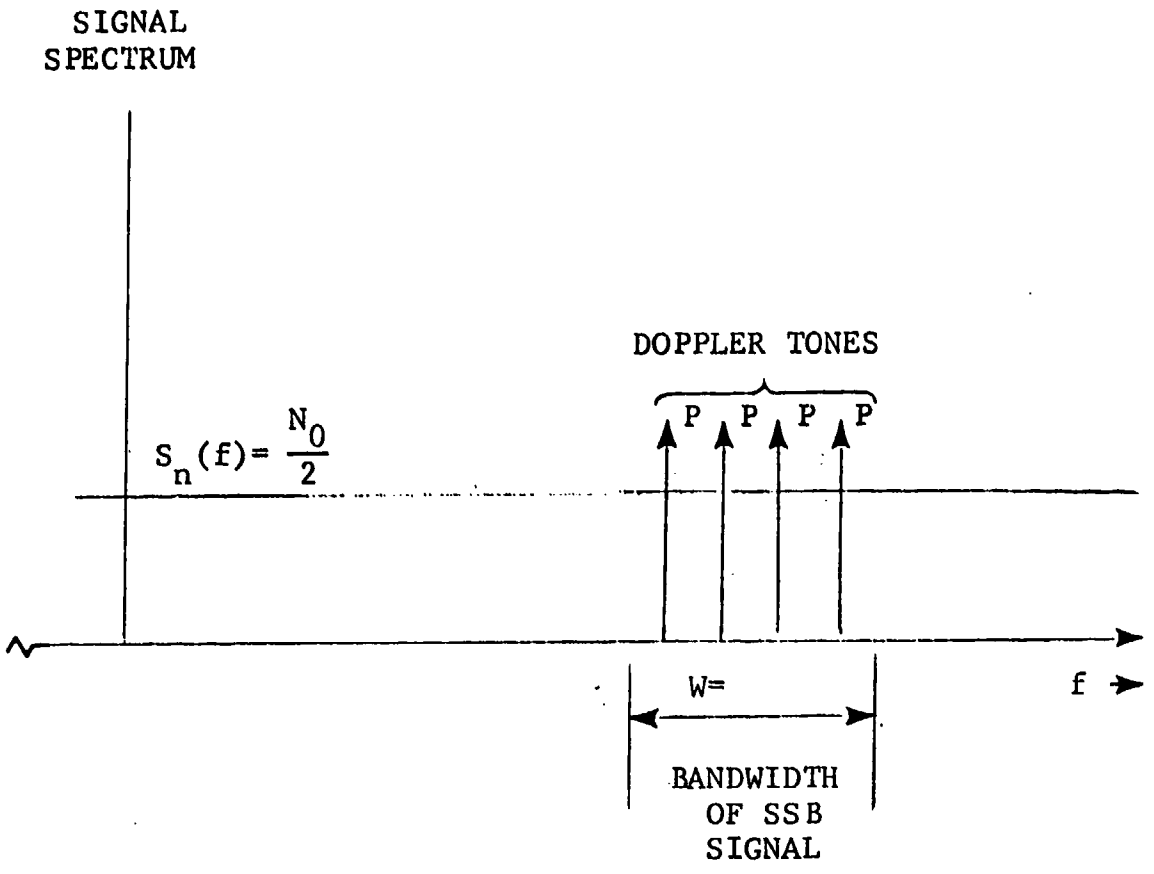

Figure 3.1 Spectral Characteristics of Signal and Noise

Successive noise samples $n\left(\frac{k}{W}\right)$ are uncorrelated zero-mean Gaussian and have variance given by

$$\overline{\left|n\left(\frac{k}{W}\right)\right|^2} = 2N_0W \tag{3.7}$$

where $\frac{N_0}{2}$ is the (two-sided) power spectral density of the noise. Thus the SNR of the waveform being processed is given by

$$\frac{2P \sum_{j=1}^{N_{path}} |\alpha_j|^2}{\left|n\left(\frac{k}{W}\right)\right|^2} = \frac{P}{N_0W} \tag{3.8}$$

3.1.2 Variable Bandwidth Bandpass Filters

The variable bandwidth filters used to isolate the Doppler tones consist of the cascade of two identical first-order recursive filters. Consider first the baseband equivalent of a single filter:

$$y_k = (1 - \mu)y_{k-1} + \mu x_k \tag{3.9}$$

The transfer function of this filter is given by

$$H_1(j\omega) = \frac{1}{\mu^{-1} - (\mu^{-1} - 1)\, e^{-j\omega T}} \tag{3.10}$$

and

$$|H_1(j\omega)|^2 = \frac{1}{1 + \gamma - \gamma \cos \omega T} \tag{3.11}$$

where

$$\gamma = 2\mu^{-2} - 2\mu^{-1} \tag{3.12}$$

The 3 dB frequency of the cascade may be found by setting $|H_1(j\omega)|^2 = \frac{1}{\sqrt{2}}$ yielding

$$\omega_{3dB} = \frac{1}{T} \cos^{-1}\left(1 - \frac{\sqrt{2}-1}{\gamma}\right) \tag{3.13}$$

or equivalently

$$\gamma = \frac{\sqrt{2} - 1}{1 - \cos\ \omega_{3dB}T} \tag{3.14}$$

In terms of γ the parameter μ is given by

$$\mu = \frac{\sqrt{1+2\gamma} - 1}{\gamma} \tag{3.15}$$

The resulting amplitude response for f_{3dB}=75 Hz is shown in Figure 3.2.

In the simulation an equivalent second-order recursive filter was used rather then separate first-order filters and the filtering was performed at bandpass. For an assumed center frequency ω_0 the filtering operation is defined by

$$y_k = A_1 e^{j\omega_0 T} y_{k-1} + A_2 e^{2j\omega_0 T} y_{k-2} + A_3 x_k \tag{3.16}$$

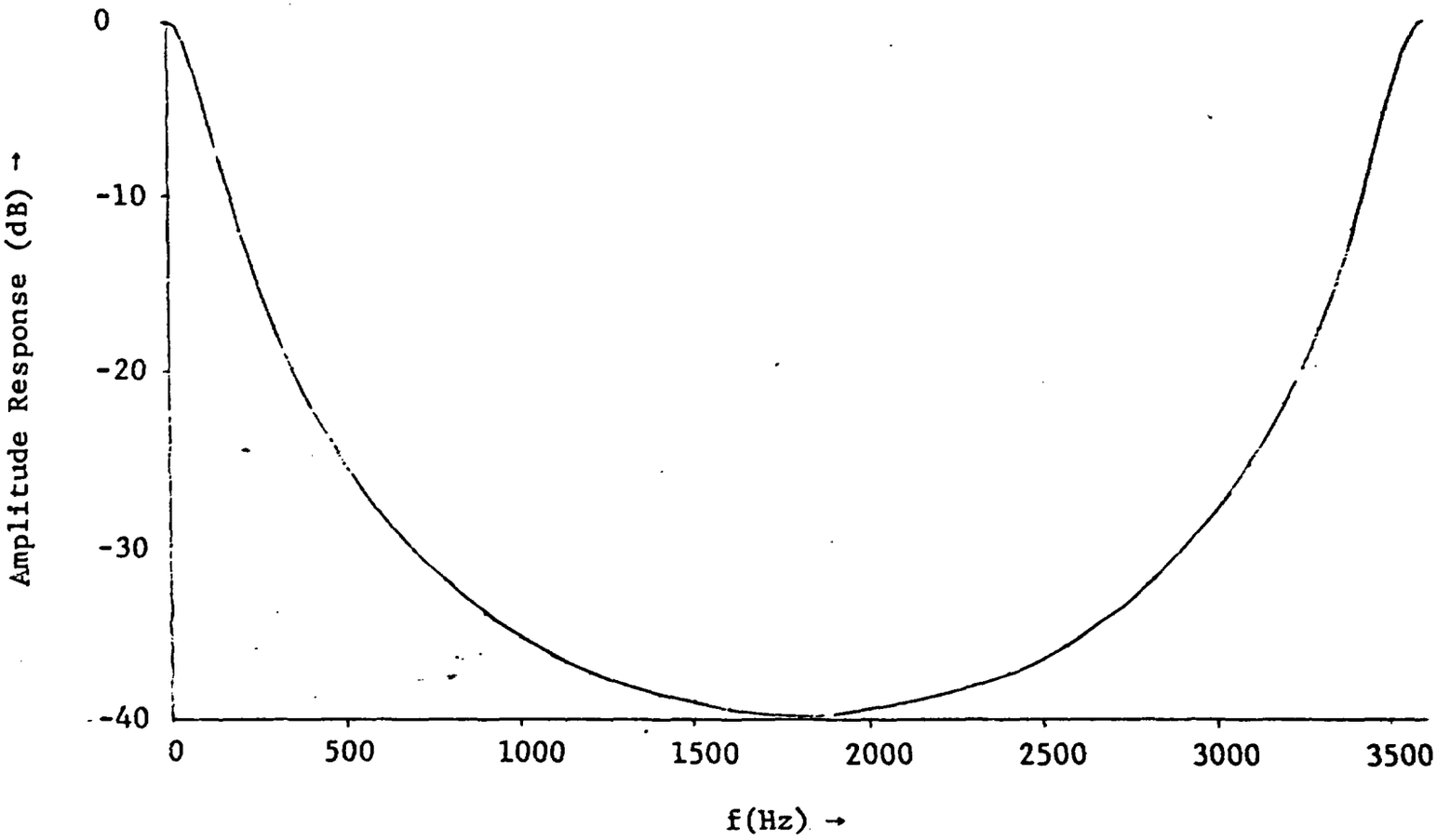

Figure 3.2 Frequency Response of Lowpass Equivalent Second-order Filter
f_{3dB} = 75 Hz Sampling Rate = 3600 sec^{-1}

where

$$A_1 = 2(1-\mu) = 2\left[1 - \frac{\sqrt{1+2\gamma} - 1}{\gamma}\right] \tag{3.17}$$

$$A_2 = -(1-\mu)^2 = -\left[1 - \frac{\sqrt{1+2\gamma} - 1}{\gamma}\right]^2 \tag{3.18}$$

$$A_3 = \mu^2 = \left(\frac{\sqrt{1+2\gamma} - 1}{\gamma}\right)^2 \tag{3.19}$$

To achieve a desired 3 dB bandwidth these coefficients must be evaluated using Eq. (3.14).

Filter outputs are sampled for further processing at an interval sufficient to ensure that the noise in successive samples is substantially uncorrelated. In [3.1] the recommended separation is $3t_c$ where t_c appears in the equivalent first-order continuous-time filter model as

$$H(f) = \frac{t_c^{-1}}{j2\pi f + t_c^{-1}} \tag{3.20}$$

By straightforward manipulation, it can be shown that for this model t_c is related to the overall 3-dB frequency by

$$t_c = \frac{\sqrt{\sqrt{2} - 1}}{2\pi f_{3\,dB}} = \frac{0.1024}{f_{3\,dB}} \tag{3.21}$$

3.1.3 Doppler Estimation

Although the Doppler estimation has been discussed in detail elsewhere [3.1], we present a somewhat different formulation which enables a slight reduction in the number of arithmetic operations required. Consider first a single complex envelope sampled at time kT:

$$z_k = x_k + jy_k \tag{3.22}$$

The Doppler estimate based on this signal is

$$\hat{\nu}_k = \frac{1}{2\pi} \frac{x_k \dot{y}_k - y_k \dot{x}_k}{x_k^2 + y_k^2} = \frac{1}{2\pi} \frac{\mathrm{Im}\left[z_k^* \dot{z}_k\right]}{|z_k|^2} \tag{3.23}$$

For a constant-envelope noise-free signal with fixed Doppler ($z = |z| e^{j\omega T}$) this relationship is exact. However, the derivative will be approximated by a simple difference

$$\dot{z}_k = \frac{1}{T}\left(z_k - e^{j\omega T} z_{k-1}\right) \tag{3.24}$$

where z_{k-1} represents the previous sample at the basic sampling rate and the factor $e^{j\omega T}$ is included because the desired signal imbedded in z(t) is the output of a bandpass filter centered at ω. Substituting (3.24) into (3.23) we find that the first term is identically zero, yielding

$$\hat{\nu}_k = \frac{1}{2\pi T} \frac{\mathrm{Im}\left\{e^{-j\omega T} z_k z_{k-1}^*\right\}}{|z_k|^2} \tag{3.25}$$

Calculation of the numerator of (3.25) requires 6 multiplications and 3 additions, while the original approach (calculating $\dot{x}_k$ and $\dot{y}_k$ before forming $x_k\dot{y}_k - y_k\dot{x}_k$) requires 6 multiplications and 7 additions.

At N instants in time (separated by approximately t_c seconds), the numerator and denominator of (3.25) are computed for each of the four bandpass filter outputs and accumulated separately. Thus, the Doppler estimate may be regarded as a weighted average of individual Doppler measurements

$$\nu = \frac{\sum_{n=1}^{N} \sum_{i=1}^{4} |Z_{n,i}|^2 \nu_{n,i}}{\sum_{n=1}^{N} \sum_{i=1}^{4} |Z_{n,i}|^2} \qquad (3.26)$$

where $\nu_{n,i}$ represents the measurement obtained from the i^{th} tone at time $t=3nt_c$ and $Z_{n,i}$ is the corresponding complex envelope.

3.1.4 Simulation Results

In running the simulation software, the following parameter values were selected:

Tone Frequencies (phases): 675.00(0), 1237.50(0), 1800.0(0), 2362.50(180^o)

Noise filter center frequencies: 956.25, 1518.75, 2081.25, 2643.75

Complex samples per second: 3600

Window for signal presence detection $\left(t_{WIN}\right)$ .0417 sec (N=10)

Signal presence threshold: 2.65

Signal presence filter bandwidth = 75 Hz

Doppler estimation filters:

Stage	Bandwidth (Hz)	N	Sample Separation (ms)
1	75	16	4.17
2	16.2	3	18.89
3	3.5	1	87.78

Duration of Doppler estimation (including transient build-up): 0.3136 sec

Initial frequency offset: 0

The parameters most important to the design are the bandwidths of the tone filters for each stage, the time separation between samples taken at the output of these filters, and the number (N) of samples averaged. Values for these parameters, as shown above, were taken from the preliminary design presented in [3.1]. The sample separation must, of course, be an integral multiple of the basic sampling rate, which was assumed to be 3600 Hz, so these values differ slightly from the original.

The simulation software is written to carry out signal presence detection and Doppler estimation in sequence. However, if signal presence detection does not occur during the first t_{WIN} seconds, Doppler estimation is not attempted and the trial is recorded as an acquisition failure. (In the actual processor, acquisition might occur subsequent to the window, but Doppler estimation would then overlap the wideband sync pulses and be substantially degraded.) Thus, we may compare the observed probability of incorrect dismissal with theoretical calculations made earlier. (The probability of false alarm was also predicted theoretically, but for the threshold settings of interest it is too small to observe in the simulations.) Recall that calculations

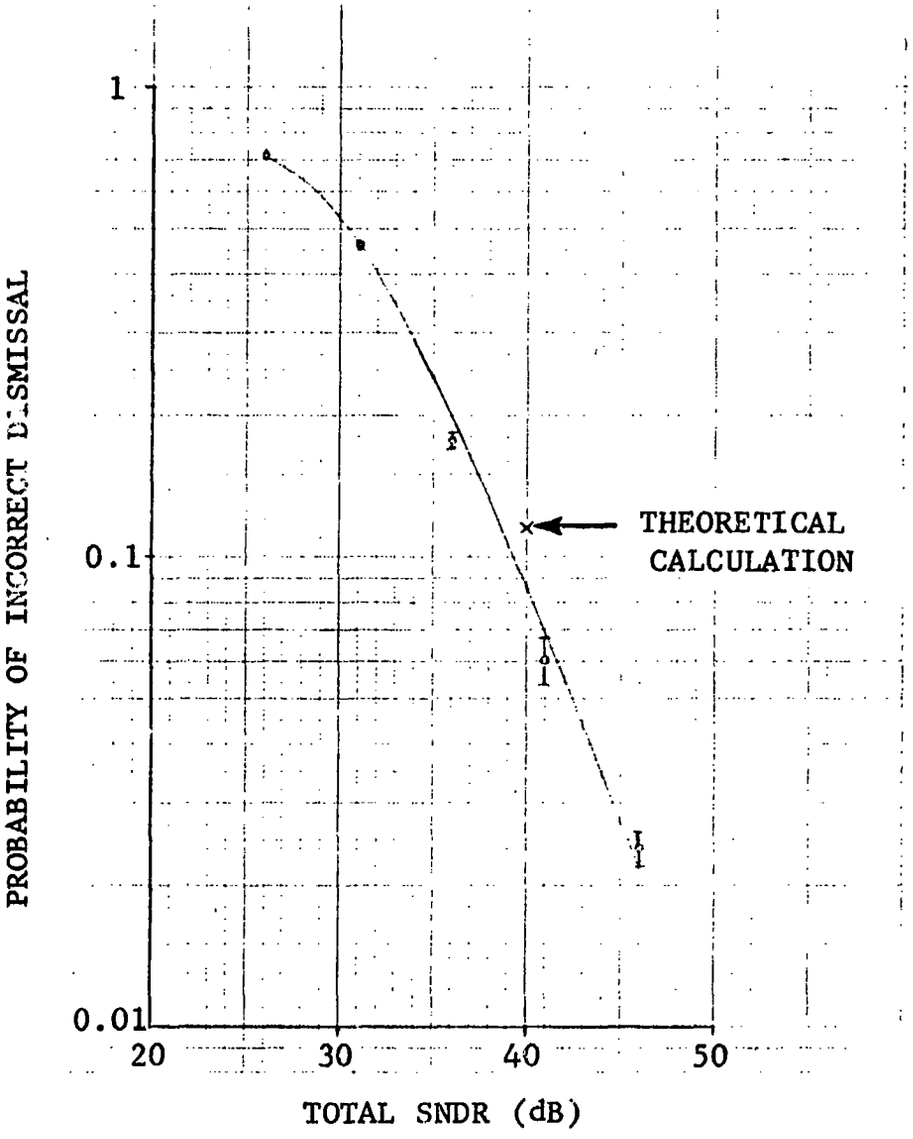

Figure 3.3 Simulated Performance of Signal Processing Detection in Flat Fading (Single-Path Channel)

were made under two assumptions: completely correlated fading of the tones and independent fading. The former case corresponds to the model of Eq. (3.1). However, as the number of paths increases, the tones will tend to become uncorrelated. Therefore, we have compared simulation results for the two- and six-path models with the predictions based on independent fading in Figure 3.4. These results also show good agreement in the region for which the simulation results are valid. However, the effect of correlation between the tones would be more pronounced at higher values of SNDR.

RMS Doppler estimation error as a function of SNDR is shown in Figures 3.5 and 3.6 for the two- and six-path channel models. Also shown are theoretical predictions based on Eq. (2.121) of [3.1]. In general, the simulations show better performance than the predictions. This is because Eq. (2.121) assumes that in each stage the tones fall at the 3 dB point of the bandpass filter, resulting in a loss of 3 dB in SNR. In the simulations, the tones were located at the center of the first stage filters; in subsequent stages, tone location depends on the estimate made in the preceding stage during that particular trial. Thus, the theoretical predictions are overly conservative while the simulations more accurately represent operational conditions Examinations of the curves does in fact show a displacement of roughly 3 dB at the higher SNDR's. At the lower SNDR's, performance of the second and especially the third stage is degraded as a result of earlier estimates placing the signal outside of the filter passband. In view of these considerations, agreement between theory and simulation seems to be excellent.

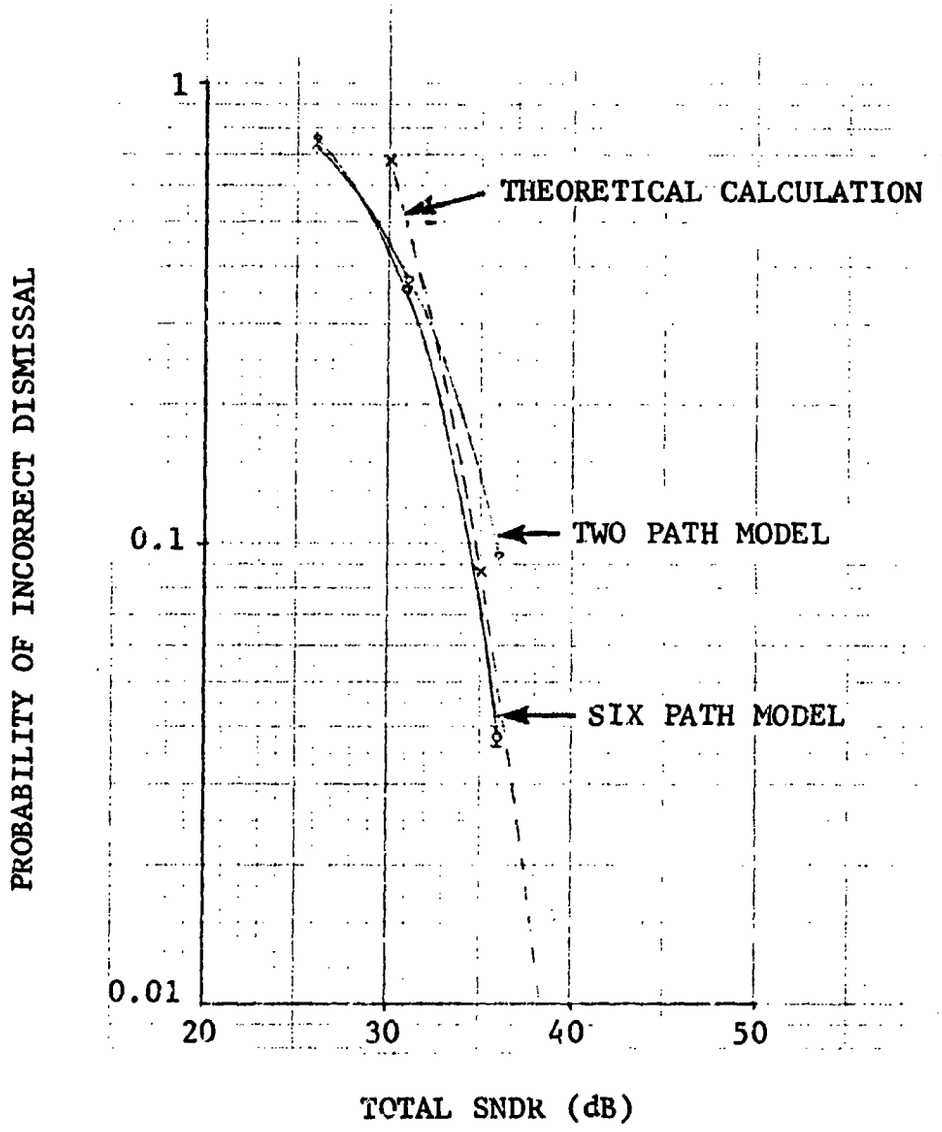

Figure 3.4 Simulated Performance of Signal Presence Detection

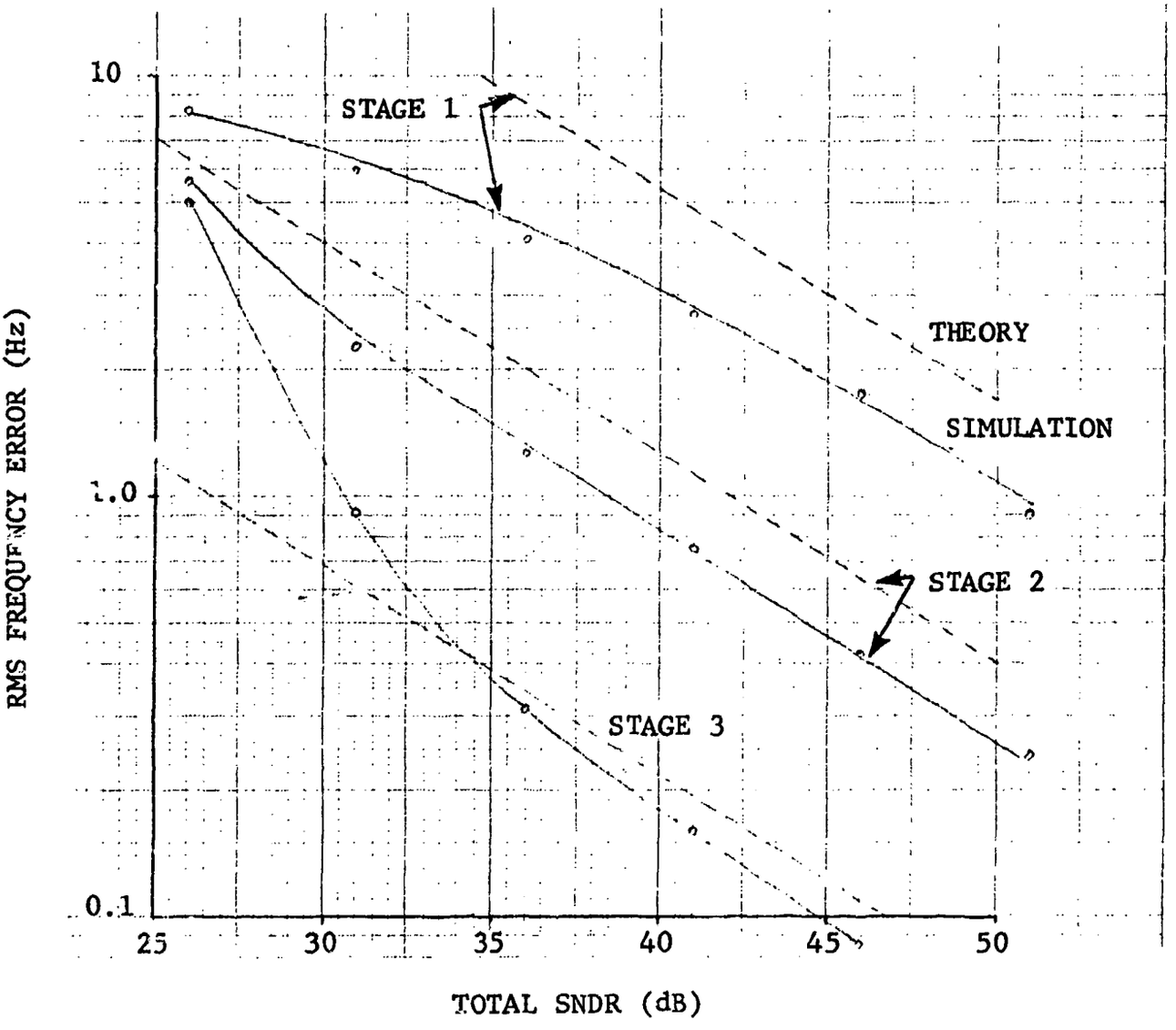

Figure 3.5 Simulated Performance of Three-Stage Doppler Estimator for Two-Path Channel

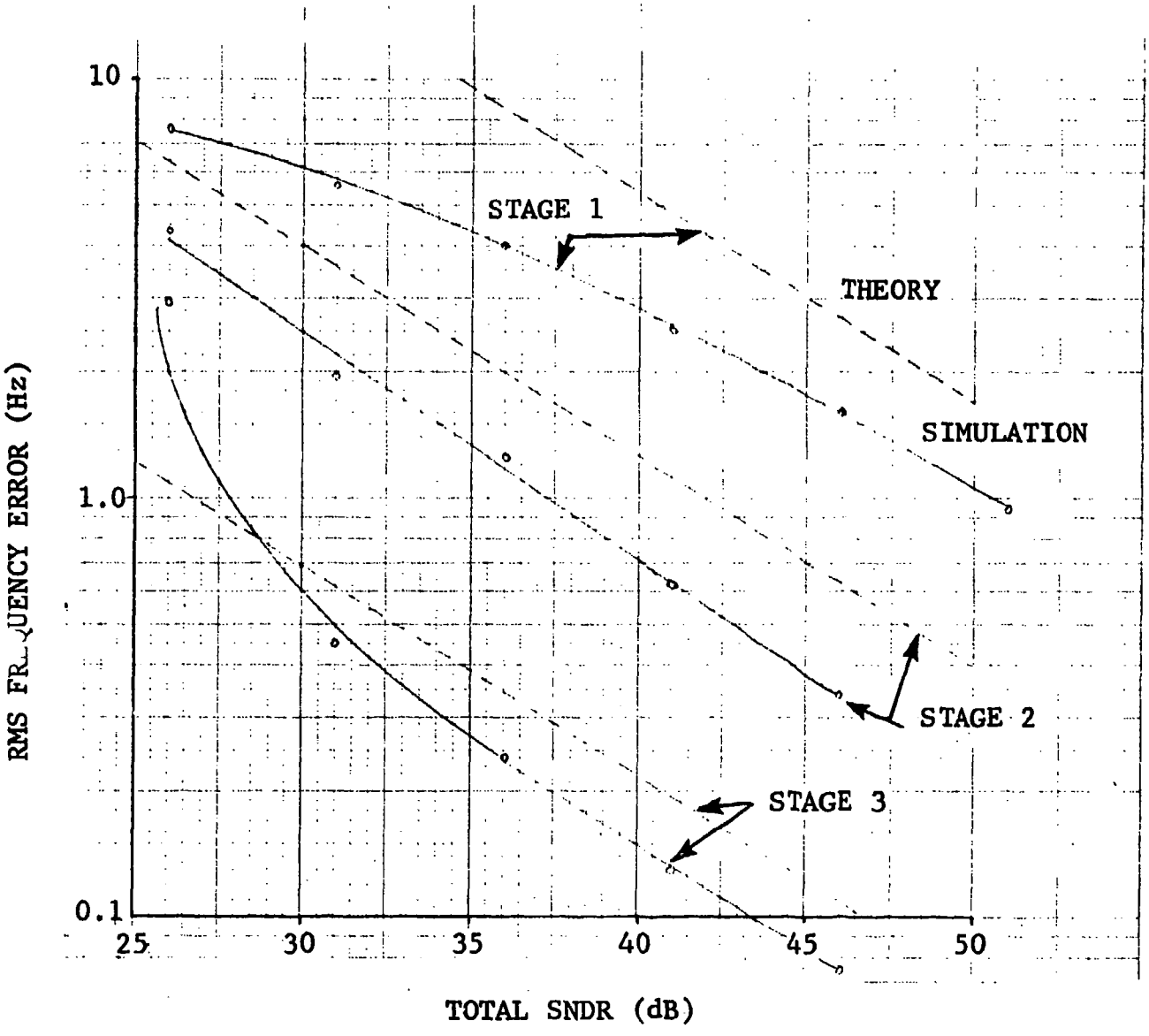

Figure 3.6 Simulated Performance of Three-Stage Doppler Estimator for Six-Path Split Ray Channel

3.2 Frame Sync Detection

3.2.1 Wideband Sync Waveform

The wideband sync waveform consists of a sequence of bipolar bandlimited pulses modulating a carrier:

$$s(t) = \sqrt{2P_T} \sum \gamma_m p(t-m\Delta) e^{j2\pi f_0 t} \qquad (3.27)$$

The frequency f_0 is chosen so that the pulse spectrum falls within the equipment passband, as shown in Figure 3.7. The sequence $\{\gamma_m\}$ consists, in this case, of three repetitions of a length 31 m-sequence, chosen for its desirable autocorrelation properties, as discussed in Section 2.

In the receiver signal processing consists of an approximate matched filter $\hat{p}(t)$, followed by a tapped delay line structure which forms the correlation between the original sequence $\{\gamma_m\}$ and appropriate samples of the output of the matched filter. This structure is shown in Fig. 3.8 for a pulse separation Δ equal to 5 times the sampling interval t_s of the modem; the choice of this parameter will be motivated below. The output of the shift register, available every t_s seconds, is compared over one full period of the m-sequence or 31 Δ seconds, and the largest value is selected. The initiation of this procedure is timed so that the sync waveform is present at the input during the entire interval to avoid end efforts. This is the basis for the receiver's estimate of the arrival time of the signal.

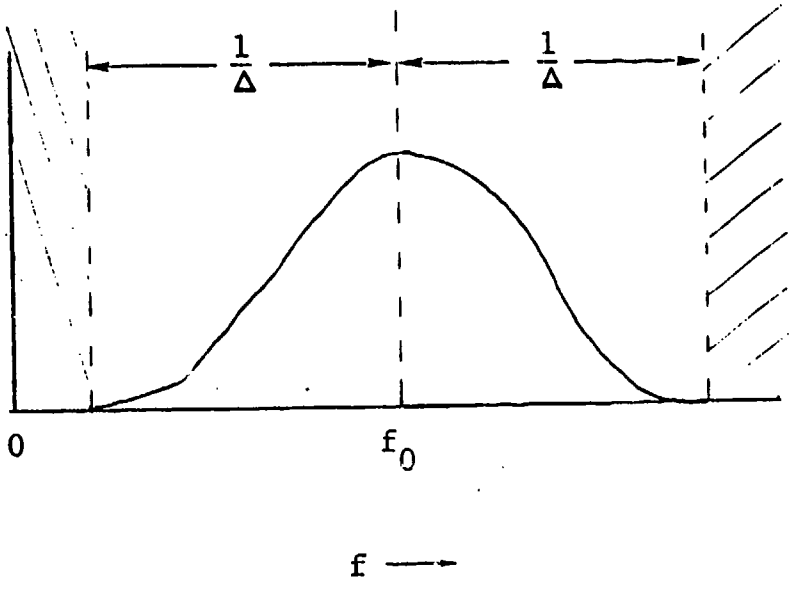

Figure 3.7 Transmitted Pulse Spectrum for Sync Preamble Pulse Train

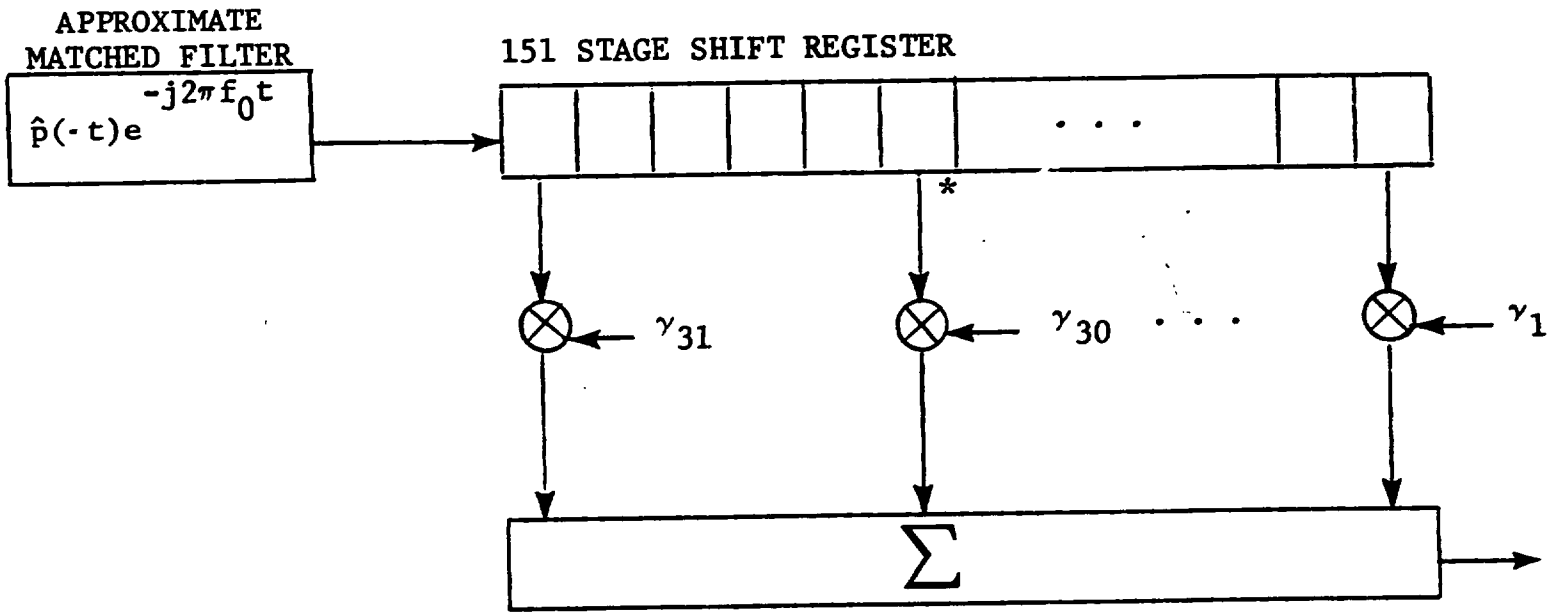

*OUTPUT TAKEN FROM EVERY 5^{th} STAGE.

Figure 3.8 Receiver Signal Processing for Sync Detection

Before processing the sync preamble the receiver has a timing uncertainty of 41.7 ms resulting from the time (t_{WIN}) allowed for signal presence detection. In order that no timing ambiguity result from sync preamble detection, it is desirable that the period of the sync preamble be somewhat greater than this value. For a sampling rate of 3600 sec^{-1}, the 31 bit m-sequence will satisfy this goal if $\Delta \geq 4.84\, t_s$. However, Δ must be an integral multiple of t_s in order for the structure of Fig. 3.8 to be valid. Thus, we are led to the value of $\Delta = 5t_s$ for a preliminary design. Note, however, that more timing accuracy could be obtained with a shorter pulse width ($\Delta = 4t_s$, for example). This would require a longer m-sequence to avoid ambiguity or some entirely different means of resolving the resulting ambiguity.

The transmitted pulse p(t) was selected to have a band-limited "raised-cosine" spectrum and unit power. Thus p(t) and its transform P(f) have the form*

$$p(t) = \sqrt{\frac{4}{3}}\ \frac{\sin 2\pi\left(\frac{t}{\Delta}\right)}{2\pi\left(\frac{t}{\Delta}\right)\left[1-4\left(\frac{t}{\Delta}\right)^2\right]} \tag{3.28}$$

$$P(f) = \begin{cases} \sqrt{\frac{4}{3}}\,\Delta\cos^2\left(\frac{\pi}{2}\,f\Delta\right) & |f| < \frac{1}{\Delta} \\ 0 & \text{elsewhere} \end{cases} \tag{3.29}$$

*This represents a departure from [3.1] where it was proposed that the convolution of p(t) and the receiver pulse matched filter have periodic zeros rather than p(t) as in (3.28). As a consequence, the sidelobe levels of the correlation function are somewhat degraded from ideal. However, p(t) and the matched filter are more readily realized because of their reduced "tails". Resources available did not permit a tradeoff study of the many waveforms available.

This baseband signal is shifted so that it occupies a bandwidth of $2/\Delta$ located within the passband of the HF SSB equipment as shown in Fig. 3.7. For $\Delta = 5t_s$ as established above and $t_s = \frac{1}{3600}$ sec, the required bandwidth is 1440 Hz, easily within the equipment's capability. In selecting the center frequency f_0, it is profitable to consider the receiver signal processing shown in Fig. 3.8. Since the output of the approximate matched filter will be centered at f_0, successive samples at its output will be shifted in phase by $2\pi f_0 t_s$ radians, and successive samples taken from the shift register will be shifted by $5 \cdot 2\pi f_0 t_s$. Combining these samples in the summer to produce a baseband output would ordinarily require multiplying each by the proper multiple of $e^{-j5 \cdot 2\pi f_0 t_s}$ in addition to multiplication by γ_m. However, this can be avoided by choosing f_0 so that this factor is unity; in other words

$$5 \cdot 2\pi f_0 t_s = k(2\pi) \tag{3.30}$$

where k is any integer. Selecting $k = 2$ results in $f_0 = 1440$ Hz so that the transmitted spectrum falls conveniently between 720 and 2160 Hz.

Since p(t) in Eq. (3.28) has infinite duration, some approximation must occur in the receiver pulse matched filter in Fig. 3.2. For the simulations, this filter was formed by truncating p(t) to 9 samples symmetrically located about $t = 0$ and using these

samples as the coefficients of a FIR filter. Since the next samples in either direction are zero, this represents an accurate approximation to p(t). Fig. 3.9 shows the output of the receiver processing (Fig. 3.8) when its input is the noise-free transmitted signal.

In simulating wideband sync detection, a signal model similar to that used in simulating signal presence and Doppler estimation was used. The only significant difference is that the transmitted signal structure is given by Eq. (3.27) rather than by Eq. (3.3); other details of channel structure and sampling are identical.

3.2.2 Simulation Results

Theoretical predictions of sync detection performance are presented in Section 2. To compare simulation with predictions, we have plotted simulation results for a one-path channel and the corresponding (L = 1) prediction in Fig. 3.10. The two curves are in good agreement in spite of the different assumptions made in obtaining them.

First, the theoretical calculation assumes an idealized autocorrelation function having zero width, while the simulation uses the actual autocorrelation function for the bandlimited transmitted waveform, including the effect of the approximate matched filter in the receiver.

Second, simulation of sync detection is performed in sequence following signal presence detection and Doppler estimation. Any error in the final Doppler estimate is present during sync detection, an effect not considered in the theoretical predictions.

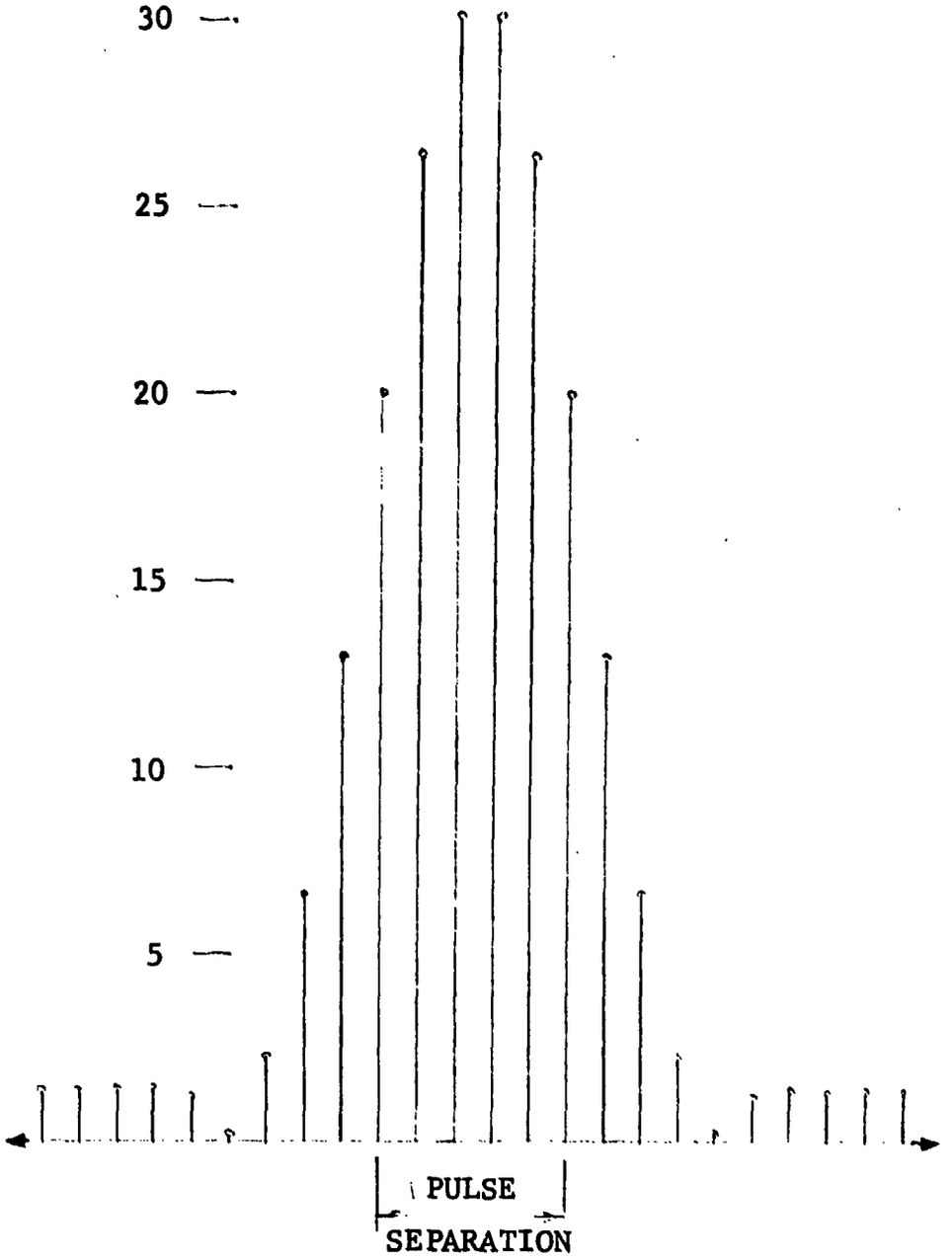

Figure 3.9 Discrete "Autocorrelation" Resulting from Approximate Matched Filter

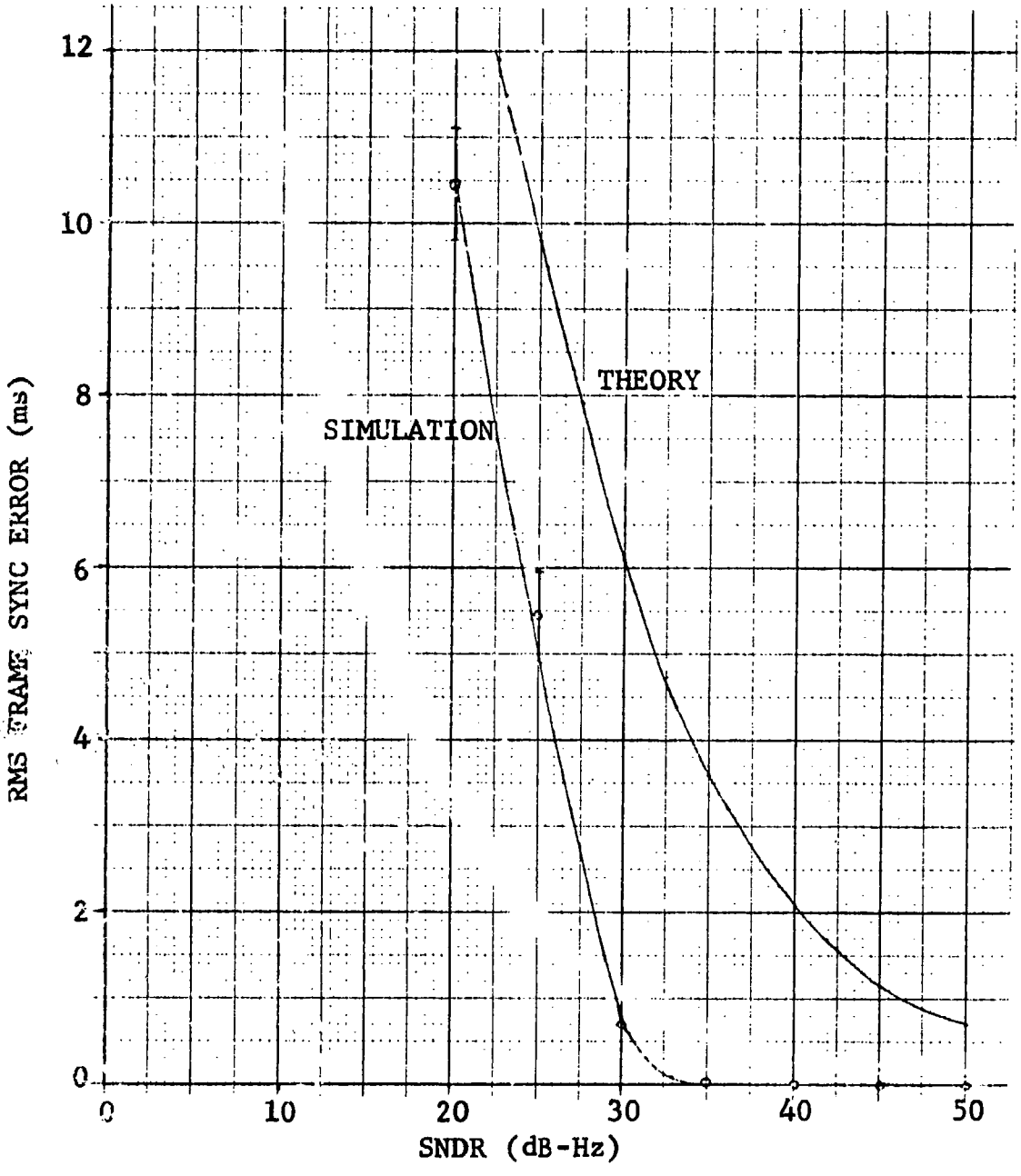

Figure 3.10 Simulated and Theoretical Performance of Wideband Sync Waveform

A third effect occurs when more than one path is present. With multipath spreads of less than 3 ms, interference (constructive or destructive) between paths will occur in the receiver processing. This effect is, of course, modeled in the simulation but not taken into account in the theoretical predictions. For this reason, we will not compare theory and prediction when multiple paths are present.

Simulation results for the two-path and six-path channel models are plotted on Fig. 3.11. When additional paths are included, three effects occur. First, the multipath spread of the channel itself causes a residual error in the sync estimation which will be present even at high SNR. This effect is evident in the two- and six-path curves of Fig. 3.11. Second, the presence of additional independent paths adds diversity which tends to reduce the probability of detection errors due to noise peaks. However, this effect is offset to some degree by the effective loss of power resulting from the fact that the receiver partially resolves the paths. It turns out that, for rms errors larger than the residual, performance in the two-path case is roughly 3 dB worse than in the one-path situation. For the six-path channel, the paths are spread uniformly over a 2.5-ms delay interval. The width of the autocorrelation function is such that six individual paths cannot be resolved by the receiver. However, received energy is smeared over this interval, resulting in further degradation from the two-path case, as shown in Fig. 3.11.

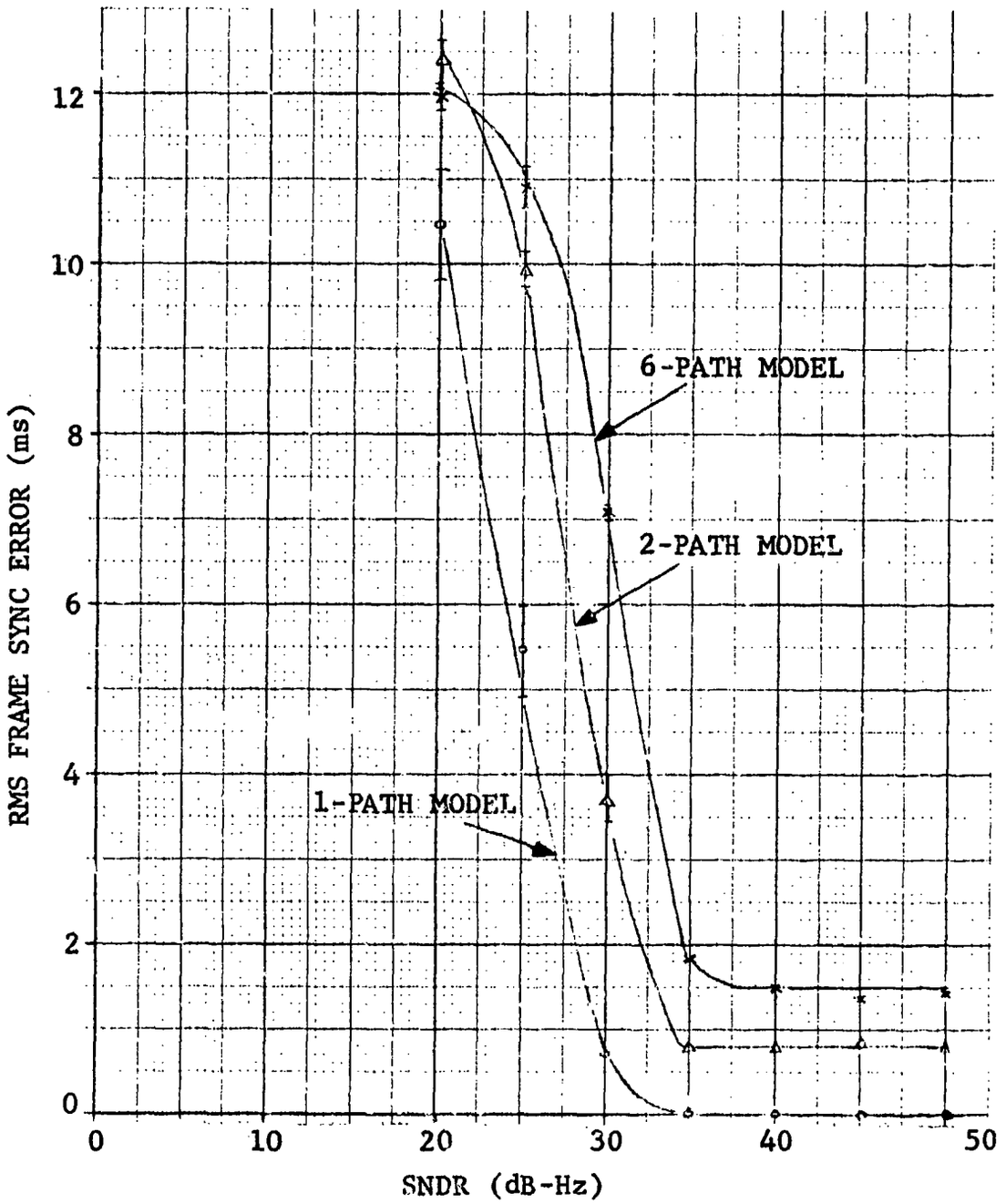

Figure 3.11 Simulated Performance of Wideband Sync Waveform

3.3 Doppler Tracking

3.3.1 Decision-Directed Doppler Tracking

Computer simulations of Doppler tracking in the ANDVT modem were performed. The goals of this effort were to evaluate the suitability of the decision-directed error signal proposed previously [3.1] and to design a suitable loop filter. A block diagram of the tracking loop is shown in Fig. 3.12a. At time pT, the Doppler error signal ϵ_p is derived by the demodulator as a sum of terms obtained from each of the 39 demodulated tones:

$$\epsilon_p = \sum_{k=1}^{39} \epsilon_{kp} \tag{3.31}$$

If S_{kp} denotes the complex output of the k'th tone filter at time pT, the DPSK demodulation process involves forming the product

$$S_{kp}^* S_{k,p-1} = R_{kp} + jQ_{kp} \tag{3.32}$$

The signs of the real and imaginary parts R_{kp} and Q_{kp} give the decisions on the transmitted data. In terms of these quantities, the Doppler error signal for this tone is given by

$$\epsilon_{kp} = (|Q_{kp}| - |R_{kp}|) \operatorname{sgn}(R_{kp}) \operatorname{sgn}(Q_{kp}) \tag{3.33}$$

It has been shown earlier [3.1] that with slow fading and in the absence of noise

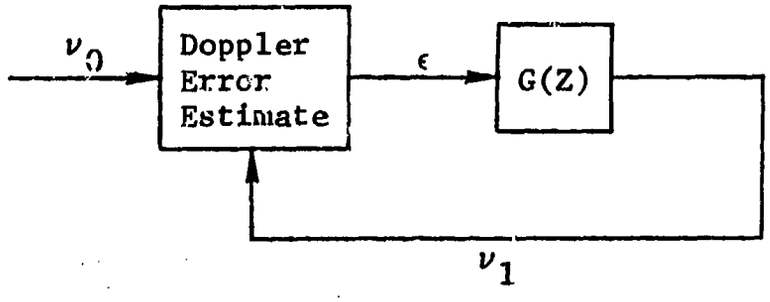

a) Doppler Tracking Loop

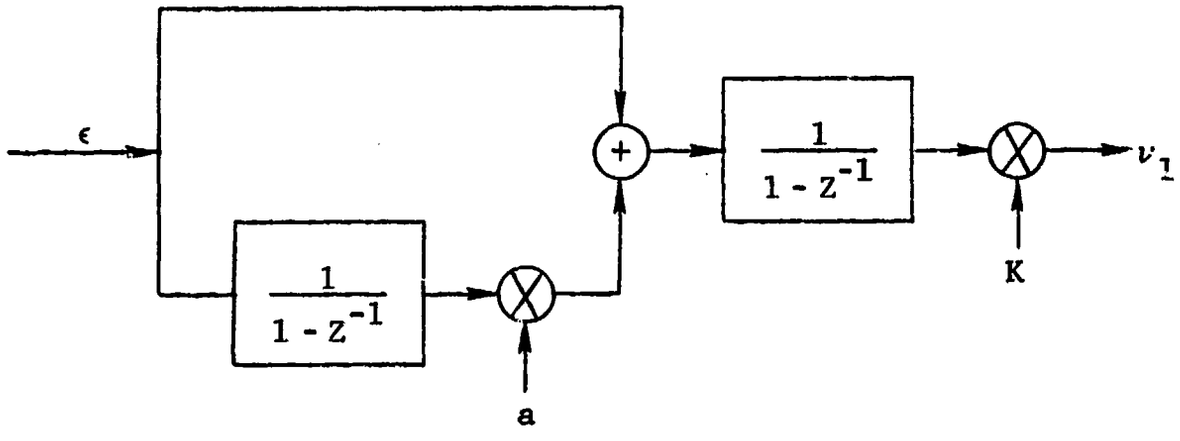

b) Second-Order Loop Filter G(Z)

Figure 3.12 Block Diagram of Doppler Tracking Loop

$$\epsilon_k = \sqrt{2}\ |T(kF,pT)|\ |T[kF,(p-1)T]|\ \sin 2\pi T(\nu_0 - \nu_1) \qquad (3.34)$$

where T(f,t) is the time-varying transfer function of the channel.

The design goal has been operation of the tracking loop in the presence of a 3.5 Hz/sec frequency offset. A second-order loop filter (see Fig. 3.12b) was selected to give zero steady-state tracking error for a ramp input. Additional goals which have been satisfied are:

(1) Successful tracking at the initiation of a 3.5 Hz/sec ramp in frequency

(2) Successful tracking at the initiation of a 1 Hz/sec step in frequency

Figure 3.13 shows acquisition of a 3.5 Hz/sec ramp (for a noise-free, nonfading signal) for loop constants K = 0.05 and a = 0.03. Figure 3.14 shows the acquisition of a 1-Hz frequency step under these same conditions. These values of loop constants a and K represent a compromise; increasing loop bandwidth would improve transient response but increase susceptibility to noise.

Since Doppler tracking is a sampled data process operating at the frame rate, the channel model used for simulating signal presence detection, Doppler estimation, and sync detection would be inappropriate. The channel model used for simulating long-term Doppler tracking has been described earlier [3.1, Appendix B]. The only modification necessary has been the inclusion of the frequency ramp representing the Doppler offset.

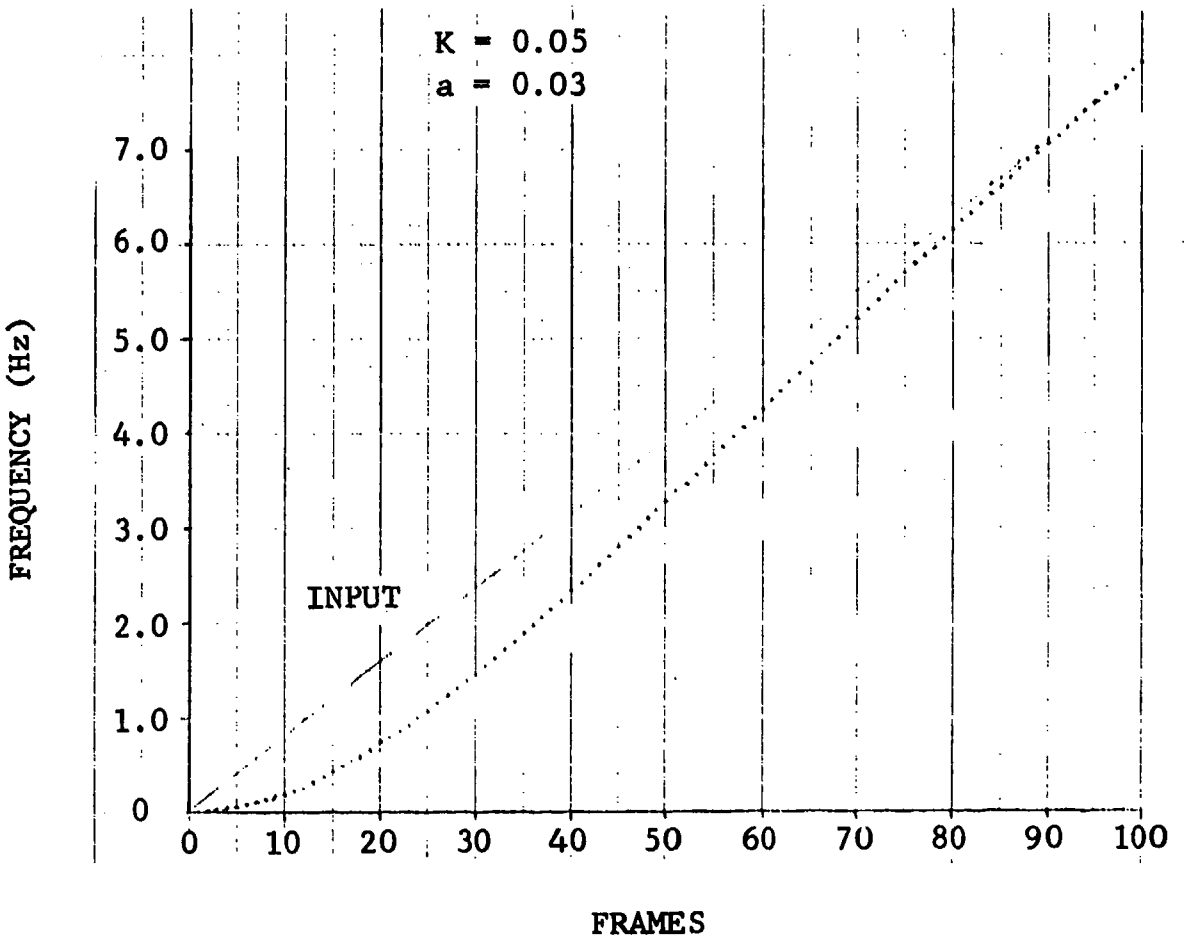

Figure 3.13 Response to a Ramp in Frequency

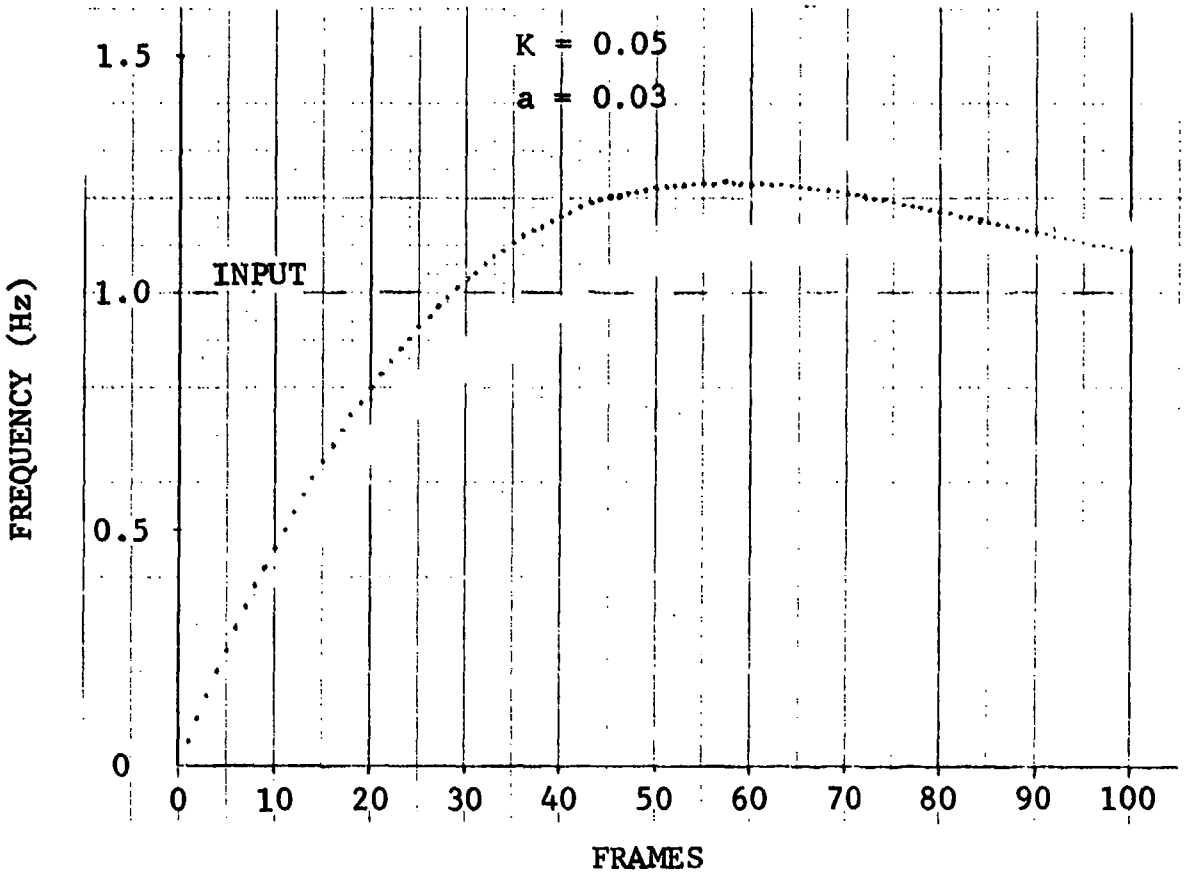

Figure 3.14 Response to a Step in Frequency

3.3.2 Simulation Results

To provide a comparison for the decision-feedback tracking simulation results, some simulations of conventional single-tone tracking have been carried out. In this scheme an unmodulated tone of equal amplitude is added to the ANDVT format at 562.5 Hz. At the receiver this tone is selected by a bandpass filter and passed through a discriminator to generate the error signal for the Doppler tracking loop. The structure and bandwidth of this loop were the same as that used for decision feedback tracking so that the single-tone tracking simulation differs only in the error signal used. In the single-tone tracking scheme the bandwidth of the bandpass filter together with the received noise level establish the noise power at the input to the discriminator. As signal fading occurs, the instantaneous signal-to-noise ratio of the discriminator will fall below threshold, causing an error signal consisting primarily of noise to be supplied to the tracking loop until the received signal level increases again. Clearly, the bandpass filter should be made as narrow as possible to minimize this effect.

We first consider simulation results for the two-path channel. Shown in Fig. 3.15 are rms tracking errors as a function of E_b/N_0 for bandwidths of $\pm$ 22.22 and $\pm$ 44.44 Hz and for the decision-directed scheme. Table 3-1 shows the values of E_b/N_0 below which loss of lock occurs with each technique. Together with Fig. 3.15, these results indicate that, of the three systems being compared, decision-directed tracking gives the smallest tracking error, while single-tone tracking with a bandwidth of $\pm$ 22.22 Hz gives the lowest threshold.

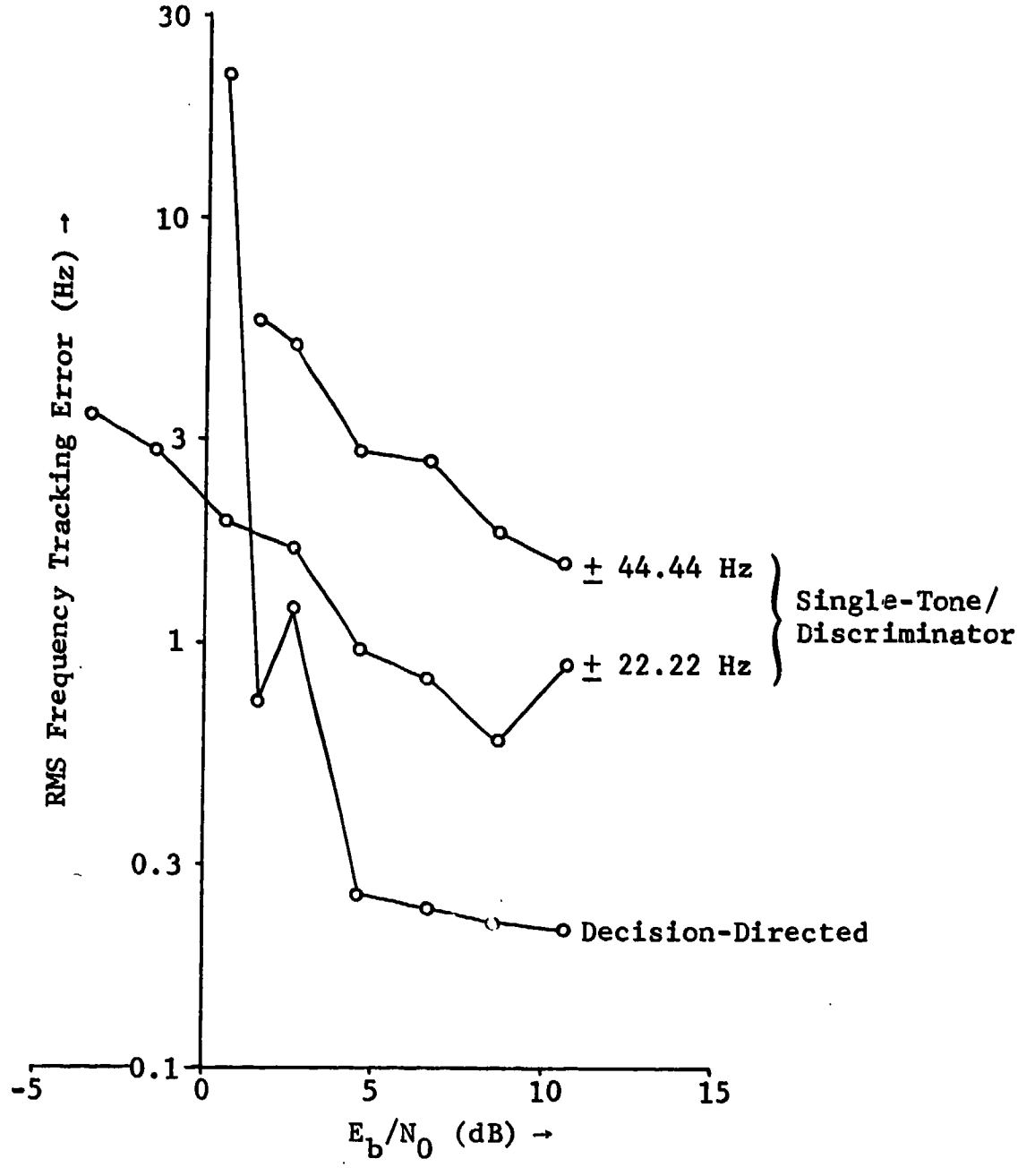

Doppler = 3.5 Hz/sec

2-Path Channel: Multipath Spread = 1 ms
Double-Sided Doppler Bandwidth = 1 Hz

Loop Constants: K = 0.05, a = 0.03

Figure 3.15 Tracking Performance of Various Doppler Correction Loops

TABLE 3-1

TRACKING LIMITS FOR DIFFERENT LOOP DESIGNS;
TWO-PATH CHANNEL

Tracking Method	Smallest E_b/N_0 for Which Loop is Locked
Decision-Directed	0.6 dB
Single-Tone/Discriminator	
Bandwidth = ± 22.22 Hz	-3.4 dB
Bandwidth = ± 44.44 Hz	1.6 dB

The effect of these tracking loops on error rate is shown in Fig. 3.16. Performance of the decision-directed technique falls on top of the reference curve at all E_b/N_0 for which the loop is in lock. The same is true of single-tone/discriminator tracking with a bandwidth of $\pm$ 22.22 Hz. For a bandwidth of $\pm$ 44.44 Hz the curve shown in Fig. 3.16 was obtained, showing a performance loss of 1 - 2 dB. It should be noted that in the latter simulation for the single-tone/discriminator no correlation was assumed between fading of the Doppler tone and fading of the data tones. The effect of this assumption on the results is expected to be small.

We next consider simulation results for the six-path channel. Shown in Fig. 3.17 are rms tracking errors as a function of E_b/N_0 for bandwidths of $\pm$ 22.22 and $\pm$ 44.44 Hz and for the decision-directed scheme. Table 3-2 shows the limiting values of E_b/N_0 below which successful tracking is not possible. Together with Fig. 3.17 these results indicate that, for the six-path channel, decision-directed tracking is superior to single-tone/discriminator tracking in both threshold and rms tracking error.

The effect of these tracking loops on error rate is shown in Fig. 3.18. The curve for discriminator tracking with a bandwidth of $\pm$ 22.22 Hz falls on top of the reference curve at all E_b/N_0 for which the loop is in lock. The same is true of decision-directed tracking except for values of E_b/N_0 just above threshold. With discriminator tracking in a $\pm$ 44.44 Hz bandwidth, there is significant degradation in error rate at all E_b/N_0.

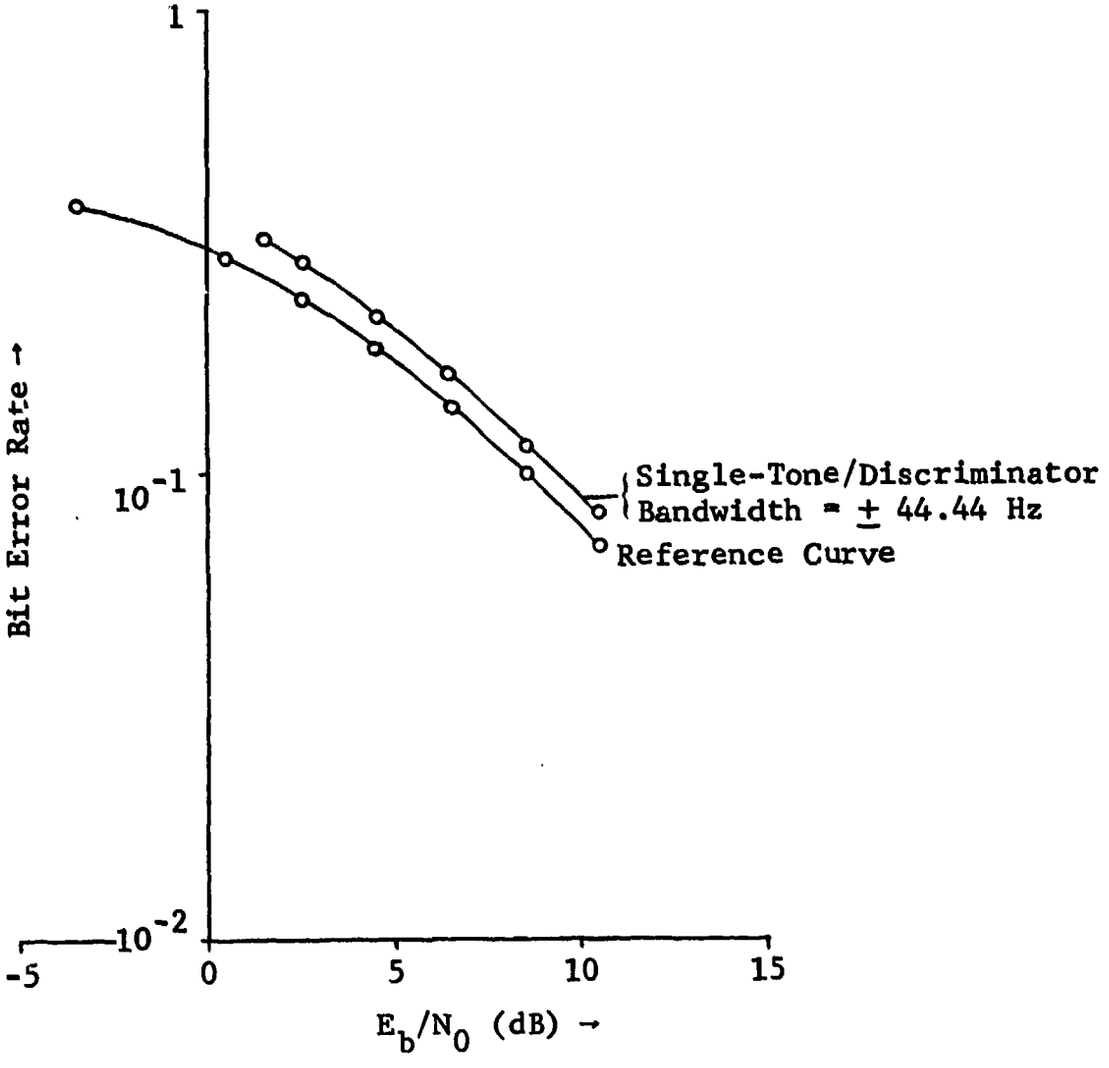

Doppler: 3.5 Hz/sec

Two Path Channel: Multipath Spread = 1 ms
Double-Sided Doppler
Bandwidth = 1 Hz

Loop Constants: K = 0.05, a = 0.03

Figure 3.16 Simulated Raw Bit Error Rates showing Effect of Closed Loop Frequency Tracking

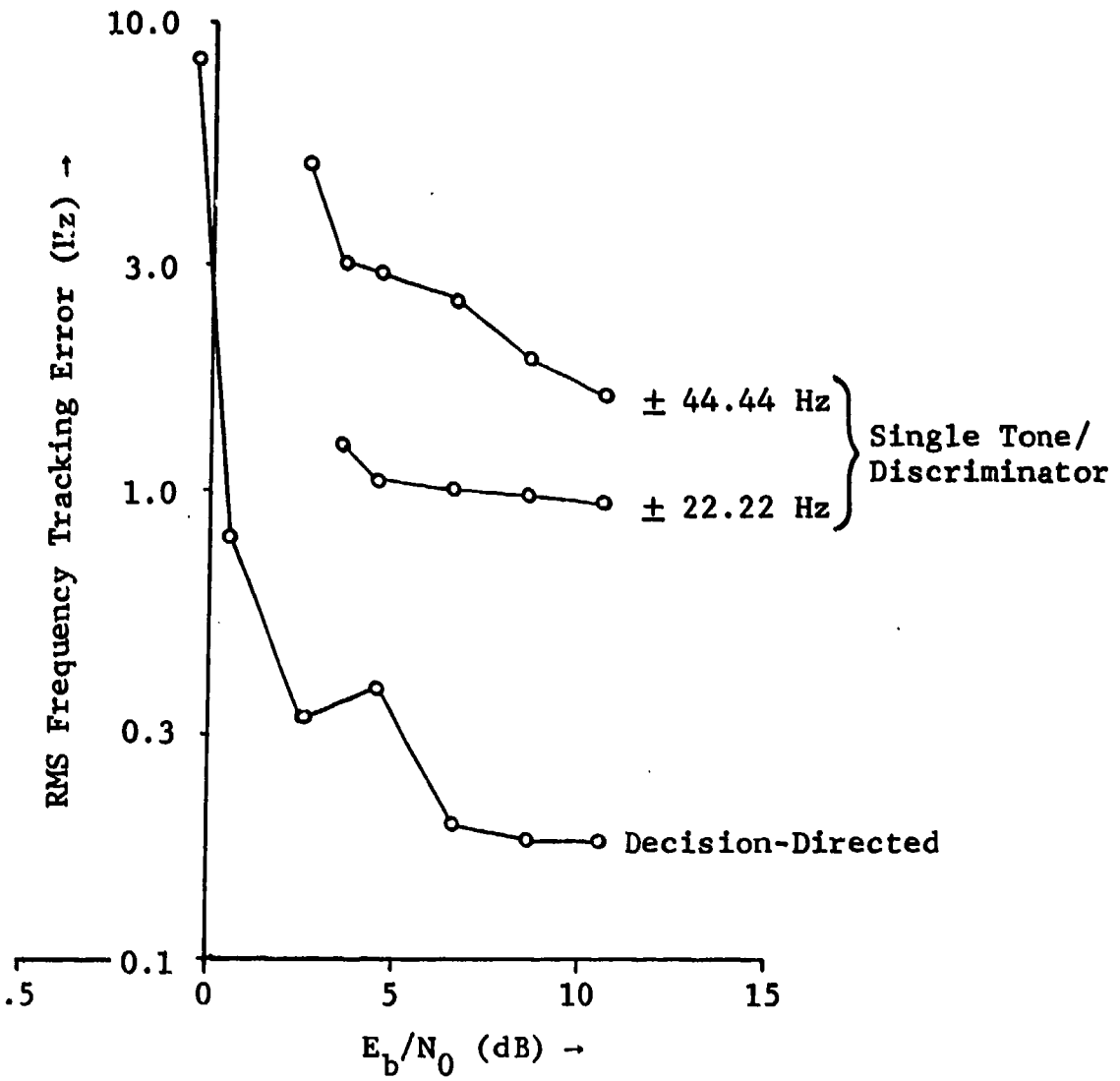

Doppler = 3.5 Hz/sec

Six-Path Split Ray Channel: Multipath Spread = 26 msec

Double-Sided Doppler
Bandwidth = 1.5 Hz

Loop Constants: K = 0.05, a = 0.03

Figure 3.17 Tracking Performance of Various Doppler Correction Loops

TABLE 3-2

TRACKING LIMITS FOR DIFFERENT LOOP DESIGNS
SIX-PATH CHANNEL MODEL

Tracking Method	Smallest E_b/N_0 for Which Loop is Locked
Decision-Directed	-0.4 dB
Single-Tone/Discriminator	
Bandwidth = ± 22.22 Hz	3.6 dB
Bandwidth = ± 44.44 Hz	2.6 dB

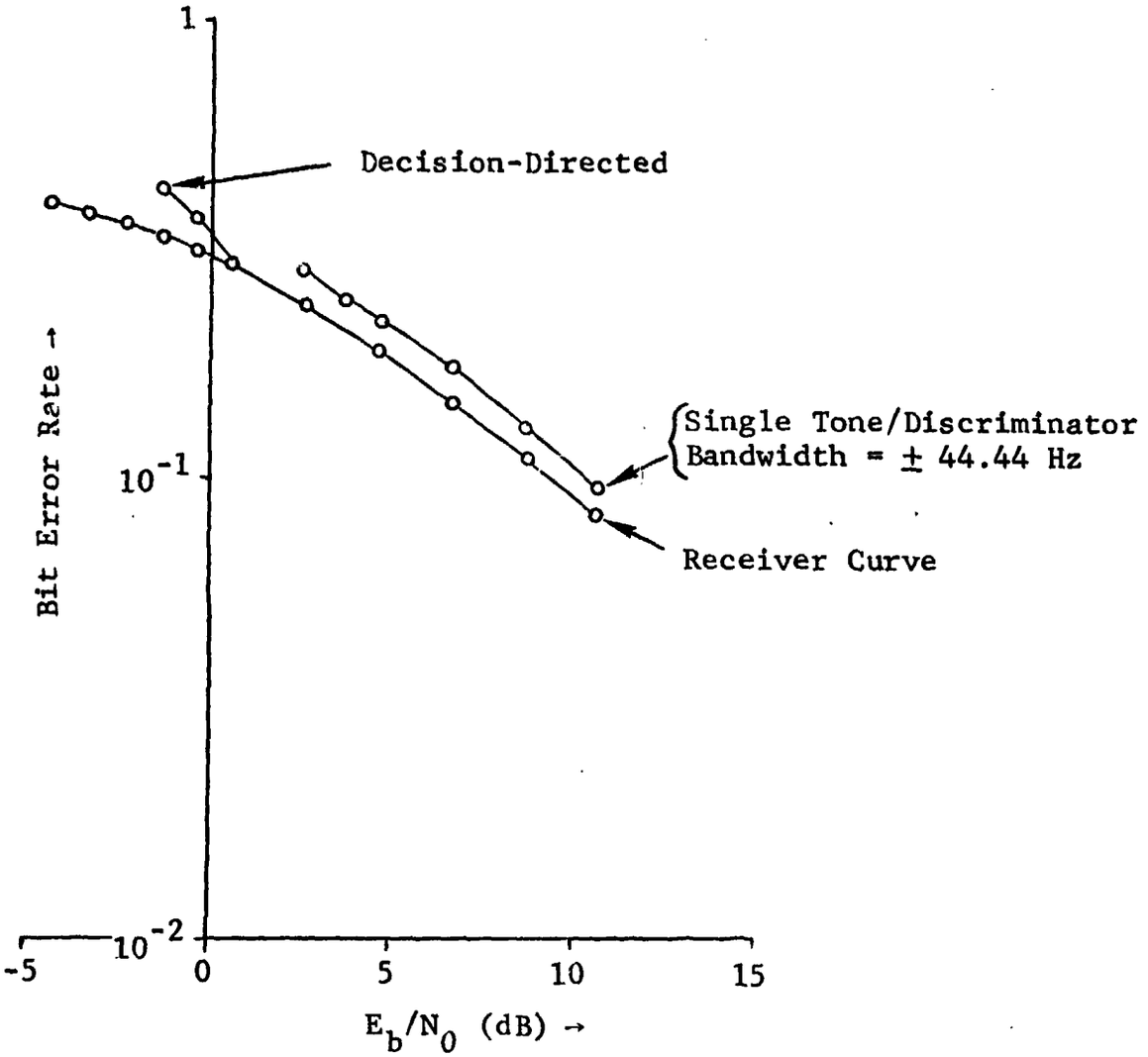

Doppler: 3.5 Hz/sec

Six-Path Split Ray Channel: Multipath Spread = 26 msec

Double-Sided Doppler Bandwidth = 1.5 Hz

Loop Constants: K = 0.05, a = 0.03

Figure 3.18 Simulated Raw Bit Error Rates Showing Effect of Closed Loop Frequency Tracking

REFERENCES

[3.1] D. Chase, et al., "HF Modem Design for the Advanced Narrowband Digital Voice Terminal (ANDVT)," November 1977, Final Report on Contract N00039-77-C-0190.

SECTION 4

CODING AND MODULATION FORMAT FOR THE KG SYNCHRONIZATION SEQUENCE

4.1 Introduction

The results obtained during the previous effort indicated that the (250,100;46), (252,128;37), and (250,150;27) BCH codes, combined with eighth-order diversity, represent attractive candidates for providing the COMSEC synchronization. In addition to these long BCH codes, it is of interest to consider the use of several (24,12;8) Golay codewords to protect the KG synchronization sequence. For example, if ten Golay codewords are used with eighth-order diversity, one may view the overall code as a (240,120), which may be compared to long BCH codes. In this section we first compare these coding approaches by using analysis techniques which are based on a Rayleigh fading channel model with code symbols assumed to be independent. These theoretical results are shown to be somewhat optimistic when compared to simulated results obtained for the two-path and six-path HF models used throughout this project. In fact, the theoretical results, given in Section 4.2, indicate that a long BCH codeword with just hard decoding is somewhat superior to the use of multiple Golay codes with soft decoding. The simulation results, given in Section 4.3, which include the correlation between code symbols, renders the multiple Golay codes with soft decoding superior to the long BCH codes decoded with just binary information. The recommended coding techniques for the KG synchronization sequence is also given in Section 4.3. It should be pointed out at the onset of this section that both the multiple Golay coding approach

and the long BCH codes are attractive choices since these codes provide performance capabilities such that KG synchronization can be achieved even when the channel conditions are such that the quality of the digitized voice would be unacceptable.

4.2 Theoretical Evaluations Based on the Independent Rayleigh Fading Model

We have begun this investigation by obtaining the performance of four candidate KG codes for the COMSEC synchronization. Any remaining code bits with a code block may be used for net control. The codes are a BCH (250,100;46) code, a BCH (252,128;37) code, a BCH (250,150;27) code, and ten (24,12;8) Golay codewords, which can be viewed as a (240,120) code.

Both hard decoding and soft decoding are investigated. The results are compared on the basis of both decoded bit error rate and block error rate. In addition, both slow and fast fading cases are considered. The results are plotted in Figures 4.1 through 4.8.

In addition to comparing performance, it is of interest to modify the processing time study for Contract N00039-77-C-0190 to provide results for the (252,128) code and (250,150) code as well as results already obtained for the (250,100) code. The time required for hard-decision decoding of the (24,12) Golay code has also been isolated from the study of the processing time for a 16-iteration soft-decision decoding of the (24,12) extended Golay code.

Table 4-1 summarizes the processing times for the various codes and algorithms. The processing time is given in terms of the t_{ALU} and t_{memory} parameters which have been described in the previous final report. A value of 350 ns is assumed in Table 4-1 to provide

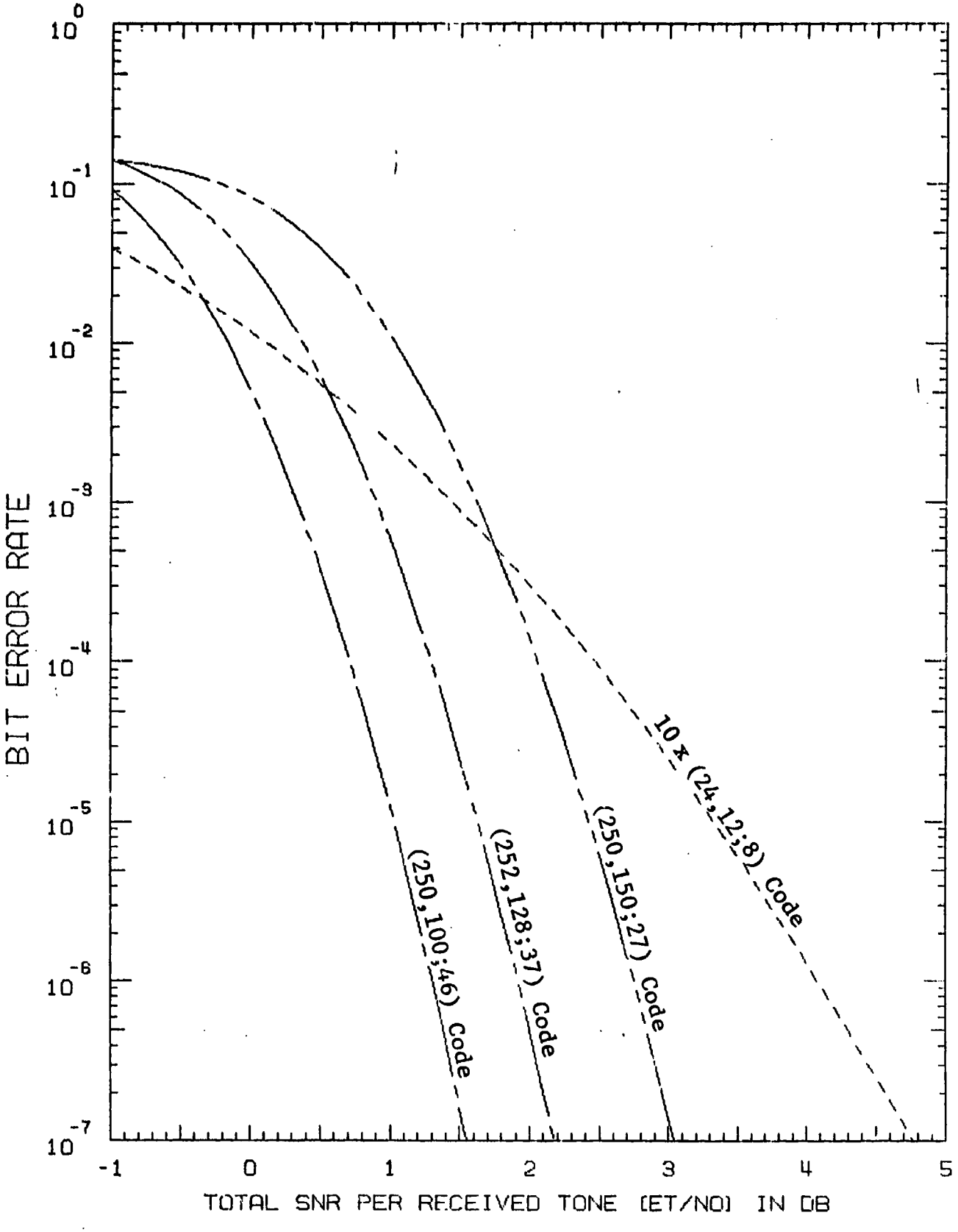

Figure 4.1 Hard-Decoded Bit Error Rates of KG Codes over a Slowly Fading HF Channel with 4-Phase DPSK Modulation using Eighth-Order Post-Detection Equal Gain Diversity Combining

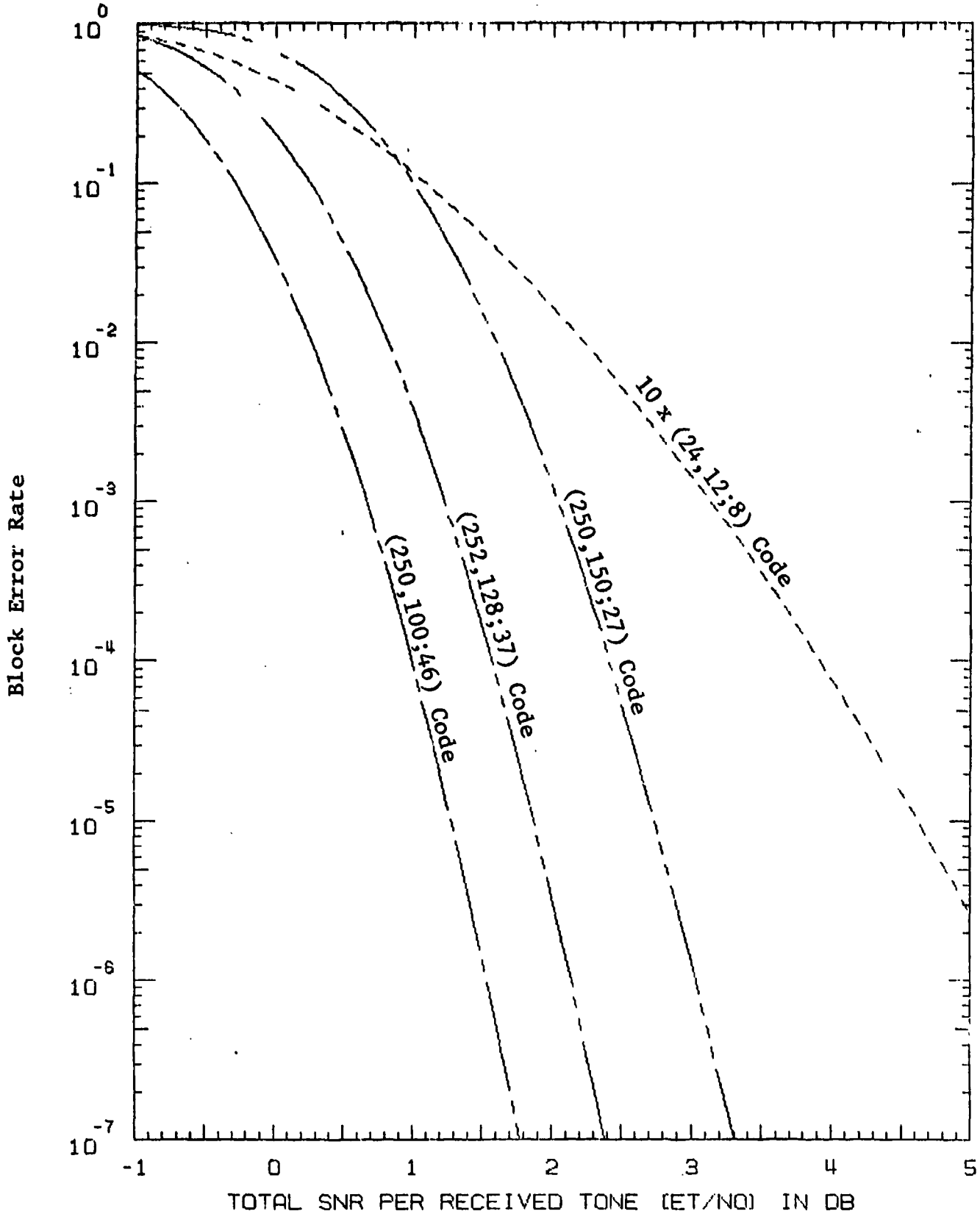

Figure 4.2 Hard-Decoded Block Error Rates of KG Codes over a Slowly Fading HF Channel with 4-Phase DPSK Modulation using Eighth-Order Post-Detection Equal Gain Diversity Combining

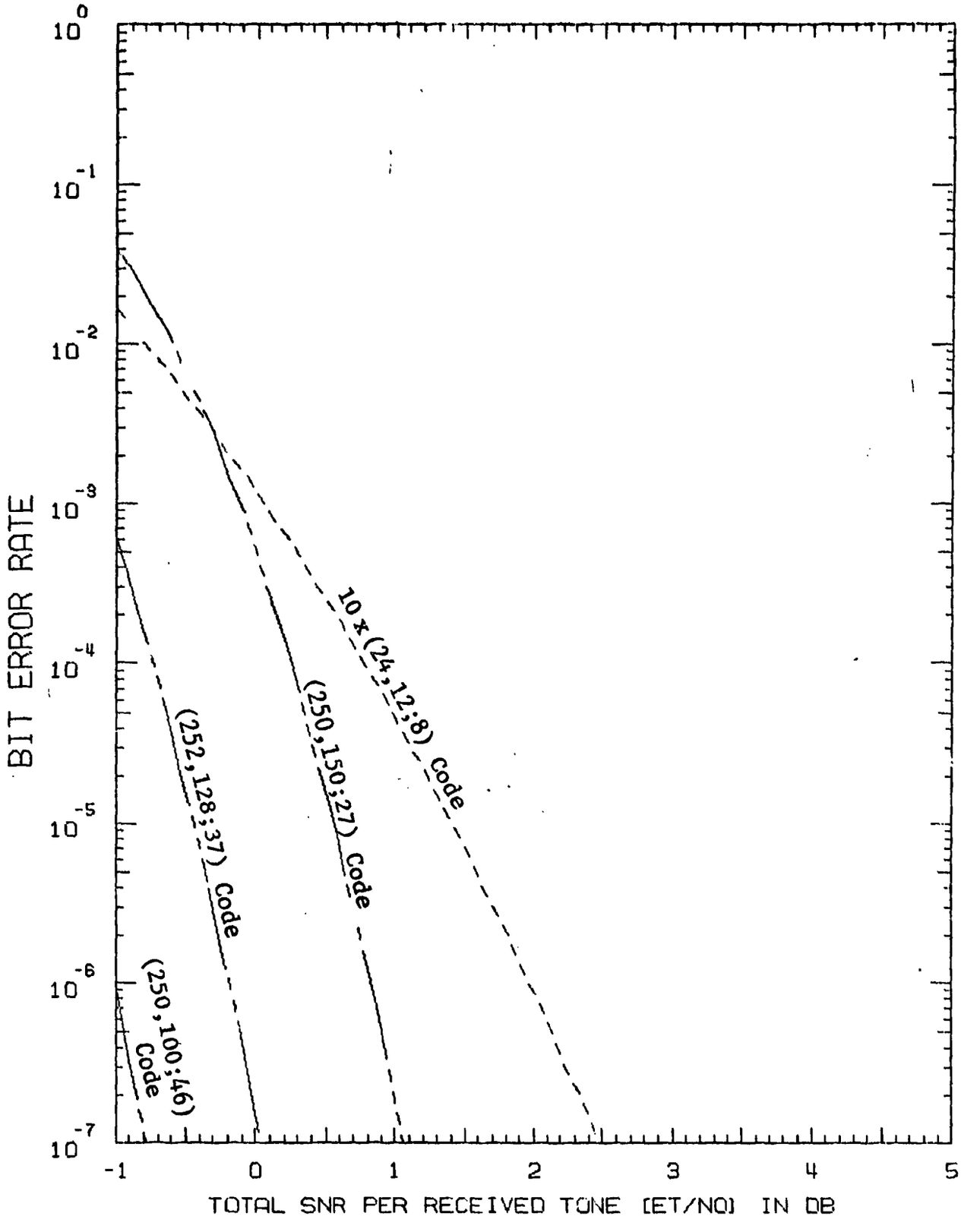

Figure 4.3 Estimated Soft-Decoded Bit Error Rates of KG Codes over a Slowly Fading HF Channel with 4-Phase DPSK Modulation using Eighth-Order Post-Detection Equal Gain Diversity Combining

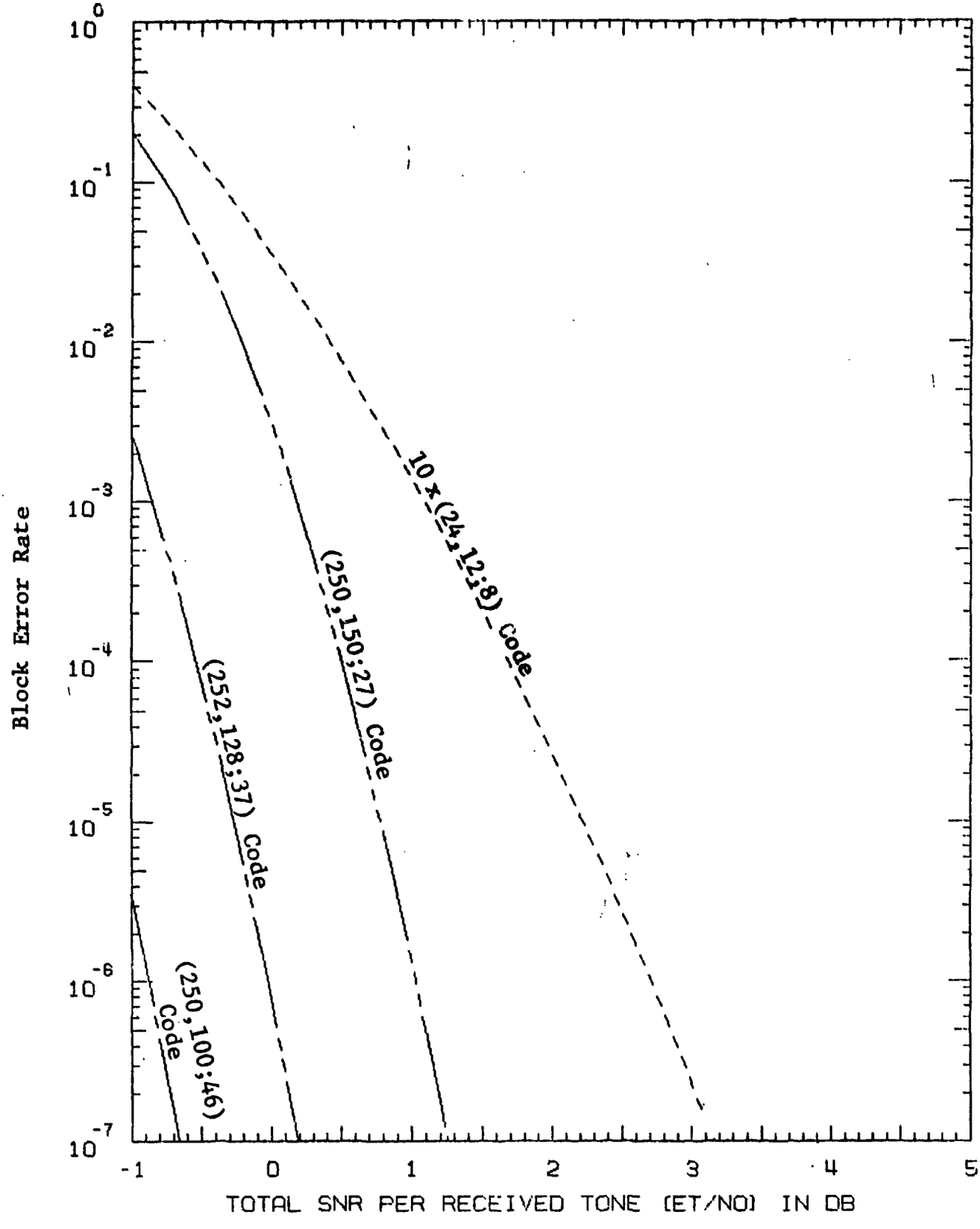

Figure 4.4 Estimated Soft-Decoded Block Error Rates of KG Codes over a Slowly Fading HF Channel with 4-Phase DPSK Modulation using Eighth-Order Post-Detection Equal Gain Diversity Combining

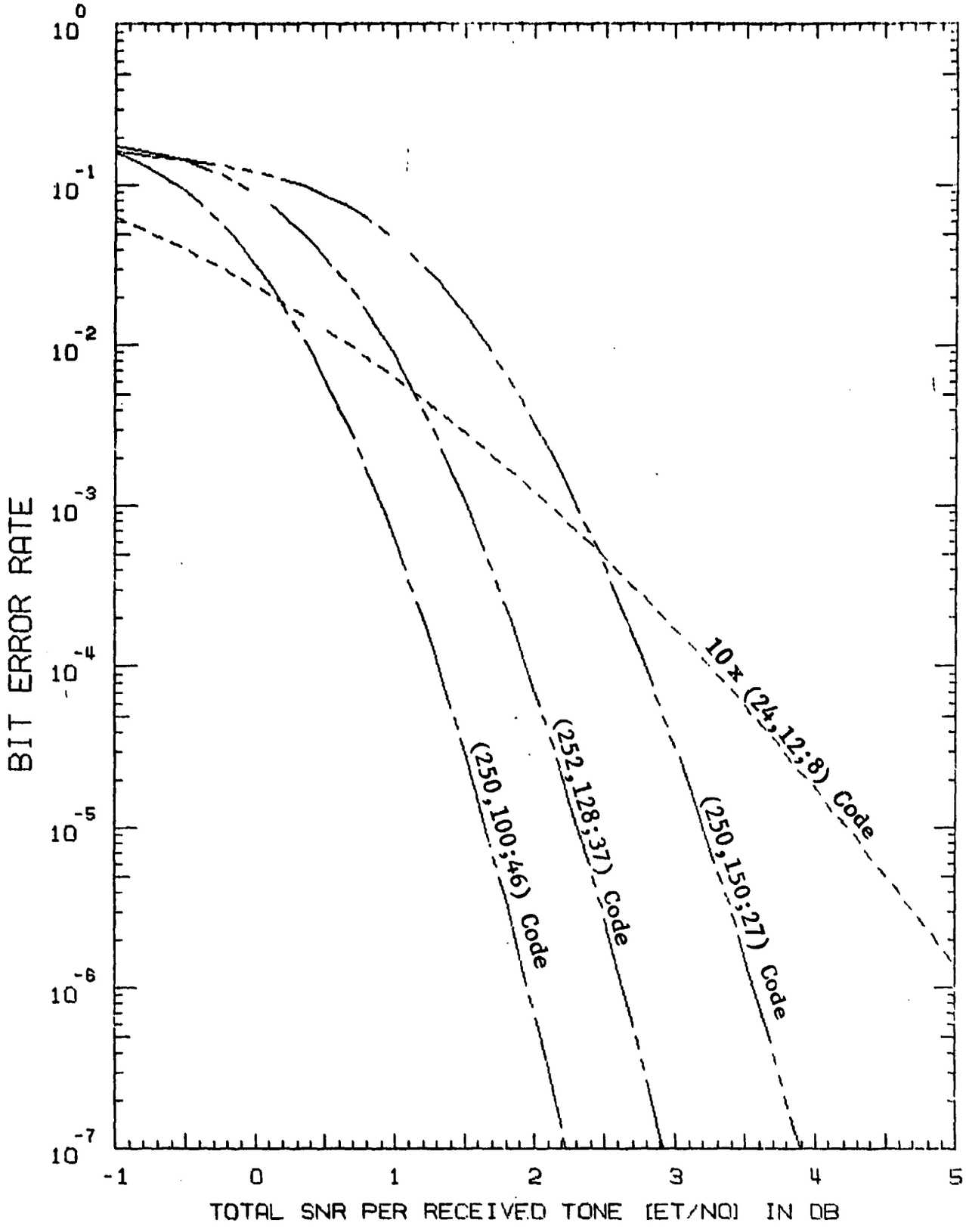

Figure 4.5 Hard-Decoded Bit Error Rates of KG Codes over a Time-Varying HF Channel with 4-Phase DPSK Modulation (Frame Rate = 44.44 Frames/Second, B = 5 Hz) using Eighth-Order Post-Detection Equal Gain Diversity Combining

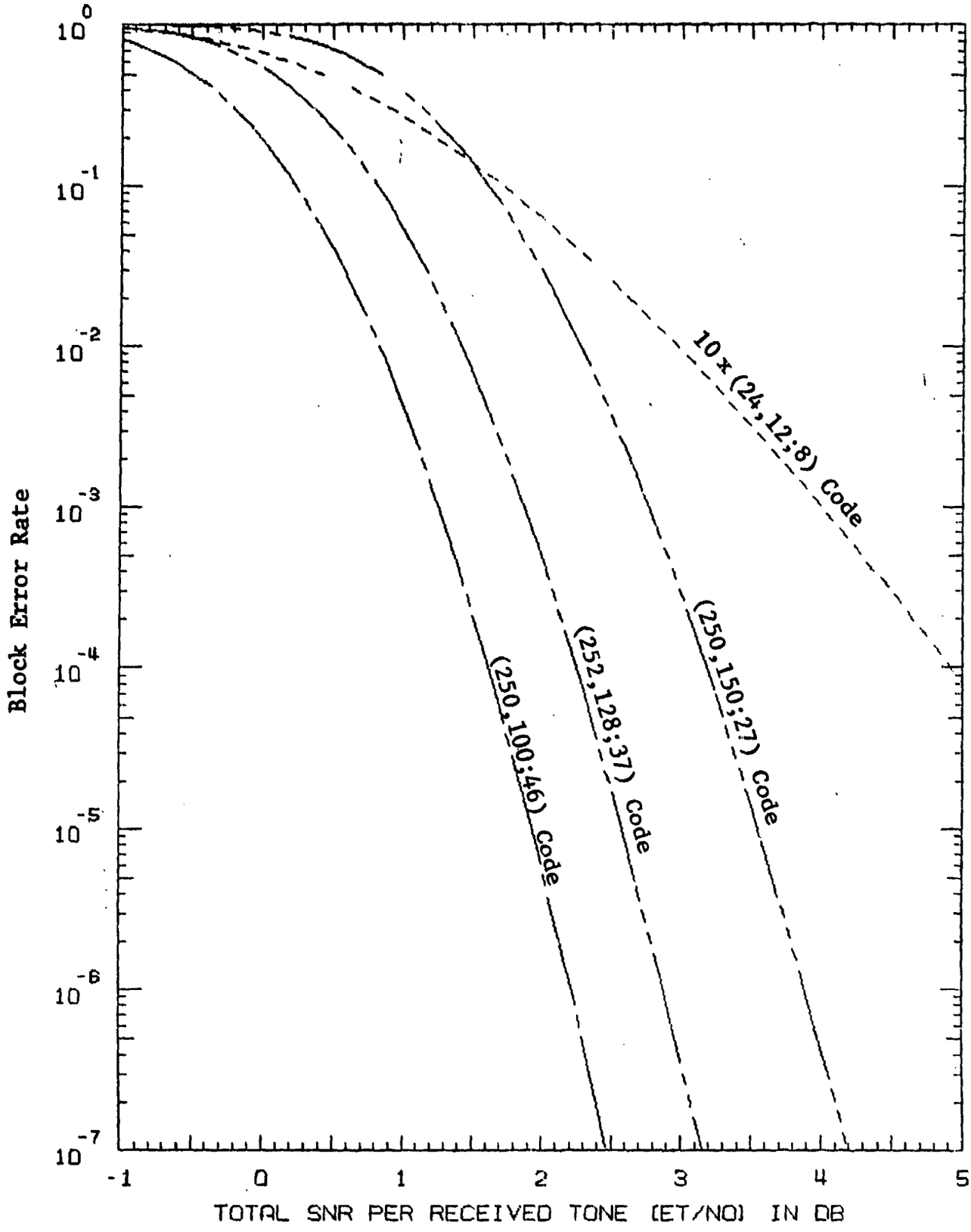

Figure 4.6 Hard-Decoded Block Error Rates of KG Codes over a Time-Varying HF Channel with 4-Phase DPSK Modulation (Frame Rate = 44.44 Frames/Second, B = 5 Hz) using Eighth-Order Post-Detection Equal Gain Diversity Combining

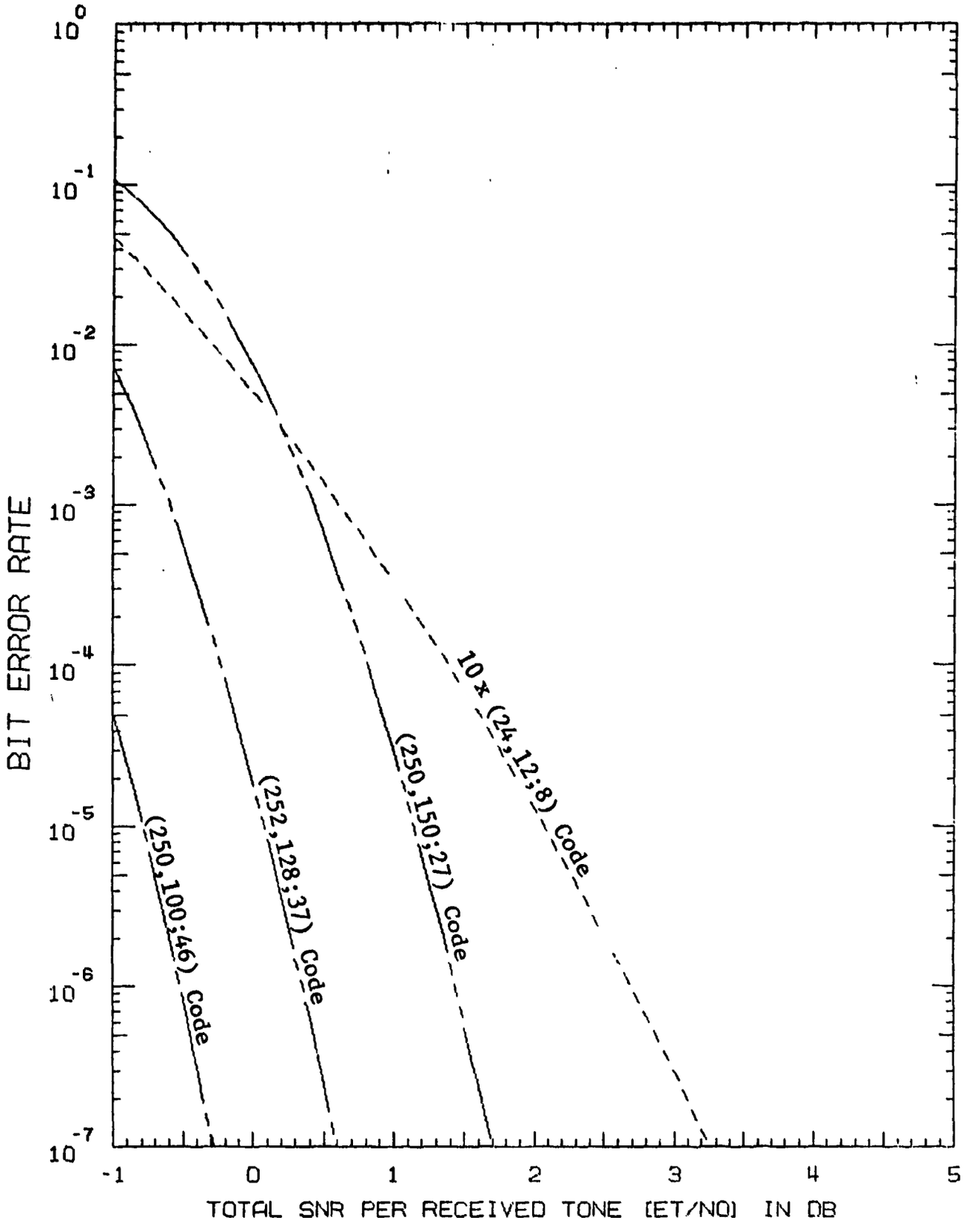

Figure 4.7 Estimated Soft-Decoded Bit Error Rates of KG Codes over a Time-Varying HF Channel with 4-Phase DPSK Modulation (Frame Rate = 44.44 Frames/Second, B = 5 Hz) using Eighth-Order Post-Detection Equal Gain Diversity Combining

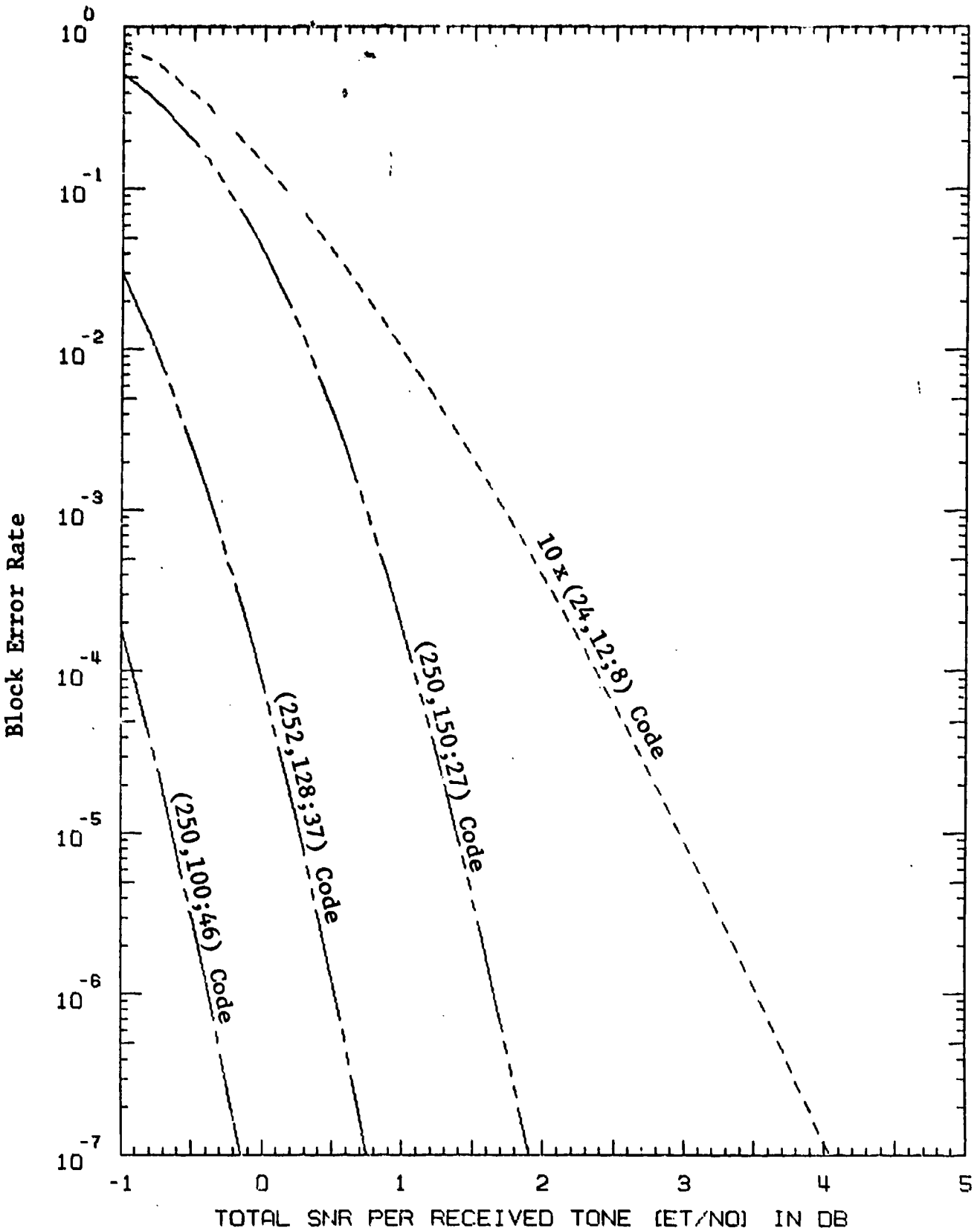

Figure 4.8 Estimated Soft-Decoded Block Error Rates of KG Codes over a Time-Varying HF Channel with 4-Phase DPSK Modulation (Frame Rate = 44.44 Frames/Second, B = 5 Hz) using Eighth-Order Post-Detection Equal Gain Diversity Combining

TABLE 4-1

DECODER PROCESSING TIMES

Code and Algorithm	Processing Time	Estimate for $t = t_{ALU} = 350$ ns
(249,101;45) BCH (Hard Decode)	$104837\ t_{ALU} + 36136\ t_{memory}$	49.34 ms
(252,128;37) BCH (Hard Decode)	$84292\ t_{ALU} + 28678\ t_{memory}$	39.54 ms
(250,150;27) BCH (Hard Decode)	$58504\ t_{ALU} + 19546\ t_{memory}$	27.32 ms
10 Codewords using a (24,12) Extended Golay Code (16 Iteration Soft Decode)	$134560\ t_{ALU} + 28500\ t_{memory}$	56.13 ms
10 Codewords using a (24,12) Extended Golay Code (Hard Decode)	$6480\ t_{ALU} + 530\ t_{memory}$	2.45 ms

an approximate timing estimate. These processing times also favor the use of a long BCH code with hard decoding, insread of the use of a multiple soft-decoded Golay coding approach.

However, before a firm recommendation can be made, a complete simulation over realistic channel models is necessary. These results are given in the following section.

4.3 Simulation Results for the Two-Path and Six-Path Channel Model

In this section a detailed simulation is conducted for the (252,128;37) BCH code and 11 (24,12;8) Golay codes. Thus, the BCH code protects 128 bits which may be used of KG synchronization net control, and the 11 Golay codes protect 132 bits.*

Transmission of the encoded sequence is to be accomplished by a 39 parallel tone modem using 4-phase DPSK modulation. Seventy-eight bits of data are relayed during each 22.5-ms frame. Since the block length of the encoded sequence, N, must be greater or equal to 128, more than one frame will be required to transmit each data sequence. For the purposes of providing time diversity, each encoded sequence will be repeated L times. The number of frames required to transmit the multiple repeats of the encoded sequence is simply $\left\lceil \frac{N \cdot L}{78} \right\rceil$ where $\lceil . \rceil$ denotes the ceiling operator. The receiver uses equal gain predetection combining to assemble the results of the L sequence transmissions.

A block code selected for the encoding process must satisfy the dual criteria of excellent performance at the signal-to-noise ratios of interest and relatively simple encoding and decoding algorithms.

---

*A simulation of this type slightly favors the BCH code since fewer bits are protected. However, it is expected that the results for the Golay codes, when only 120 bits are protected, will be quite similar to these simulated results.

One of the protection schemes of interest incorporates a (252,128;37) BCH code. The bits representing the first transmission of the encoded KG synchronization sequences are placed on the tone array as diagrammed in Figure 4.9. All subsequent repetitions of the KG codeword are placed on the tone array in packed format. An example of the packing for the second KG codeword occurs during frame i+3 in Figure 4.9.

Each of the L repetitions of the j^{th} ($1 \leq j \leq N$) codeword bit will be combined before demodulation. In order to benefit from the available inband diversity, the L bit repetitions should appear to be evenly dispersed across the tone array. An example of this dispersal for the modulation format of Figure 4.9 is depicted in Figure 4.10. Tone placements of the first codeword bit for a maximum of eight repetitions are easily discerned. Tone positions of the j^{th} bit can be easily determined by right-circularly-shifting the tone array index in Figure 4.10 by j-1.

An alternate protection scheme requires the use of 11 (24,12;8) Golay codewords to form a single repetition of an encoded KG synchronization sequence data block. The maximum number of data bits which can be protected is 132; the total duration of the encoded sequence is 264 bits. The modulation format bit assignments for this scheme are presented in Figure 4.11.

The 11 Golay codewords comprising each KG codeword are interleaved. However, repetitions of each KG codeword are packed into the tone array in a manner similar to that described for the BCH protection technique. This results in the j^{th} bit of each of the L KG codeword repetitions being placed on tones which are separated in frequency. In Figure 4.12, tone placements of the L repetitions ($L \leq 8$) of the first bit of the first Golay codeword is indicated.

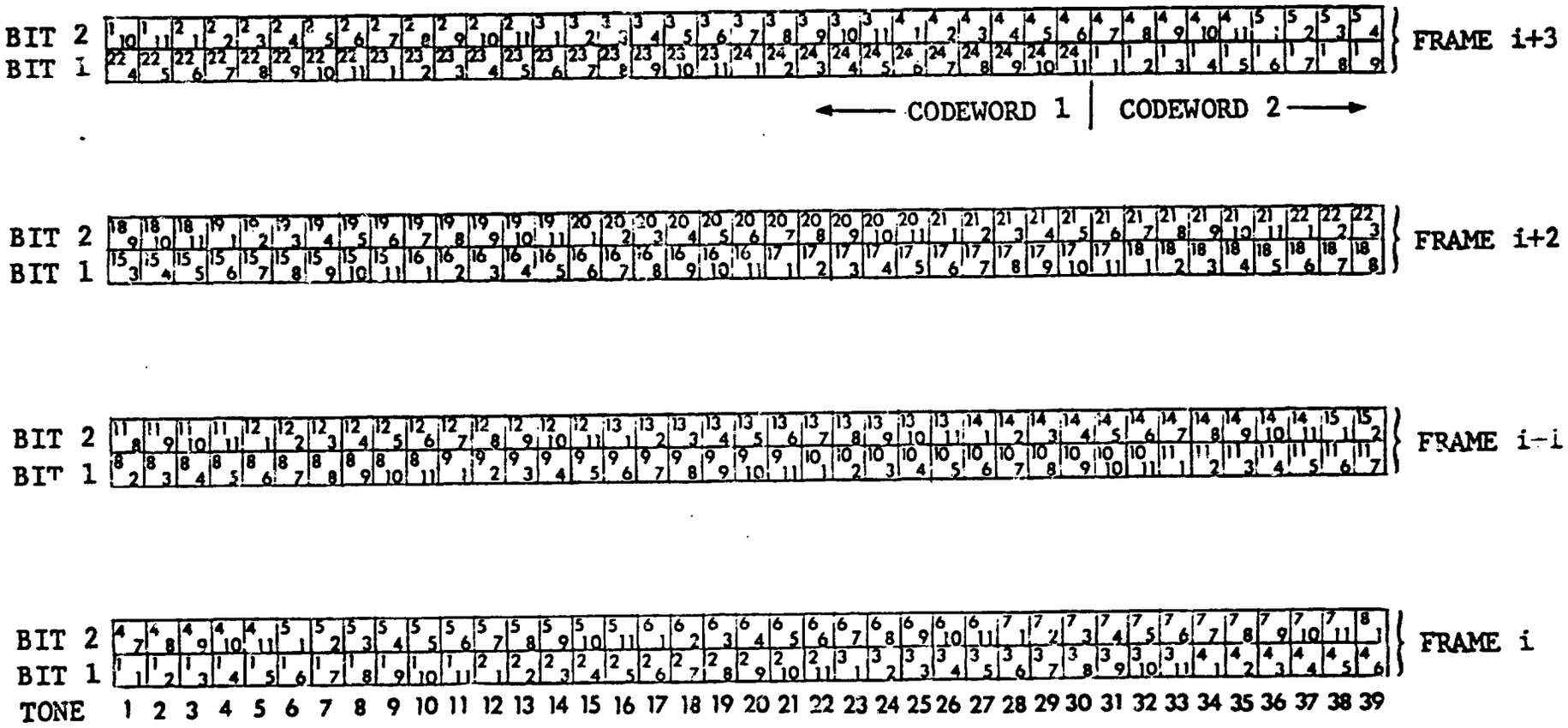

I_J → I^{th} BIT OF THE J^{th} GOLAY CODE (24,12;8). 11 GOLAY CODEWORDS COMPRISE EACH KG SYNCHRONIZATION SEQUENCE CODEWORD.

Figure 4.9 Modulation Format Bit Assignments for KG Synchronization Sequence when 11 Golay Codewords (24,12;8) Comprise Each KG Codeword

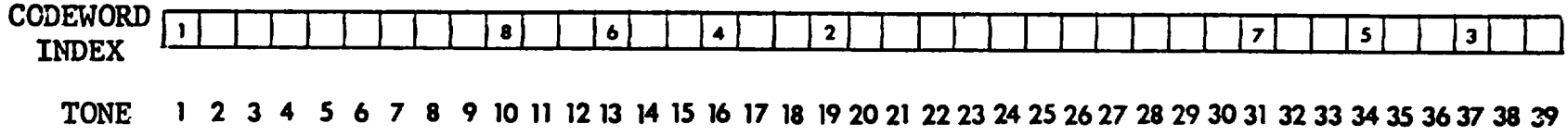

Figure 4.10 The Index of the Tone on which the First Bit of 8 Consecutive (252,128;37) Codewords Is Placed

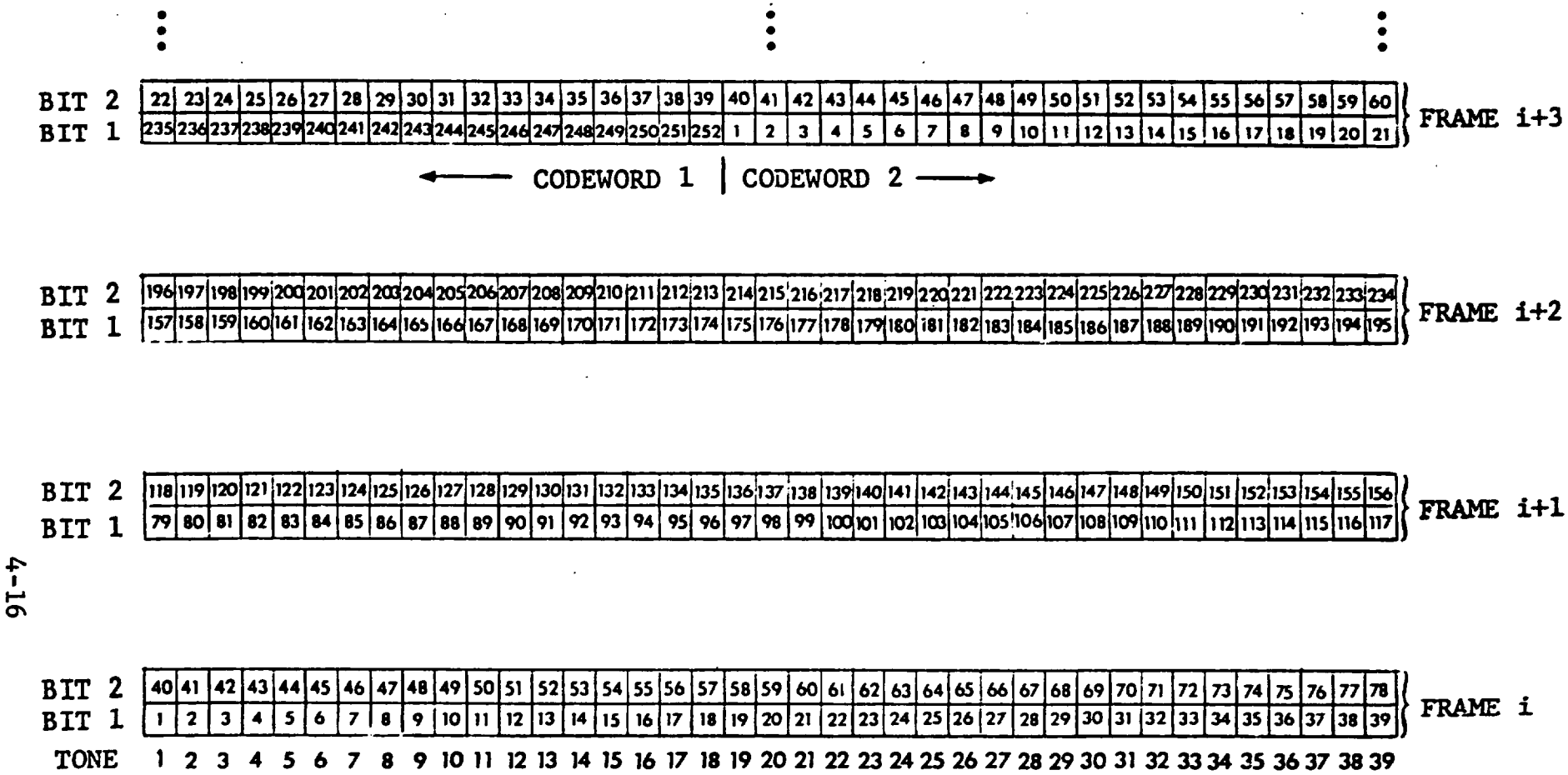

Figure 4.11 Modulation Format Bit Assignments for KG Synchronization Sequence when (252,128;37) BCH Code Is Employed

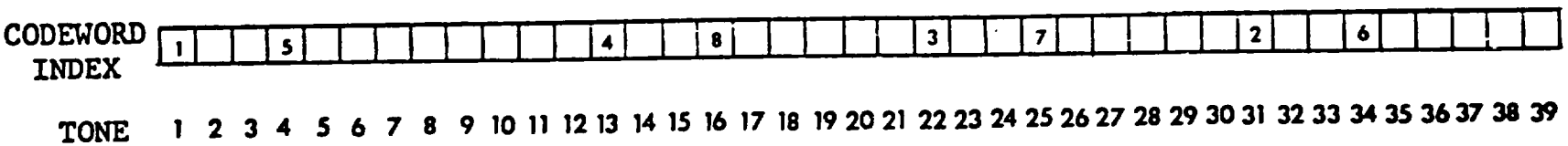

Figure 4.12 The Index of the Tone on which the First Bit of 8 Consecutive KG Synchronization Sequence Codewords 11 x (24,12;8) Is Placed

The tone placement of the 24 bits of the first Golay codeword are depicted in Figure 4.13. Both diagrams demonstrate that acceptable tone dispersement of related bits has been achieved.

To demonstrate the relative robustness of the two encoding techniques, software has been written to simulate the transmission of the KG synchronization sequence over an HF channel. Two channel models will be used for evaluation purposes:

Model 1 - The HF channel is represented by two equi-strength paths separated by 1 ms. Each path is assumed to have a double-sided Doppler bandwidth of 1 Hz. This model is representative of channel behavior when the modem is operating near the maximum usable frequency (MUF).

Model 2 - The HF channel is represented by a 6-path equi-strength split ray model with a total multipath spread of 2.6 ms. Each path is assumed to be resolvable into two components separated by 0.1 ms. The double-sided Doppler bandwidth per path is 1.5 Hz. This model is representative of channel behavior when the modem is operating significantly below the maximum usable frequency.

A summary of the details of both channel models appears in Table 4-2.

The result of the simulations is a statistical summary of the decoded KG synchronization sequence bit and block error rates. Of course, the block error rates are computed on the basis of the entire KG codeword. For the case of the Golay protection scheme, a KG block error occurs whenever one or more of the 11 Golay codewords is decoded incorrectly. For the case of the BCH protection scheme, a KG codeword is identical to the block error rate for the BCH codeword.

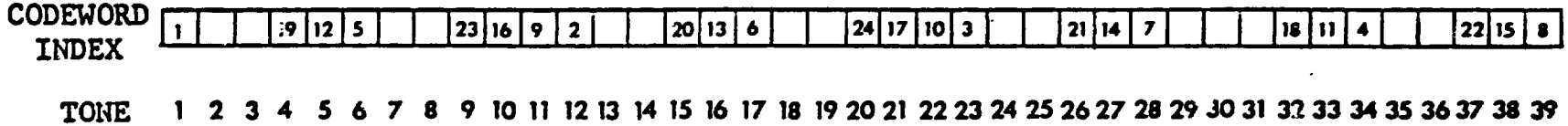

Figure 4.13 Index of the Tones on which the 24 Bits of a Typical Golay Codeword Are Placed

TABLE 4-2

SUMMARY OF THE DELAY AND DOPPLER CHARACTERISTICS
FOR TWO SIMULATED HF CHANNEL MODELS

2-Path Model			6-Path Split Ray Model		
Path Index	Delay (ms)	Double-Sided Doppler Bandwidth (Hz)	Path Index	Delay (ms)	Double-Sided Doppler Bandwidth (Hz)
1	0	1.0	1	0	1.5
2	1.0	1.0	2	0.1	1.5
			3	0.5	1.5
			4	0.6	1.5
			5	1.0	1.5
			6	1.1	1.5
			7	1.5	1.5
			8	1.6	1.5
			9	2.0	1.5
			10	2.1	1.5
			11	2.5	1.5
			12	2.6	1.5

Statistics have been kept for both hard and soft decoding of the Golay codewords. The soft decoding algorithm employed is Chase's Algorithm 2. This method requires a maximum of 16 hard decoder iterations to complete a soft decision decode of the (24,12;8) Golay codeword. Unfortunately, the large minimum distance of the (252,128;37) BCH code renders impractical any contemplated application of Chase's Algorithm 2. As a result, only a hard decoding simulation has been done for the BCH protection scheme.*

In Figures 4.14 through 4.19, block error rates as a function of signal-to-noise ratio per received tone (E_T/N_0) are presented. The curves are drawn with parametric dependence on encoding technique, HF channel model, and the number of KG codeword repetitions. Figures 4.20 through 4.25 present bit error rates as a function of signal-to-noise ratio per received tone (E_T/N_0) with similar parameterizations.

Both the BCH technique and the Golay technique demonstrate approximately equal performance when the Golay codewords are hard decoded. This is especially true for the two-path HF channel model. However, the BCH technique does suffer an increased disadvantage with respect to the hard-decoded Golay technique for the six-path split ray HF channel model.

As noted earlier, the relationship between the three SNR's used in this report is given by

*A simple two iteration soft decoding algorithm, based on one conventional hard decode and one additional hard decode with the 37 least reliable bits complemented, may prove useful if this code is finally selected for the ANDVT.

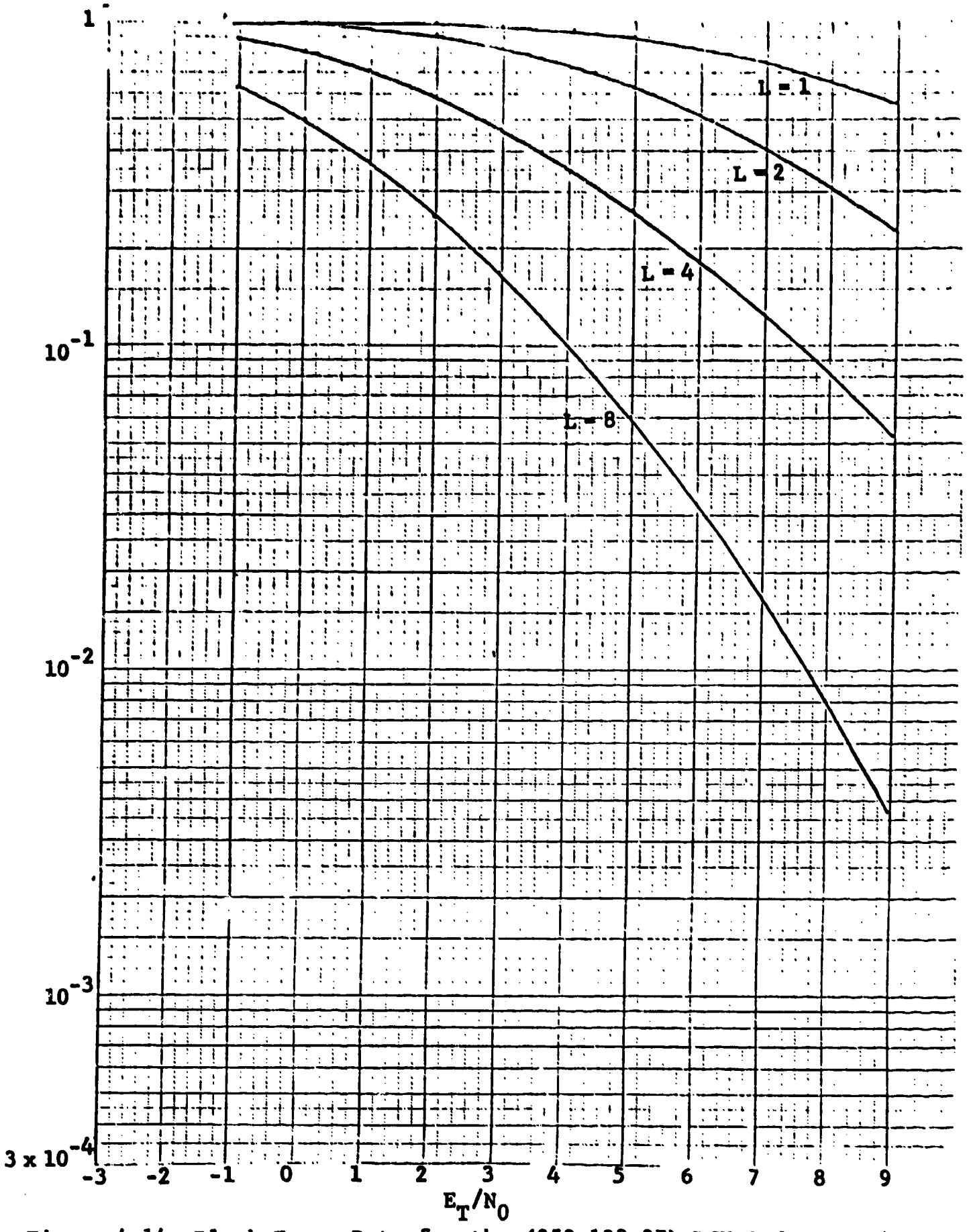

Figure 4.14 Block Error Rate for the (252,128;37) BCH Code Assuming a 2-Path HF Channel Model (L ➡ No. of KG Codeword Repetitions)

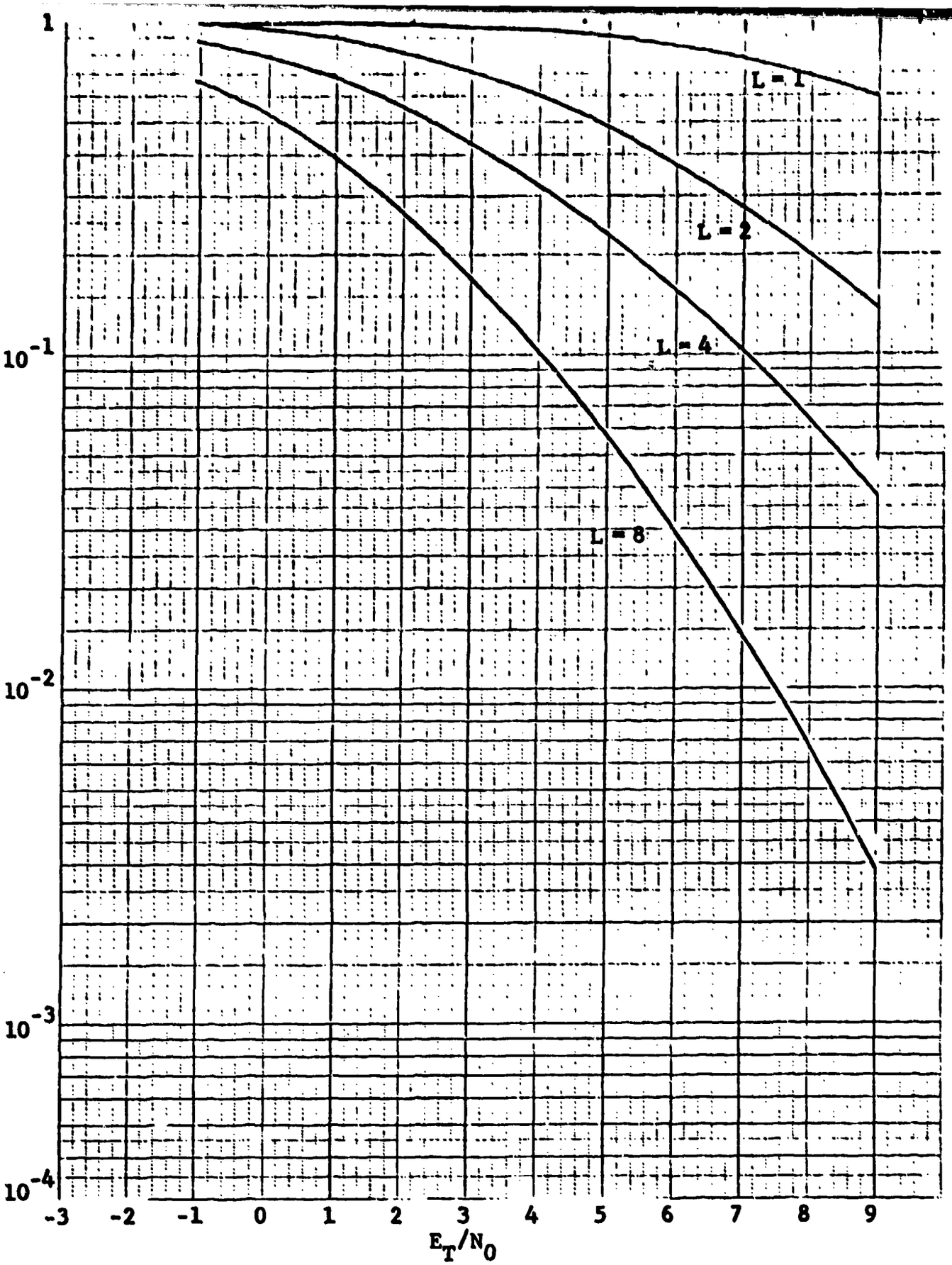

Figure 4.15 Block Error Rate for a Hard-Decoded Golay Protection Scheme Assuming a 2-Path HF Channel Model (L ⇒ No. of KG Codeword Repetitions)

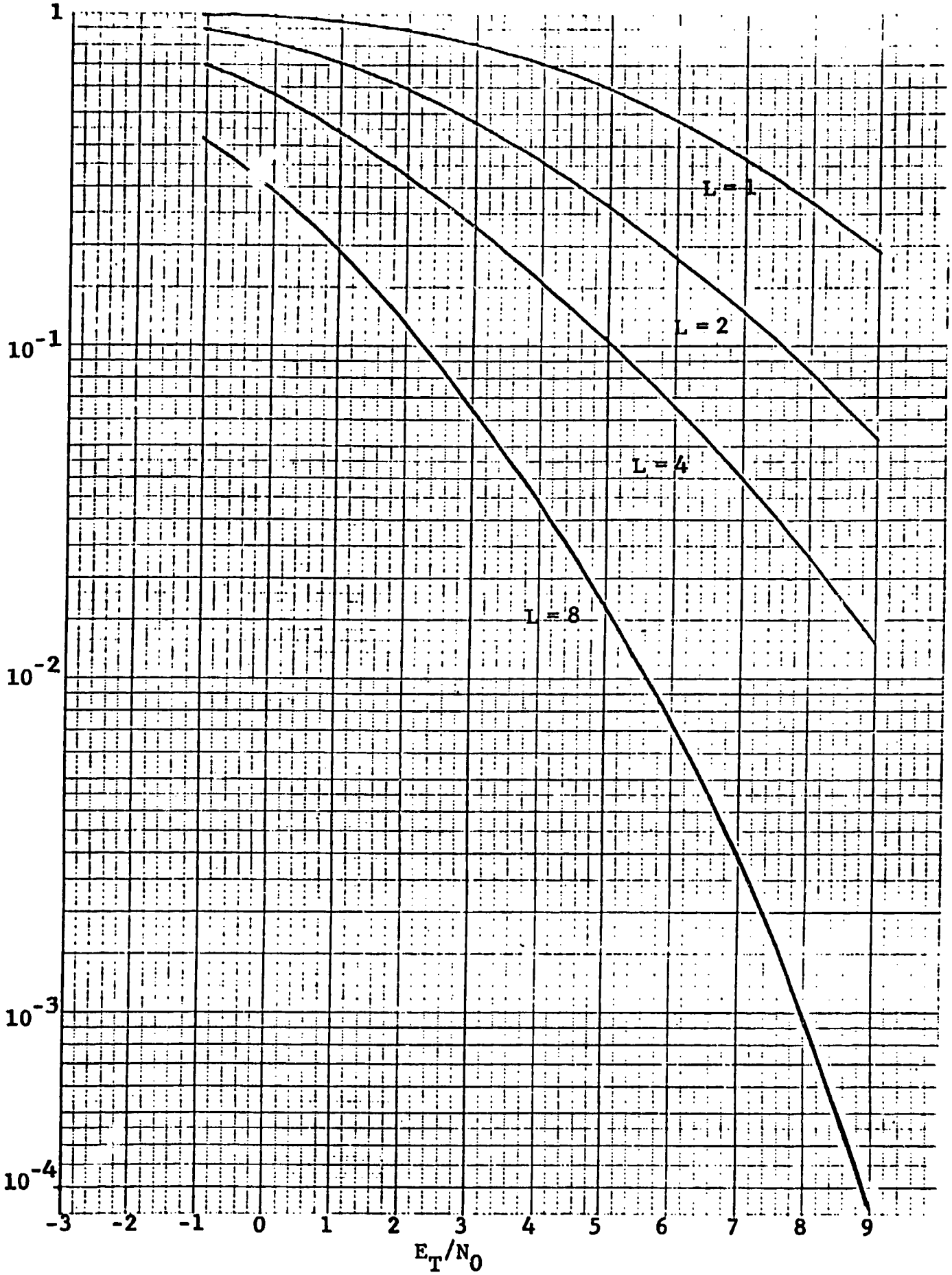

Figure 4.16 Block Error Rate for a Soft-Decoded Golay Protection Scheme Assuming a 2-Path HF Channel Model (L ⇒ No. of KG Codeword Repetitions)

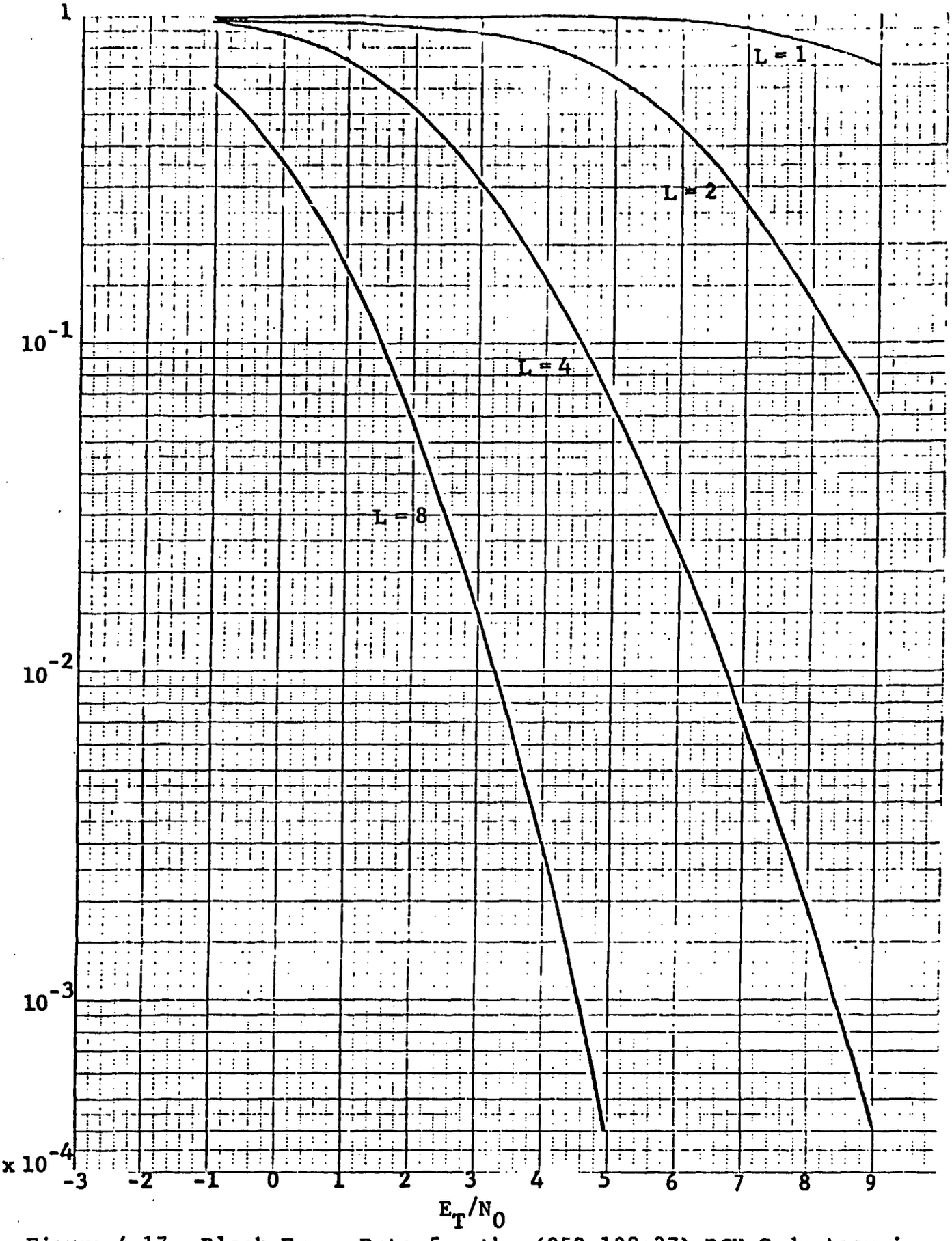

Figure 4.17 Block Error Rate for the (252,128;37) BCH Code Assuming a 6-Path Split Ray HF Channel Model (L ⇒ No. of KG Codeword Repetitions)

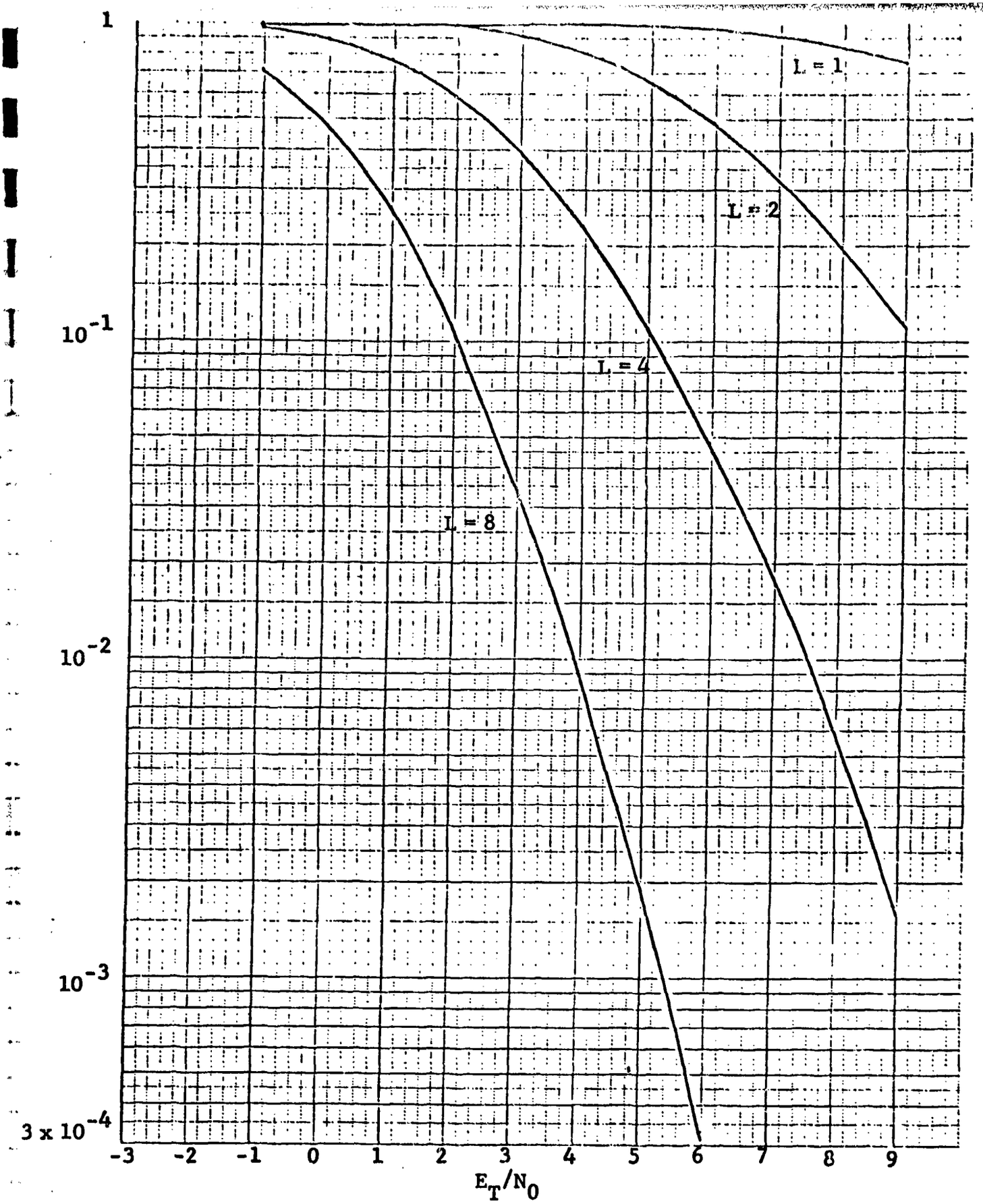

Figure 4.18 Block Error Rate for a Hard-Decoded Golay Protection Scheme Assuming a 6-Path Split Ray HF Channel Model (L ⇒ No. of KG Codeword Repetitions)

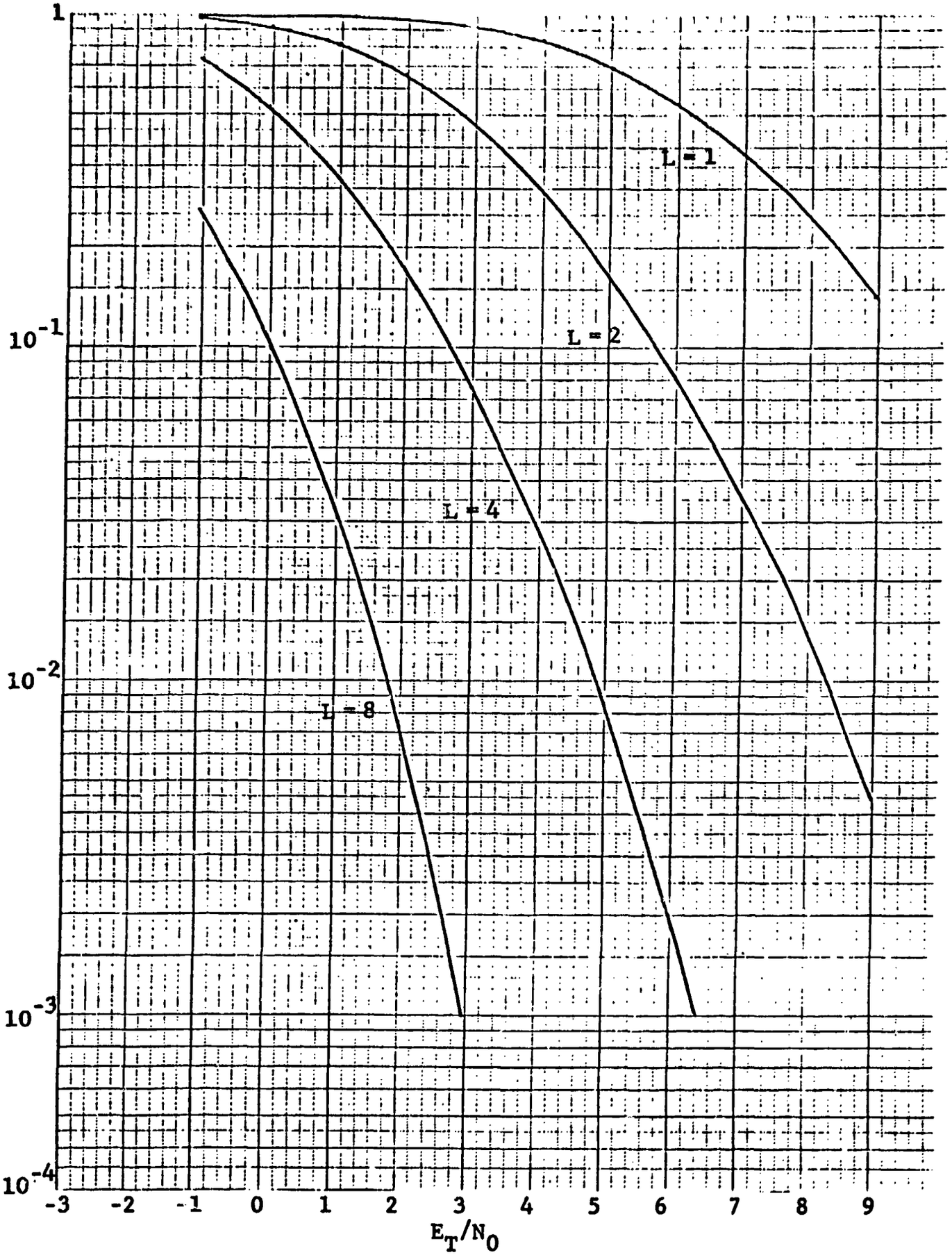

Figure 4.19 Block Error Rate for a Soft-Decoded Golay Protection Scheme Assuming a 6-Path Split Ray HF Channel Model (L ⇒ No. of KG Codeword Repetitions)

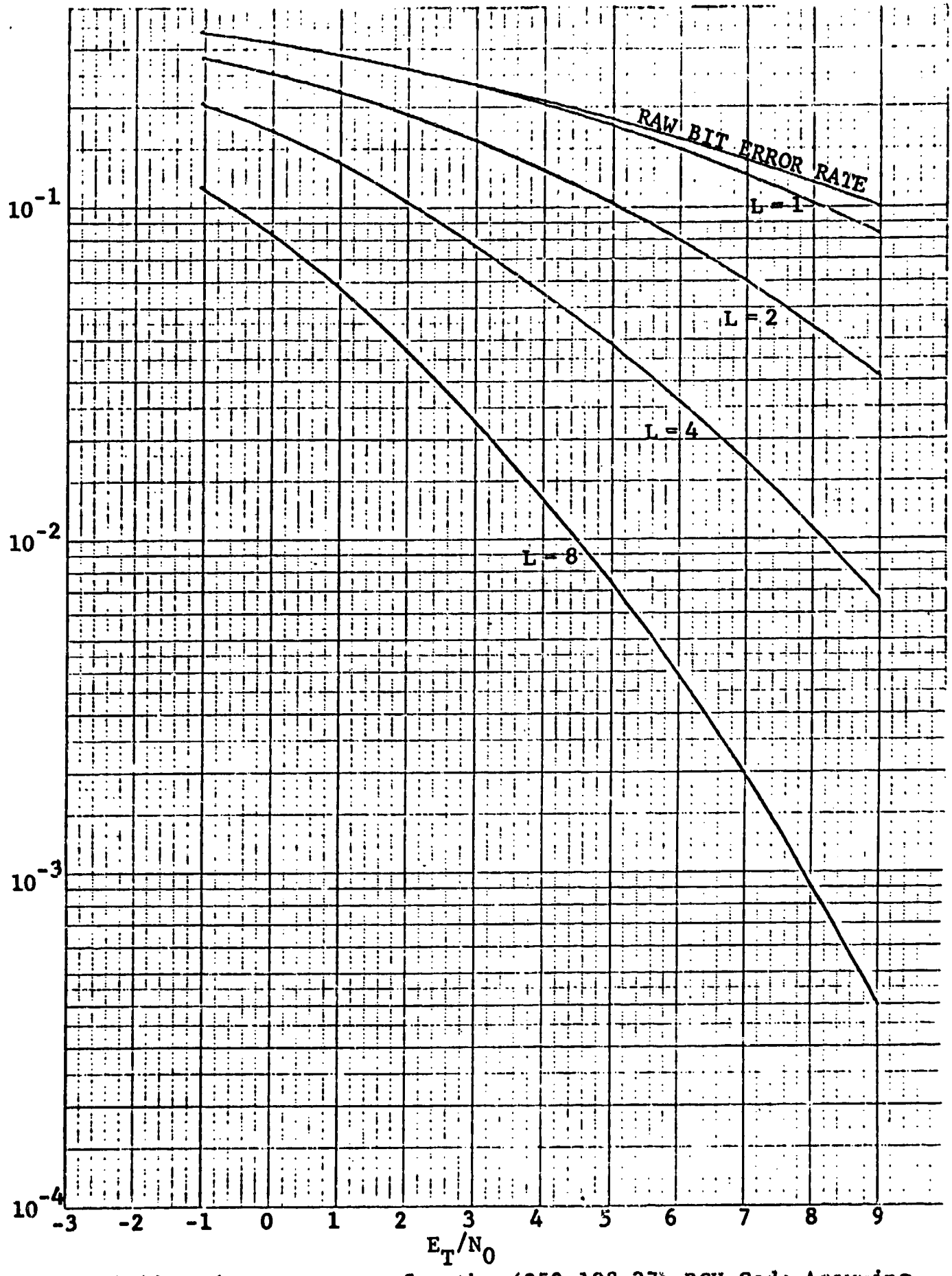

Figure 4.20 Bit Error Rate for the (252,128;37) BCH Code Assuming a 2-Path HF Channel Model (L ⇒ No. of KG Codeword Repetitions)

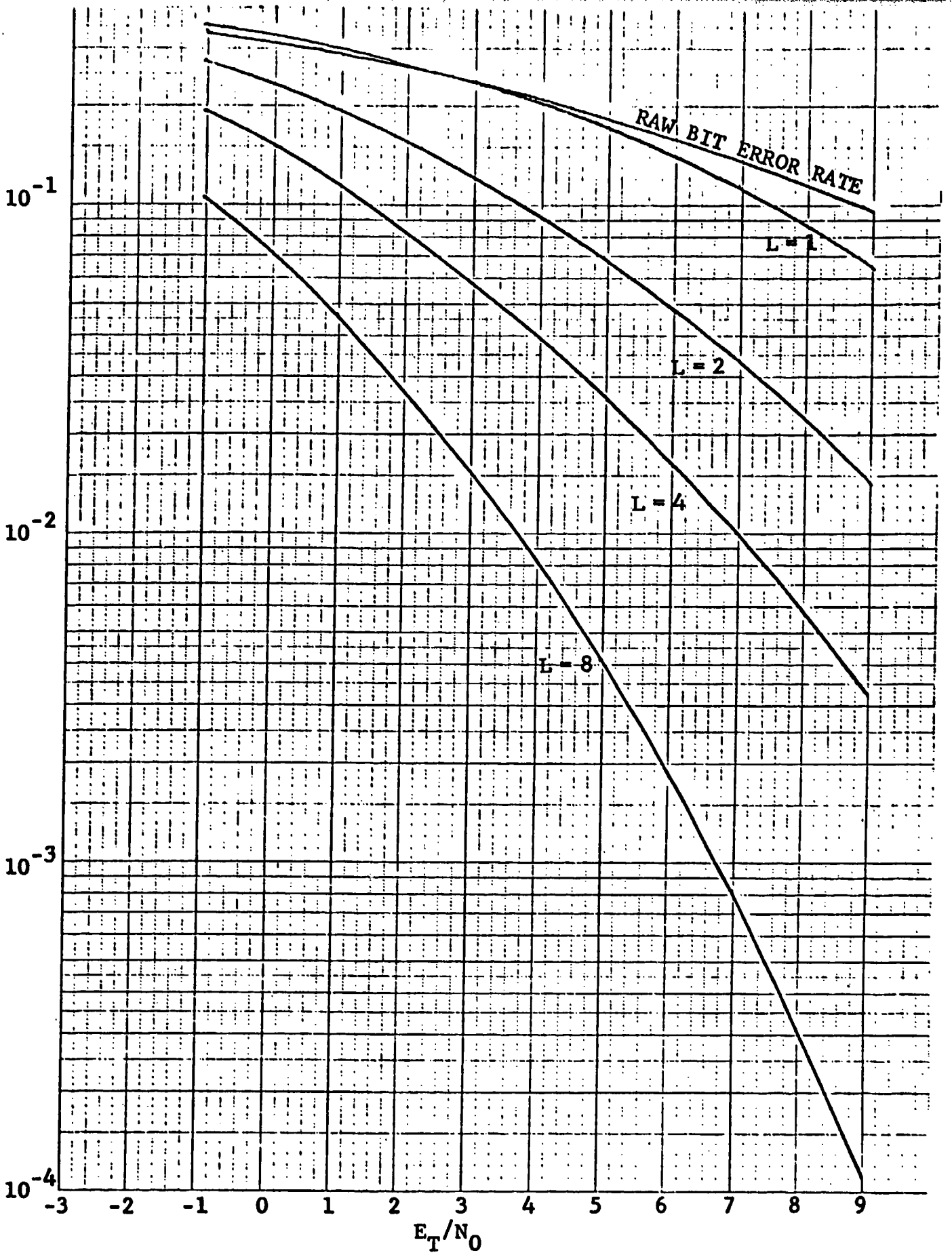

Figure 4.21 Bit Error Rate for a Hard-Decoded Golay Protection Scheme Assuming a 2-Path HF Channel Model (L ⇒ No. of KG Codeword Repetitions)

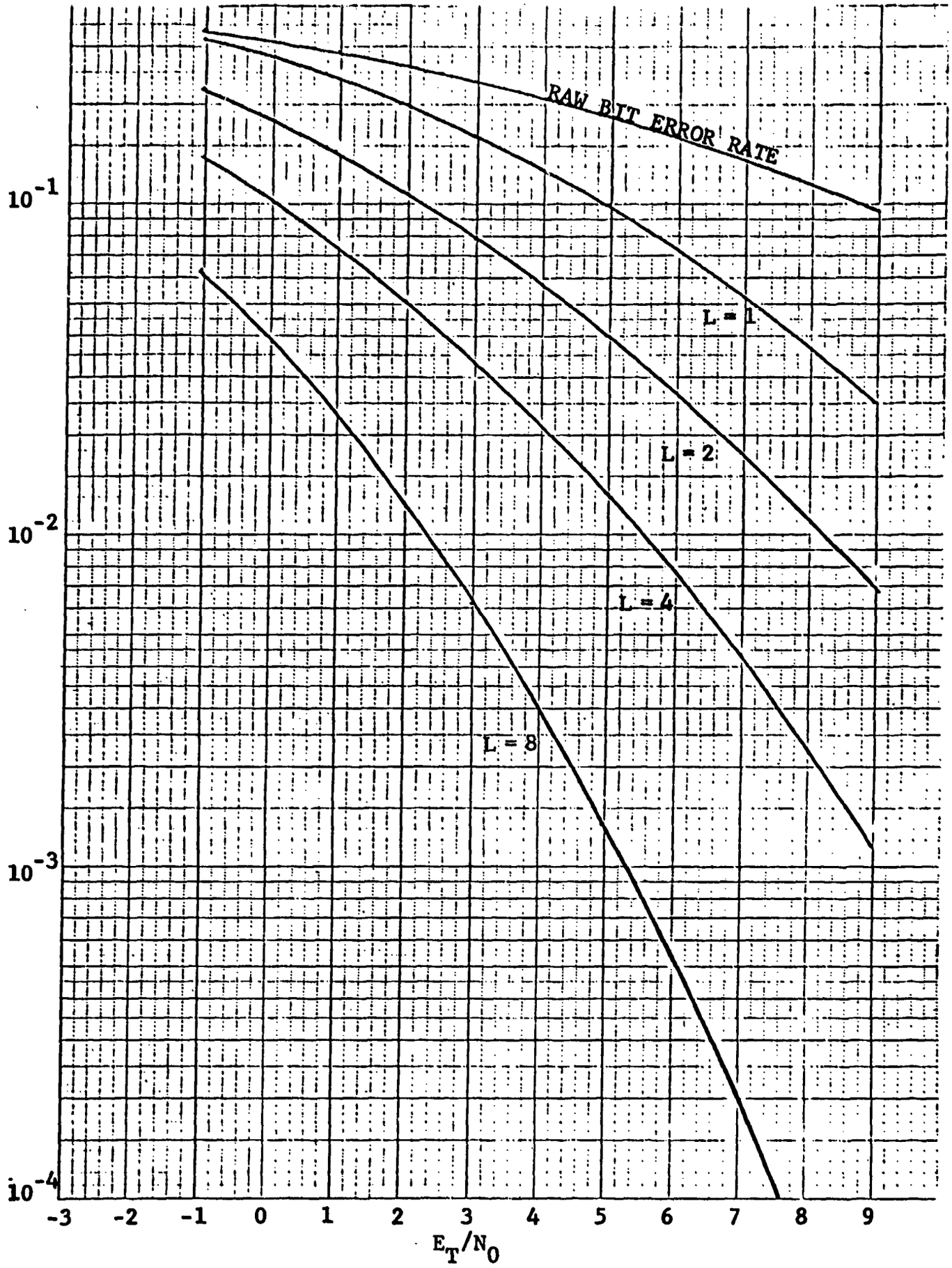

Figure 4.22 Bit Error Rate for a Soft-Decoded Golay Protection Scheme Assuming a 2-Path HF Channel Model (L ⇒ No. of KG Codeword Repetitions)

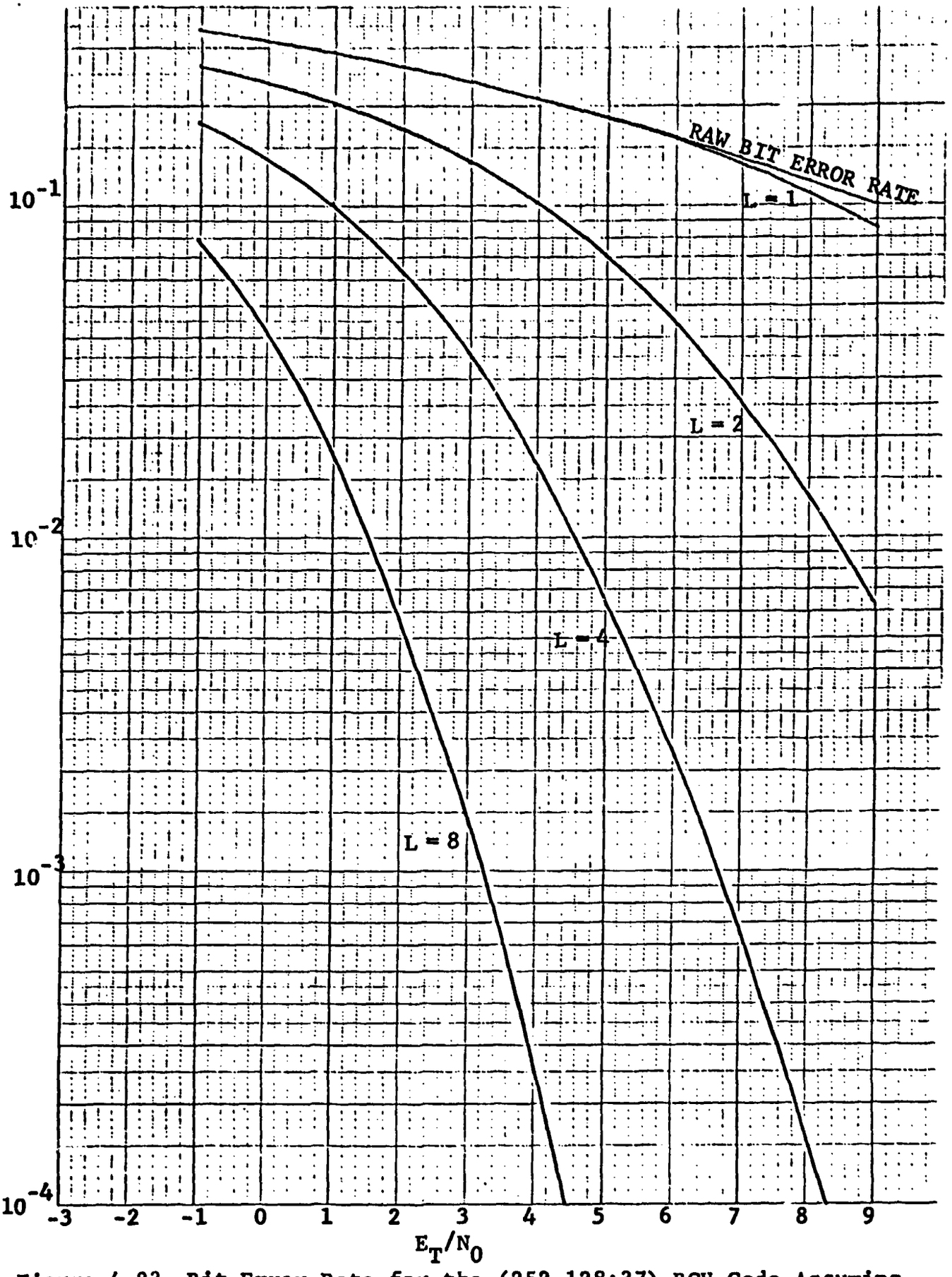

Figure 4.23 Bit Error Rate for the (252,128;37) BCH Code Assuming a 6-Path Split Ray HF Channel Model (L ⇒ No. of KG Codeword Repetitions)

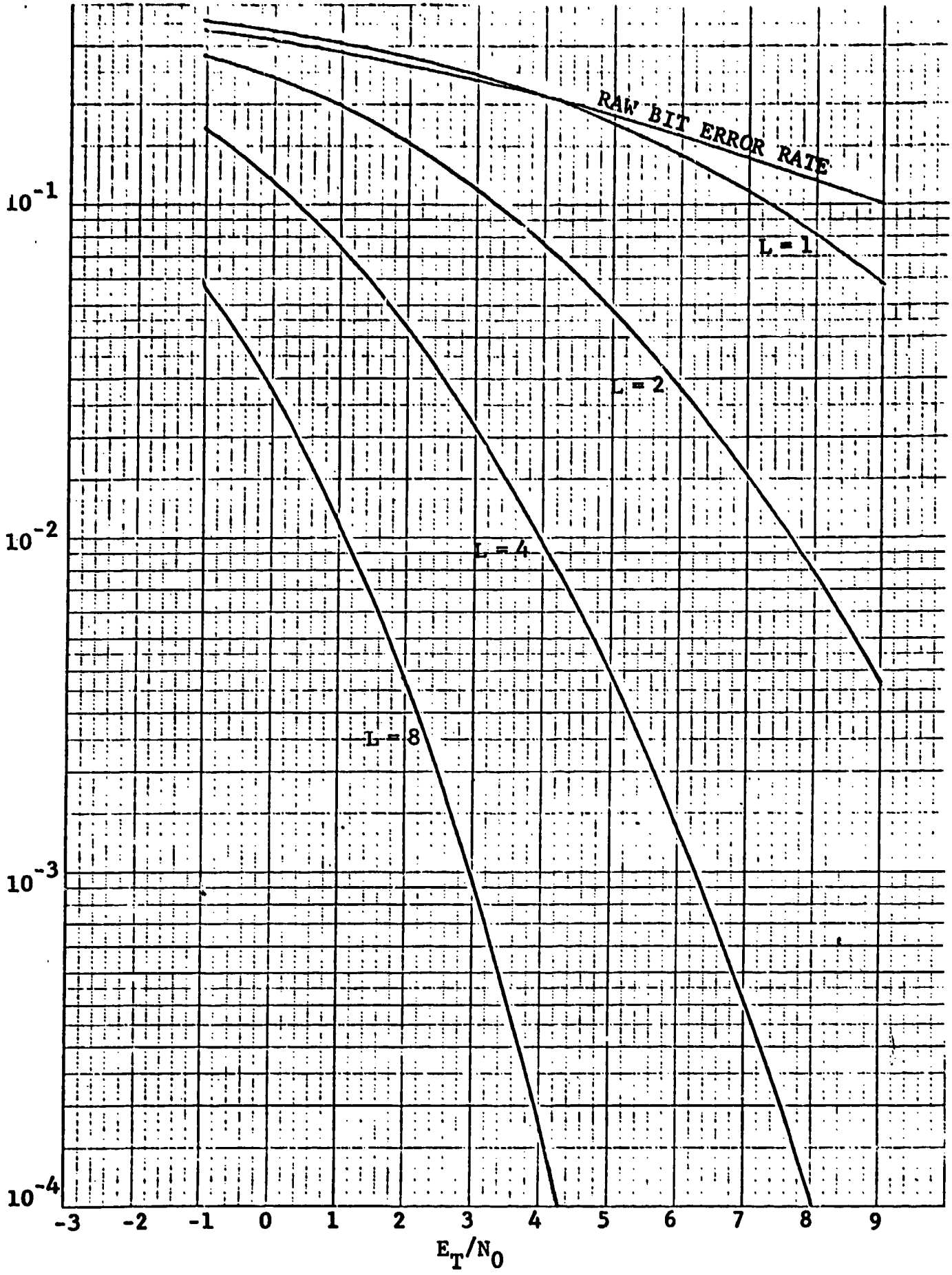

Figure 4.24 Bit Error Rate for a Hard-Decoded Golay Protection Scheme Assuming a 6-Path Split Ray HF Channel Model (L ⇒ No. of KG Codeword Repetitions)

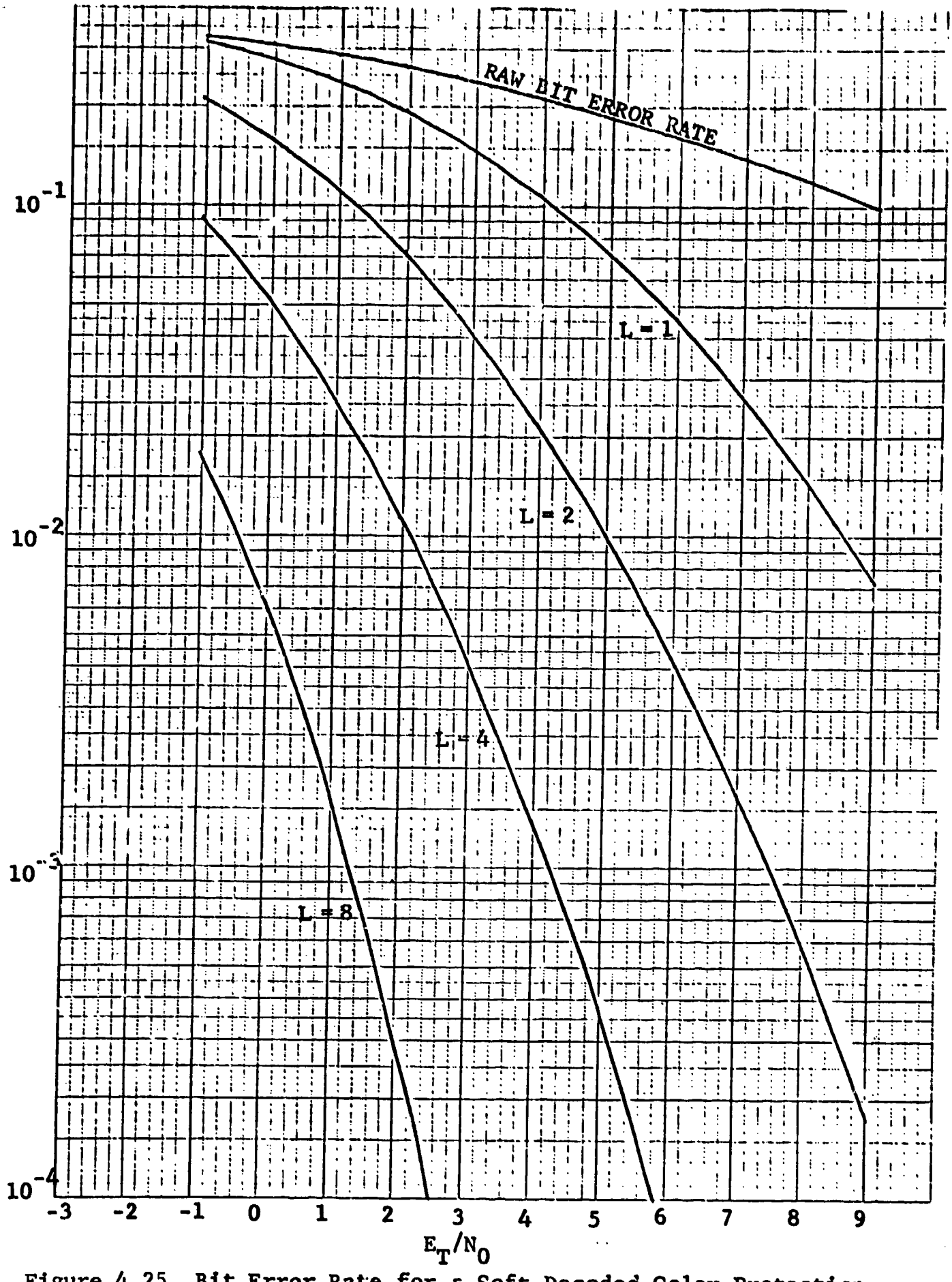

Figure 4.25 Bit Error Rate for a Soft-Decoded Golay Protection Scheme Assuming a 6-Path Split Ray HF Channel Model (L ⇒ No. of KG Codeword Repetitions)

$$\frac{P}{N_0} = \left(\frac{E_T}{N_0}\right)_{KG} + 33.4 = \left(\frac{E_b}{N_0}\right)_{voice} + 33.8$$

and, thus,

$$\frac{E_T}{N_0} = \left(\frac{E_b}{N_0} + 0.4\right) dB$$

For acceptable quality speech on a two-path model, an E_b/N_0 of 14 dB is required, and an E_b/N_0 of 11 dB is required for the six-path model. Thus, both the long BCH code and the soft-decoded Golay code, used with eighth-order diversity, represent attractive codes for KG synchronization. However, the Golay code with soft decoding offers somewhat better performance than that obtained for the long BCH code with just hard decoding. Based on performance results alone, the Golay coding approach is recommended. A choice of ten Golay codes, protecting 120 bits, appears somewhat more suitable than the eleven Golay codes actually simulated. The computation is somewhat greater for the Golay coding approach, as indicated in Table 4-1; however, this increase in computation must be weighted against the additional software program required for decoding the long BCH code.

It should be noted that the early analysis, assuming independent Rayleigh fading, indicated that the BCH technique would be superior to the soft-decoded Golay scheme. The importance of detailed simulations such as undertaken above should be evident.

APPENDIX A

APERIODIC CORRELATION FUNCTION

In this appendix we briefly summarize the development of the aperiodic autocorrelation function and record for future reference (and comparison with more general results) the relevant expressions.

The transmitted preamble is the result of convolving an impulse train of length K-1 with a pulse shaping filter p(t) to obtain

$$z(t) = \sum_{k=0}^{K-1} \gamma_k p(t - kT) \tag{1}$$

At the receiver the preamble is processed with a pulse-shaping filter q(-t) and a discrete matched filter. The output of the receiver pulse-shaping filter is given by

$$w_1(t) = \sum_{k=0}^{K-1} \gamma_k r(t - kT) \tag{2}$$

where

$$r(t) = \int q(\tau)p(t+\tau)\, d\tau \tag{3}$$

The output w(t) of the discrete matched filter is the result of convolving the impulse response of the discrete matched filter with (2). We have

$$w(t) = \int \left(\sum_{i=-(K-1)}^{0} \gamma_{-i}^{*} \delta(\tau - iT) \right) \left(\sum_{j=0}^{K-1} \gamma_j r(t-\tau-jT) \; d\tau \right)$$

$$= \sum_{i=-(K-1)}^{0} \sum_{j=0}^{K-1} \gamma_{-i}^{*} \gamma_j r[t - (i+j)T]$$

$$= \sum_{\ell=0}^{K-1} \sum_{j=0}^{K-1} \gamma_{\ell}^{*} \gamma_j r[t - (j-\ell)T] \qquad (4)$$

To simplify we use the function definition

$$[a,b](m) = \begin{cases} 1 & a \leq m \leq b \\ 0 & \text{otherwise} \end{cases} \qquad (5)$$

Then w(t) becomes

$$w(t) = \sum_{i=-\infty}^{+\infty} \sum_{j=-\infty}^{+\infty} \gamma_i^{*} \gamma_j r[t - (j-i)T][0, K-1](i)[0, K-1](j) \qquad (6)$$

which, with a change of variables $k = j-1$, becomes

$$w(t) = \sum_{-\infty}^{+\infty} C(k) r(t - kT) \qquad (7)$$

where

$$C(k) = \sum_{i=-\infty}^{+\infty} \gamma_i^* \gamma_{i+k} [0, K-1](i)[0, K-1](i+k)$$

$$= \sum_{i=-\infty}^{+\infty} \gamma_i^* \gamma_{i+k} [0, K-1](i)[-k, K-1-k](i) \qquad (8)$$

from which we finally obtain

$$C(k) = \begin{cases} \sum_{i=0}^{K-1-k} \gamma_i^* \gamma_{i+k} & \cdots\cdots \quad 0 \le k \le K-1 \\ \sum_{i=-k}^{K-1} \gamma_i^* \gamma_{i+k} & \cdots\cdots \quad -(K-1) \le k \le 0 \\ 0 & \cdots\cdots \quad |k| > K-1 \end{cases} \qquad (9)$$

The above expression can be simply manipulated to obtain the general relation

$$C(k) = C(-k) \qquad (10)$$

which can be used to write (9) in alternative forms.

Note that (9) is the output of a non-realizable filter. This is because the matched filter used in (4) was noncausal. To analyze practical systems so that we can keep track of the

timing it is necessary to insert a delay in the matched filter impulse response. A shift of (K-1)T puts the first non-zero value of the matched filter impulse response at k=0. C(k) is affected similarly. Instead of running from -(K-1) to +(K-1) the matched filter output (correlation function) runs from 0 to 2(K-1) with 2K-1 non-zero elements.

APPENDIX B

SIGNAL-TO-NOISE RELATIONSHIPS FOR HF MODEMS

For completeness, we include this appendix which relates the various signal-to-noise ratios used in this report. A 39-tone modem is specified with a frame rate of 22.5 ms, and an integration time of 17.78 ms, i.e., a guard time of 4.72 ms, is used. A complex signaling rate of 3600 Hz is consistent with a digital implementation using a 64-point FFT for the above tone specifications. The modulation format for the preamble design is based on using only four parallel tones followed by a wideband pulse sequence. Thus, any definition of SNR must also be suitable for preamble evaluation.

In all cases it is meaningful to obtain results in terms of the ratio of the total received power to noise power density. This signal-to-noise density ratio (SNDR) is given by the ratio of the total received power, P, to the noise power per Hz of bandwidth, denoted by N_0, as

$$\text{SNDR} = \frac{P}{N_0} \tag{1}$$

For preamble evaluation in Sections 2 and 3, results are given in terms of this SNDR. The above is called a signal-to-noise density ratio since the denominator is the noise density, rather than the more conventional noise power, in the bandwidth of the signal. To avoid the ambiguity which results from different bandwidth definitions, one may define the signal-to-noise ratio per information bit

$$\frac{E_b}{N_0} = \frac{P}{N_0 R} \tag{2}$$

where R is the actual data rate of the modem. For speech transmission R = 2400 b/s and thus Eqs. (1) and (2) can be related by

$$\frac{P}{N_0} = \left(\frac{E_b}{N_0} + 33.8\right) \text{dB - for R = 2400 b/s} \qquad (3)$$

For digitized speech the modulated signal is approximately contained in a bandwidth of 2400 Hz, and thus, E_b/N_0 can also be viewed as the ratio of signal-to-noise power measured in a bandwidth of 2400 Hz.

In addition to obtaining results in terms of P/N_0 and E_b/N_0, which are easily related, it is customary for parallel tone evaluations to present results in terms of the average signal-to-noise ratio per tone defined by

$$\frac{E_T}{N_0} = \frac{E[r^2]}{E[n_c^2] + E[n_s^2]} \qquad (4)$$

where r is the tone amplitude and n_c and n_s are the cosine and sine noise components at the output of the integrate-and-dump circuits. This SNR is also closely related to the signal-to-noise power measured in a bandwidth equal to that of the modulated signal.

The components of Eq. (4) are obtained by first noting that a multiple tone received signal can be written as

$$y(t) = \sqrt{2} \sum_{i=1}^{N} r_i \cos(\omega_i t + \theta_i) + n(t) \qquad (5)$$

where n(t) is assumed to be a white Gaussian noise process normalized such that $E[n(t)n(t+\tau)] = (N_0/2)\delta(\tau)$.

The cosine and sine components per tone are given by

$$y_{c_i} = \frac{\sqrt{2}}{T}\int_0^T y(t) \cos \omega_i t \, dt = r_i \cos \theta_i + n_{c_i}$$

$$y_{s_i} = \frac{\sqrt{2}}{T}\int_0^T y(t) \sin \omega_i t \, dt = r_i \sin \theta_i + n_{s_i} \qquad (6)$$

Note, the multiple tones are orthogonal over the integration time T, which is less than a baud interval by the allowable guard time.

The average signal energy per tone is given by

$$E_T = E[r_i^2 \cos^2 \theta_i + r_i^2 \sin^2 \theta_i] = E[r_i^2] \qquad (7)$$

and the energy per noise component is given by

$$E[n_{c_i}^2] = E[n_{s_i}^2] = N_0/2 \qquad (8)$$

The total received power can be written as

$$P = \frac{NE_T}{T} \qquad (9)$$

where N is the total number of tones and T is the integration time per tone. Thus, we can relate (1) and (2) to E_T/N_0 by the following:

$$\frac{P}{N_0} = \frac{N}{T}\left(\frac{E_T}{N_0}\right) \tag{10}$$

and

$$\frac{E_b}{N_0} = \frac{N}{TR}\left(\frac{E_T}{N_0}\right) \tag{11}$$

For a conventional 16 tone modem* operating at 2400 b/s, and including a Doppler correction tone of twice the amplitude, ($N_{effective} = 20$), equation (11) gives the relationship between E_b/N_0 and E_T/N_0 as

$$\frac{E_b}{N_0} = \frac{20}{\frac{1}{110}\ 2400}\left(\frac{E_T}{N_0}\right) \tag{12}$$

or

$$\frac{E_b}{N_0} = \left[\frac{E_T}{N_0} - .38\right] \text{ dB - 16 tone modem} \tag{13}$$

For an ANDVT modem operating at 2400 b/s with two Golay codes, using 39 tones and an integration of 17.78 ms, we have

$$\frac{E_b}{N_0} = \frac{39}{17.78 \times 10^{-3} \times 2400}\left(\frac{E_T}{N_0}\right) \tag{14}$$

*D. Chase, "A Combined Coding and Modulation Approach for Communication Over Dispersive Channels," IEEE Trans. on Communications, Vol. COM-21, No. 3, March 1973, page 159.

or

$$\frac{E_b}{N_0} = \left[\frac{E_T}{N_0} - .39\right] \text{ dB - 39 tone ANDVT modem} \qquad (15)$$

Thus, in this case, a comparison based on E_T/N_0 is essentially equivalent (adjustment is only .01 dB) to the fair comparison based on E_b/N_0.

If the ANDVT modem is used without coding a data rate of 2400 bps can be achieved with 27 tones which are keyed every 22.5 ms with one of four phases (2 bits/tone). In this case the relationship between E_b/N_0 and E_T/N_0 is given by

$$\frac{E_b}{N_0} = \frac{27}{17.78 \times 10^{-3} \times 2400}\left(\frac{E_T}{N_0}\right) \qquad (16)$$

$$\frac{E_b}{N_0} = \left[\frac{E_T}{N_0} - 1.99\right] \text{ dB - 27 tone ANDVT modem} \qquad (17)$$

Note, by comparing Eqs. (13) and (17), without coding the ANDVT modem offers a 1.61 dB advantage in E_b/N_0 when compared to the 16-tone modem. This gain is due to the fact that the loss due to guard time is smaller for the ANDVT modem and also due to the Doppler tracking algorithm for the ANDVT modem which does not require an external tone.

The ANDVT speech modem results are usually presented in terms of E_b/N_0 and the preamble results are presented in terms of P/N_0. Equation (3) results relate these two measures. The results for the KG synchronization sequence are presented in terms of E_T/N_0.

which has the desirable property that guard time and code redundancy does affect this SNR measure. As a consequence of the low data rate used for the KG sync sequence, E_b/N_0 is considerably greater than E_T/N_0 for this case, and thus, it is more meaningful to make comparisons based on P/N_0. Equation (10) relates P/N_0 to E_T/N_0, which for a 39-tone preamble and integration of 17.78 ms yields

$$\frac{P}{N_0} = [E_T/N_0 + 33.4]\ \text{dB} \quad \text{- 39-tone KG preamble} \qquad (18)$$

In summary, the preamble, KG sync sequence, and multiple tone modems can be compared in terms of P/N_0 but, by convention, E_b/N_0 and E_T/N_0 are sometimes used. Equation (3) provides the appropriate conversion for the ANDVT speech modem, and Eq. (18) provides the conversion for the KG sync results given in Section 4.